



**A SYSTEM FOR ANALYSIS OF
SOIL-STRUCTURE INTERACTION**

VERSION 3

THEORETICAL MANUAL

Farhang Ostadan

APRIL 2007

ACKNOWLEDGEMENT

Original SASSI Development Team

John Lysmer, Farhang Ostadan,
Mansour Tabatabaie, Fredrick Tajirian, and Shahriar Vahdani

Geotechnical Engineering Division
Civil Engineering Department
University of California, Berkeley, CA 94720

SASSI2000

REVISION 1

November 1999

John Lysmer, Farhang Ostadan, Chih Cheng Chin

SASSI2000

Version 2

January 2006

Farhang Ostadan

DISCLAIMER

Every reasonable effort was made to provide a comprehensive and flexible computer program. However, the computer program itself and associated documentation are supplied without representation of warranty, expressed or implied, as to its content, accuracy, or freedom from defects or errors.

RECORD OF REVISION

Version Number	Date of Revision	Description
3	April 2007	Upgraded version from version 2

LIST OF DOCUMENT PAGES

Sheet	Latest Revision	Sheet	Latest Revision
Cover Sheet	3		
i	3	3-1	3
ii	3	3-2	3
iii	3	3-2	3
iv	3	3-4	3
v	3	3-5	3
vi	3	3-6	3
vii	3	3-7	3
viii	3	3-8	3
ix	3	3-9	3
x	3	3-10	3
xi	3	3-11	3
		3-12	3
		3-13	3
		3-14	3
1-1	3	3-15	3
1-2	3	3-16	3
		3-17	3
2-1	3	3-18	3
2-2	3	3-19	3
2-3	3	3-20	3
2-4	3	3-21	3
2-5	3	3-22	3
2-6	3	3-23	3
2-7	3	3-24	3
2-8	3	3-25	3
2-9	3	3-26	3
2-10	3	3-27	3
2-11	3	3-28	3
2-12	3		

Sheet	Latest Revision	Sheet	Latest Revision
		5-6	3
		5-7	3
		5-8	3
		5-9	3
		5-10	3
		5-11	3
		5-12	3
		5-13	3
		5-14	3
		5-15	3
		5-16	3
4-1	3	5-17	3
4-2	3	5-18	3
4-3	3	5-19	3
4-4	3	5-20	3
4-5	3	5-21	3
4-6	3	5-22	3
4-7	3	5-23	3
4-8	3	5-24	3
4-9	3	5-25	3
4-11	3	5-26	3
4-12	3	5-27	3
4-13	3	5-28	3
4-14	3	5-29	3
4-15	3	5-30	3
		5-31	3
5-1	3	5-32	3
5-2	3	5-33	3
5-3	3	5-34	3
5-4	3	5-35	3
5-5	3	5-36	3

Sheet	Latest Revision	Sheet	Latest Revision
5-37	3	5-68	3
5-38	3	5-69	3
5-39	3	5-70	3
5-40	3	5-71	3
5-41	3	5-72	3
5-42	3	5-73	3
5-43	3	5-74	3
5-44	3	5-75	3
5-45	3	5-76	3
5-46	3	5-77	3
5-47	3	5-78	3
5-48	3	5-79	3
5-49	3	5-80	3
5-50	3	5-81	3
5-51	3	5-82	3
5-52	3	5-83	3
5-53	3	5-84	3
5-54	3	5-85	3
5-55	3	5-86	3
5-56	3	5-87	3
5-57	3	5-88	3
5-58	3	5-89	3
5-59	3	5-90	3
5-60	3	5-91	3
5-61	3	5-92	3
5-62	3	5-93	3
5-63	3	5-94	3
5-64	3	5-95	3
5-65	3	5-96	3
5-66	3	5-97	3
5-67	3	5-98	3

Sheet	Latest Revision	Sheet	Latest Revision
6-1	3		
6-2	3		
6-3	3		
7-1	3		
7-2	3		
7-3	3		
7-4	3		
7-5	3		
8-1	3		
8-2	3		
8-3	3		
8-4	3		
8-5	3		
8-6	3		
8-7	3		
8-8	3		
9-1	3		
9-2	3		
9-3	3		
9-4	3		
9-5	3		
A-1	3		
A-2	3		
A-3	3		

TABLE OF CONTENTS

<u>CHAPTER</u>	<u>PAGE</u>
THEORETICAL MANUAL	i
LIST OF DOCUMENT PAGES	iv
 CHAPTER 1 INTRODUCTION.....	 1-1
 CHAPTER 2 SUBSTRUCTURING METHODS OF SASSI.....	 2-1
2.1 SUBSTRUCTURING METHODS OF SSI ANALYSIS	2-1
2.2 THE FLEXIBLE VOLUME METHOD	2-3
2.3 THE SUBSTRUCTURE SUBTRACTION METHOD	2-7
2.4 COMPUTATIONAL STEPS	2-11
 CHAPTER 3 SITE RESPONSE ANALYSIS	 3-1
3.1 SITE RESPONSE ANALYSIS MODEL.....	3-1
3.2 EIGENVALUE PROBLEM FOR SITE MODEL	3-2
3.2.1 Eigenvalue Problem for Generalized Rayleigh Wave Motion.....	3-2
3.2.2 Eigenvalue Problem for Generalized Love Wave Motion.....	3-6
3.3 TRANSMITTING BOUNDARY MATRICES	3-7
3.3.1 Transmitting Boundary Matrix for Two-Dimensional Problems ..	3-7
3.3.2 Transmitting Boundary Matrix for Axisymmetric Problems.....	3-8
3.4 FREE-FIELD MOTION.....	3-13
3.4.1 Inclined SV- and P-Waves	3-13
3.4.2 Inclined SH-Wave	3-16
3.4.3 Rayleigh Wave.....	3-18
3.4.4 Love Wave Motion	3-20
3.5 MODELLING OF SEMI-INFINITE HALFSpace AT BASE.....	3-20
3.5.1 The Variable Depth Method	3-20
3.5.2 Viscous Boundary at Base	3-24
3.6 DYNAMIC SOIL PROPERTIES AND EQUIVALENT LINEAR METHOD	3-26
3.7 COMPLEX RESPONSE METHOD	3-27
 CHAPTER 4 IMPEDANCE ANALYSIS	 4-1
4.1 COMPLIANCE MATRIX FOR TWO-DIMENSIONAL PROBLEMS	4-1
4.2 COMPLIANCE MATRIX FOR THREE-DIMENSIONAL PROBLEMS	4-6
4.3 DIRECT METHOD OF IMPEDANCE ANALYSIS	4-10
4.4 SKIN METHOD OF IMPEDANCE ANALYSIS	4-10
4.5 IMPEDANCE ANALYSIS IN SUBTRACTION METHOD	4-14
4.6 IMPEDANCE MATRICES FOR SYMMETRIC AND ANTISYMMETRIC SYSTEMS	4-14

CHAPTER 5 PILE FOUNDATIONS.....	5-1
5.1 INTRODUCTION	5-1
5.1.1 Beam-on-Winkler-Foundation Methods	5-2
5.1.2 Continuum Methods.....	5-3
5.1.3 Finite Element Methods	5-4
5.1.4 Pile Groups	5-4
5.1.5 Modeling of Pile Foundation in SASSI	5-5
5.2 SPECIAL ELEMENTS FOR PILE GROUPS IN THREE DIMENSIONS	5-5
5.2.1 Definition of the Element.....	5-6
5.2.2 Definition and Geometry of the Inter-pile Element	5-7
5.2.3 Stiffness Matrix Formulation.....	5-13
5.2.4 Mass Matrix Formulation.....	5-22
5.2.5 Global Main and Side Soil Element Mass and Stiffness Matrices	5-22
5.2.6 Development of the Transformation Matrix [A].....	5-28
5.2.7 Modification of the Transformation Matrix	5-36
5.2.8 Mass and Stiffness Matrices of the Pile	5-36
5.3 SPECIAL ELEMENTS FOR PILE GROUPS IN TWO DIMENSIONS ...	5-40
5.3.1 Definition of the Element.....	5-40
5.3.2 Definition and Geometry of the Inter-pile Element	5-40
5.3.3 Stiffness Matrix Formulation.....	5-42
5.3.4 Mass Matrix Formulation.....	5-53
5.3.5 Global Soil Element Mass and Stiffness Matrices.....	5-53
5.4 IMPLEMENTATION AND FURTHER CAPABILITIES OF THE SPECIAL ELEMENTS	5-56
5.5 PILE IMPEDANCE METHOD	5-57
5.5.1 Introduction	5-57
5.5.2 Analytical Model for Single Piles	5-57
5.5.3 Formulation of the Axisymmetric Element.....	5-59
5.5.4 Stiffness Matrix Formulation.....	5-61
5.5.5 Mass Matrix Formulation.....	5-70
5.5.6 Improving the Bending Behavior of the Elements	5-72
5.5.7 Considerations for Pipe Piles	5-78
5.5.8 The Semi-Infinite Region.....	5-79
5.5.9 Soil-Pile-Structure Systems	5-92
5.5.10 Capabilities and Limitations of the Pile Impedance Method	5-96
5.5.11 Implementation	5-97
 CHAPTER 6 STRUCTURAL ANALYSIS.....	 6-1
6.1 MODELLING OF STRUCTURE.....	6-1
6.2 MODELLING OF EXCAVATED SOIL.....	6-2
6.3 EXTENDED NEAR FIELD ZONE	6-2
6.4 FINITE ELEMENT SIZE.....	6-3

CHAPTER 7 SOLUTION OF THE EQUATION OF MOTION	7-1
7.1 STEADY STATE RESPONSE ANALYSIS.....	7-1
7.2 TRANSIENT RESPONSE ANALYSIS	7-1
7.3 SASSI INTERPOLATION TECHNIQUE	7-4
7.4 CRITERIA FOR CHOOSING FREQUENCIES OF ANALYSIS.....	7-5
 CHAPTER 8 COMPUTER PROGRAM ORGANIZATION	 8-1
8.1 PROGRAM LAYOUT	8-1
8.2 OPERATIONAL FEATURES	8-4
8.3 CAPABILITIES AND LIMITATIONS.....	8-5
8.4 PROGRAM VALIDATION AND APPLICATION.....	8-6
 CHAPTER 9 REFERENCES.....	 9-1
 APPENDIX A COMMENT FORMS AND ERROR REPORTS	 A-1

TABLES

<u>TABLE</u>	<u>PAGE</u>
Table 5-1. Equation (3.55).....	5-38
Table 5-2. Equation (3.56).....	5-39

FIGURES

<u>FIGURE</u>	<u>PAGE</u>
Figure 2.1-1. Summary of Substructuring Methods.....	2-2
Figure 2.2-1. Substructuring in the Flexible Volume Method.....	2-6
Figure 2.3-1. Substructuring in the Substructure Subtraction Method.....	2-10
Figure 3.2-1. Degrees of Freedom: (a) Rayleigh Wave, and (b) Love Wave.....	3-4
Figure 3.2-2. Assembling Submatrices of Each Layer.....	3-5
Figure 3.3-1. Degrees of Freedom on Axisymmetric Transmitting Boundary	3-12
Figure 3.4-1. Model of Plane SV-Wave Incidence.....	3-15
Figure 3.4-2. Model of Plane SH-Wave Incidence.....	3-17
Figure 3.5-1. Simulation of Halfspace.....	3-23
Figure 3.5-2. Halfspace Simulation by Viscous Dashpots	3-25
Figure 3.6-1. Average Shear Moduli and Damping Characteristics of Soils	3-27
Figure 4.1-1. Plane-Strain Model for Impedance Analysis	4-4
Figure 4.1-2. Boundary Conditions.....	4-5
Figure 4.2-1. Axisymmetric Model for Impedance Analysis.....	4-8

Figure 4.2-2. Boundary Conditions.....	4-9
Figure 4.4-1. Foundation System for Skin Method	4-13
Figure 5.2-1. General Configuration of a Pile Group	5-6
Figure 5.2-2. Three-dimensional Inter-pile Element	5-8
Figure 5.2-3. (a) Plane View of the t-plane, (b) Pile Intersection at Node t_1	5-9
Figure 5.2-4. Special Configurations of the Inter-pile Element	5-12
Figure 5.2-5. (a) Main, (b) Side Soil Element in Global Coordinate, and (c) Soil Element in Natural Coordinate System.....	5-14
Figure 5.2-6. Degrees of Freedom of Internal and Global Nodes (Main Soil Element)	5-24
Figure 5.2-7. Degrees of Freedom of Internal and Global Nodes (Side Soil Element)	5-26
Figure 5.2-8. Pile Volume Zone, Principal Axes and Global Coordinate System.....	5-30
Figure 5.2-9. Pile Segment in Local Coordinate	5-37
Figure 5.3-1. General Shape of the Two-dimensional Inter-pile Element	5-41
Figure 5.3-2. Special Cases of the 2-D Inter-pile Element	5-43
Figure 5.3-3. Soil Element with Internal Nodes (Two-dimensional Case).....	5-45
Figure 5.3-4. Soil Element for Special Cases with Internal Nodes (Two- dimensional Case)	5-46
Figure 5.3-5. Soil Element in (a) Global, and (b) Natural Coordinate System	5-48
Figure 5.3-6. Degrees of Freedom at the Global and Internal Nodes (Two- dimensional Case)	5-54
Figure 5.5-1. Single Pile in Horizontally Layered System.....	5-58
Figure 5.5-2. (a) Element in Global Coordinate System, (b) Element in Natural Coordinate System	5-63
Figure 5.5-3. Local Degrees of Freedom for (a) Zero Harmonic, and (b) First Harmonic Case	5-65
Figure 5.5-4. Cantilever Beam	5-74
Figure 5.5-5. Comparison of the Pile ($\ell/r = 10$) with beam theory. (a) Axial Displacement; (b) Head Rotation; (c) Lateral Displacement (Free Rotation); (d) Lateral Displacement (Fixed Rotation).....	5-75
Figure 5.5-6. Comparison of the Pile ($\ell/r = 30$) with beam theory. (a) Axial Displacement; (b) Lateral Displacement (Free Rotation); (c) Head Rotation; (d) Lateral Displacement (Fixed Rotation)	5-76
Figure 5.5-7. Comparison of the Pile ($\ell/r = 60$) with beam theory. (a) Axial Displacement; (b) Lateral Displacement (Free Rotation); (c) Head Rotation; (d) Lateral Displacement (Fixed Rotation)	5-77
Figure 5.5-8. Degrees of Freedom: (a) Love Wave, and (b) Rayleigh Wave.....	5-82
Figure 5.5-9. Structure of Matrices [A], [B], [G], [M]	5-83
Figure 5.5-10. Degrees of Freedom on Transmitting Boundary	5-88
Figure 5.5-11. Substructuring for the Simplified Method	5-93

CHAPTER 1

INTRODUCTION

The computer program SASSI was developed in the University of California, Berkeley, by a research team consisting of five doctoral students under the direction of Prof. J. Lysmer. The theory and the analytical methods described in this manual are extracted from the five doctoral dissertations (Refs. 5, 13, 30, 31, 32). A brief description of the theory and the program was first published in Ref. 12. The previous version of the program (SASSI2000, Rev 1 Ostadan et. al) was published in 1999. This manual contains the basic description of the analytical methods and computational steps used in the program in support of SASSI2000 Revision 2. Complete descriptions on various parts of the theory used by the program may be obtained from the five dissertations cited.

This manual is prepared in 9 chapters. In Chapter 2, an overview of the substructuring methods of soil-structure Interaction (SSI) analysis is presented. Following this background discussion, the flexible-volume substructuring method and the subtraction method, the equations of motion, and the computational steps used by SASSI are then fully described.

Chapter 3 presents the theory and techniques used by SASSI to solve the site response problem. The models along with the equations of motion used to solve for the body and surface waves are described. Formulation of the transmitting boundary matrices for two dimensional and axisymmetric problems, the techniques for halfspace simulation and the methods for incorporating the dynamic soil properties are also presented.

In Chapter 4, the method used by SASSI to solve the impedance problem is presented. This includes descriptions of the analytical models used for computing the impedance matrix for two- and three-dimensional problems.

Chapter 5 presents the methods for analysis of pile foundations. These methods include special inter-pile elements and a method for computing the impedance functions for pile foundations.

Chapter 6 describes the techniques for modeling the superstructure and basement in accordance with the flexible-volume and subtraction substructuring techniques. The analysis technique used by SASSI to obtain the steady state and transient dynamic response are described in Chapter 7, including the interpolation technique used in calculating the response transfer functions.

Finally, Chapter 8 presents the SASSI computer program layout and operational features. It also presents a brief summary of program validation and the example applications of the program to practical engineering problems.

References are cited in Chapter 9.

Appendix A includes comment forms and error reports.

CHAPTER 2

SUBSTRUCTURING METHODS OF SASSI

2.1 SUBSTRUCTURING METHODS OF SSI ANALYSIS

The soil-structure interaction problem is most conveniently analyzed using a substructuring approach. In this approach, the linear soil-structure interaction problem is subdivided into a series of simpler sub-problems. Each sub-problem is solved separately and the results are combined in the final step of the analysis to provide the complete solution using the principle of superposition.

For the case of structures with surface foundations for which the structure and the foundation interface boundary is on the surface of the foundation medium, the substructuring method is relatively simple and many solution techniques are available. For structures with embedded foundations, the substructuring method becomes considerably more complicated. Conceptually, these methods can be classified into four types depending on how the interaction at the soil and structure interface degrees-of-freedom is handled (Refs. 5 and 11). These four types are: 1) the rigid boundary method, 2) the flexible boundary methods, 3) the flexible volume method, and 4) the substructure subtraction method. The seismic SSI sub-problems that these four types of substructuring methods are required to solve to obtain the final solution are compared in Fig. 2.1-1. As shown in this figure, the solution for the site response problem is required by all four methods. This is, therefore, common to all methods. The analysis of the structural response problem is also required and involves essentially the same effort for all methods. The necessity and effort required for solving the scattering and impedance problems, however, differ significantly among the different methods. For the rigid-boundary and the flexible-boundary methods, two explicit analyses are required separately for solving the scattering and impedance problems. On the other hand, the flexible volume method and the substructure subtraction method, because of the unique substructuring technique (see Sections 2.2 and 2.3), require only one impedance analysis and the scattering analysis is eliminated. Furthermore, the substructuring in the subtraction method often requires a much smaller impedance analysis than the flexible

volume method. The SASSI computer program adopts both the flexible volume method and the substructure subtraction method of substructuring.

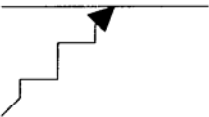
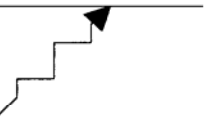
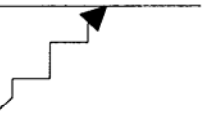
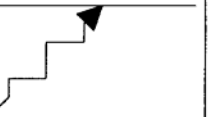
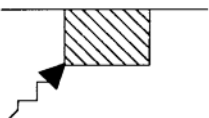
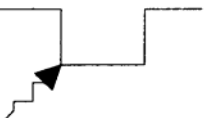
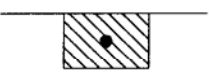

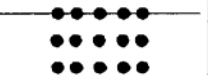

Method Analysis	Rigid Boundary	Flexible Boundary	Flexible Volume	Subtraction
Site Response Analysis (a)				
Scattering Analysis (b)			None	None
Impedance Analysis (c)				
Structural Response Analysis (d)	Standard	Standard +	Standard +	Standard +

Figure 2.1-1. Summary of Substructuring Methods

2.2 THE FLEXIBLE VOLUME METHOD

The flexible volume substructuring method is based on the concept of partitioning the total soil-structure system as shown in Fig. 2.2-1a into three substructure systems as shown in Figs. 2.2-1b, 2.2-1c and 2.2-1d. The substructure I consists of the free-field site, the substructure II consists of the excavated soil volume, and the substructure III consists of the structure, of which the foundation replaces the excavated soil volume. The substructures I, II and III, when combined together, form the original SSI system shown in Fig. 2.2-1a. The flexible volume method presumes that the free-field site and the excavated soil volume interact both at the boundary of the excavated soil volume and within its body, in addition to interaction between the substructures at the boundary of the foundation of the structure. The theory and formulation that develop in the following sections are equally applicable to two- and three-dimensional SSI problems.

The equations of motion for the SSI substructures shown in Figs. 2.2-1b, 2.2-1c and 2.2-1d can be written in the following matrix form:

$$[M] \left\{ \hat{U} \right\} + [K] \left\{ \hat{U} \right\} = \left\{ \hat{Q} \right\} \quad (2.2-1)$$

where $[M]$ and $[K]$ are the total mass and stiffness matrices, respectively. $\left\{ \hat{U} \right\}$ is the vector of total nodal point displacements and $\left\{ \hat{Q} \right\}$ are the forces due to applied external dynamic forces or seismic excitations.

For the harmonic excitation at frequency ω , the load and the displacement vectors can be written as

$$\left\{ \hat{Q} \right\} = \left\{ Q \right\} \exp(i\omega t) \quad (2.2-2)$$

and

$$\{\hat{U}\} = \{U\} \exp(i\omega t) \quad (2.2-3)$$

where $\{Q\}$ and $\{U\}$ are the complex force and displacement vectors at frequency ω .

Hence, for each frequency, the equations of motion take the form

$$[C] \{U\} = \{Q\} \quad (2.2-4)$$

where $[C]$ is a complex frequency-dependent dynamic stiffness matrix:

$$[C] = [K] - \omega^2 [M] \quad (2.2-5)$$

Using the following subscripts, which refer to degrees of freedom associated with different nodes (see Fig. 2.2-1):

<u>Subscript</u>	<u>Nodes</u>
b	the boundary of the total system
i	at the boundary between the soil and the structure
w	within the excavated soil volume
g	at the remaining part of the free-field site
s	at the remaining part of the structure
f	combination of i and w nodes

The equation of motion for the system is partitioned as follows:

$$\begin{bmatrix} C_{ii}^{III} - C_{ii}^{II} + X_{ii} & -C_{iw}^{II} + X_{iw} & C_{is}^{III} \\ -C_{wi}^{II} + X_{wi} & -C_{ww}^{II} + X_{ww} & 0 \\ C_{si}^{III} & 0 & C_{ss}^{III} \end{bmatrix} \begin{Bmatrix} U_i \\ U_w \\ U_s \end{Bmatrix} = \begin{Bmatrix} X_{ii} U_i' + X_{iw} U_w' \\ X_{wi} U_i' + X_{ww} U_w' \\ 0 \end{Bmatrix} \quad (2.2-6)$$

where superscripts, I, II and III, refer to the three substructures. The complex frequency-dependent dynamic stiffness matrix on the left of Eq. (2.2-6) simply indicate the stated partitioning according to which the stiffness and mass of the excavated soil volume are

subtracted from the dynamic stiffness of the free-field site and the structure. The frequency-dependent matrix, $\begin{bmatrix} X_{ii} & X_{iw} \\ X_{wi} & X_{ww} \end{bmatrix}$ or $\begin{bmatrix} X_{ff} \end{bmatrix}$, is called the impedance matrix, which is obtained from the model in substructure I using the methods which will be described in Chapter 4. The vector, $\begin{Bmatrix} U'_i \\ U'_w \end{Bmatrix}$ or $\begin{Bmatrix} U'_f \end{Bmatrix}$, computed from the free-field motion for the interacting nodes shown in substructure I. The motion is a function of prescribed wave field in the free-field. The methods for solving the site response problem for body and surface waves are described in Chapter 3. Degrees of freedom associated with nodes i and w are considered interacting and included in the impedance analysis and in the load vector in Eq. (2.2-6).

If the source of excitation is applied dynamic loading within the model, as in the case of foundation vibrations, impact loads, and wind loads, the free-field motions $\begin{Bmatrix} U'_i \\ U'_w \end{Bmatrix}$ vanish and Eq. (2.2-6) can be written as

$$\begin{bmatrix} C_{ii}^{III} - C_{ii}^{II} + X_{ii} & -C_{iw}^{II} + X_{iw} & C_{is}^{III} \\ -C_{wi}^{II} + X_{wi} & -C_{ww}^{II} + X_{ww} & 0 \\ C_{si}^{III} & 0 & C_{ss}^{III} \end{bmatrix} \begin{Bmatrix} U_i \\ U_w \\ U_s \end{Bmatrix} = \begin{Bmatrix} P_i \\ 0 \\ P_s \end{Bmatrix} \quad (2.2-7)$$

where the load vector has non-zero terms only where external loads are applied.

Seismic and external loads can, in principle, be considered together by simply adding the external loads $\{P\}$ to the load vector in Eq. (2.2-6). This method is not used in SASSI, since in practice, the seismic excitations and the external loads are seldom considered simultaneously.

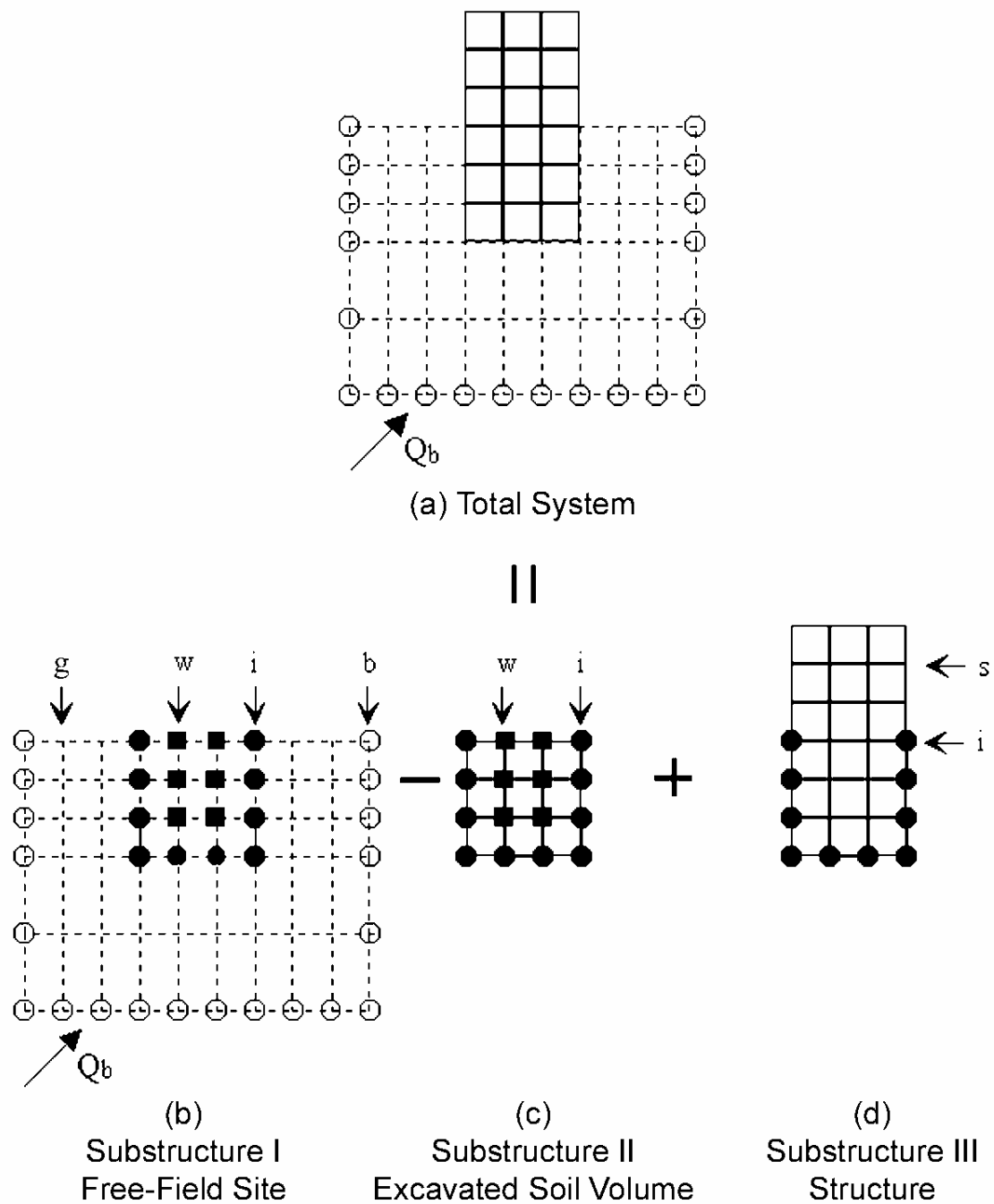


Figure 2.2-1. Substructuring in the Flexible Volume Method

2.3 THE SUBSTRUCTURE SUBTRACTION METHOD

The substructure subtraction method is basically based on the same substructuring concept as the flexible volume method. The subtraction method partitions the total soil-structure system as shown in Fig. 2.3-1a into three substructure systems as shown in Figs. 2.3-1b, 2.3-1c and 2.3-1d. The substructure I consists of the free-field site, the substructure II consists of the excavated soil volume, and the substructure III consists of the structure. The substructures I, II and III, when combined together, form the original SSI system shown in Fig. 2.3-1a. However, the subtraction method recognizes that soil-structure interaction occurs only at the common boundary of the substructures, that is, at the boundary of the foundation of the structure. This often leads to a smaller impedance analysis than the flexible volume method. The theory and formulation that develop in the following sections are equally applicable to two- and three-dimensional SSI problems.

The equations of motion for the SSI substructures shown in Figs. 2.3-1b, 2.3-1c and 2.3-1d can be written in the following matrix form as in the flexible volume method:

$$[M] \left\{ \hat{U} \right\} + [K] \left\{ \hat{U} \right\} = \left\{ \hat{Q} \right\} \quad (2.3-1)$$

where $[M]$ and $[K]$ are the total mass and stiffness matrices, respectively. $\left\{ \hat{U} \right\}$ is the vector of total nodal point displacements and $\left\{ \hat{Q} \right\}$ are the forces due to applied external dynamic forces or seismic excitations.

For the harmonic excitation at frequency ω , the equations of motion can take the form as discussed in Section 2.2:

$$[C] \{U\} = \{Q\} \quad (2.3-2)$$

where $\{Q\}$, $\{U\}$ and $[C]$ are the complex force vector, the complex displacement vector and the complex frequency-dependent dynamic stiffness matrix, respectively.

Use the same subscripts as in the flexible volume method to refer to degrees of freedom associated with different nodes (see Fig. 2.3-1):

<u>Subscript</u>	<u>Nodes</u>
b	the boundary of the total system
i	at the boundary between the ground and the structure
w	within the excavated soil volume
g	at the remaining part of the free-field site
s	at the remaining part of the structure
f	same as i nodes

The equation of motion for the system is partitioned as follows in the subtraction method:

$$\begin{bmatrix} C_{ii}^{III} - C_{ii}^{II} + X_{ii} & -C_{iw}^{II} & C_{is}^{III} \\ -C_{wi}^{II} & -C_{ww}^{II} & 0 \\ C_{si}^{III} & 0 & C_{ss}^{III} \end{bmatrix} \begin{Bmatrix} U_i \\ U_w \\ U_s \end{Bmatrix} = \begin{Bmatrix} X_{ii} U'_i \\ 0 \\ 0 \end{Bmatrix} \quad (2.3-3)$$

where superscripts, I, II and III, refer to the three substructures. The complex frequency-dependent dynamic stiffness matrix on the left of Eq. (2.3-3) indicates the stated partitioning according to which the stiffness and mass of the excavated soil are subtracted from the dynamic stiffness of the free-field site and the structure. Compared to Eq. (2.2-6) in Section 2.2 for the flexible volume method, this complex dynamic stiffness is much simpler because only the degrees of freedom associated with nodes i are considered interacting. This also leads to an impedance analysis involving less number of degrees of freedom and therefore a smaller impedance matrix, $\begin{bmatrix} X_{ii} \end{bmatrix}$ or

$\begin{bmatrix} X_{ff} \end{bmatrix}$, which will be described in Chapter 4. For the same reason, only the free-field

motions at the degrees of freedom associated with nodes i, $\{U'_i\}$ or $\{U'_f\}$, computed

from the site response analysis are part of the load vector in Eq. (2.3-3). The methods

for solving the site response problem for body and surface waves are described in Chapter 3.

If the source of excitation is applied dynamic loading within the model, as in the case of foundation vibrations, impact loads, and wind loads, the free-field motions $\{U_i'\}$ vanish and Eq. (2.3-3) can be written as

$$\begin{bmatrix} C_{ii}^{III} - C_{ii}^{II} + X_{ii} & -C_{iw}^{II} & C_{is}^{III} \\ -C_{wi}^{II} & -C_{ww}^{II} & 0 \\ C_{si}^{III} & 0 & C_{ss}^{III} \end{bmatrix} \begin{Bmatrix} U_i \\ U_w \\ U_s \end{Bmatrix} = \begin{Bmatrix} P_i \\ 0 \\ P_s \end{Bmatrix} \quad (2.3-4)$$

where the load vector has non-zero terms only where external loads are applied.

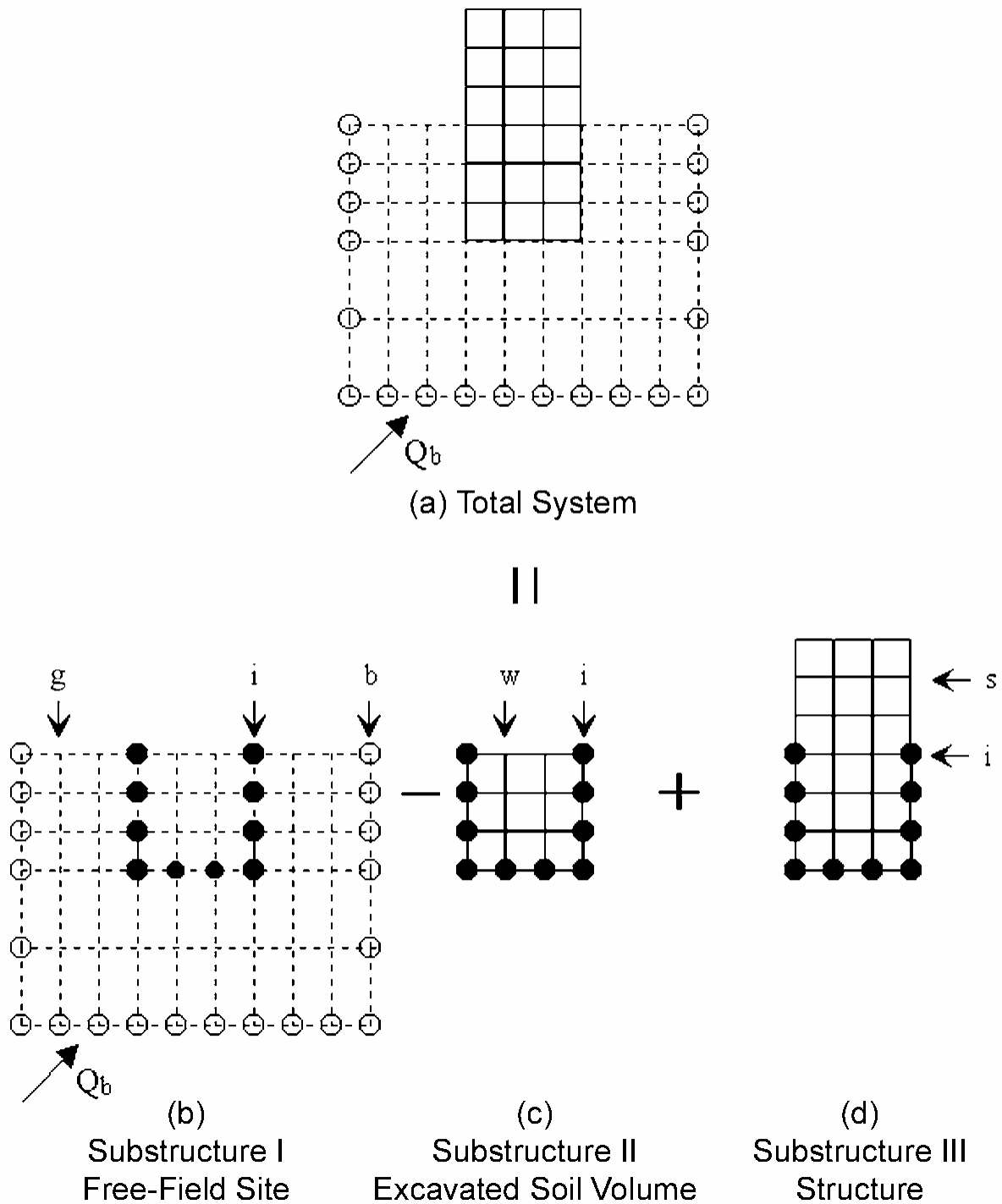


Figure 2.3-1. Substructuring in the Substructure Subtraction Method

2.4 COMPUTATIONAL STEPS

Based on the formulation presented previously, a soil-structure interaction problem with the seismic or external force excitation can be solved in the frequency domain according to the following five main steps:

1. Solve the site response problem. For the seismic excitation, this step involves determining the free-field displacement amplitudes $\{U'_f\}$ only for the interacting nodes of the free-field site. That is $\begin{Bmatrix} U'_i \\ U'_w \end{Bmatrix}$ in the flexible volume method shown in Fig. 2.2-1 or $\{U'_i\}$ in the subtraction method. For each frequency of analysis, the free-field displacement vector is a function of specified wave field (body or surface wave and incidence angle) and location of control point in the free-field soil system. Methods used for site response analysis are described in Chapter 3. The free-field displacement need not be computed for SSI problems subjected to external force excitation (see Eqs. (2.2-7) and (2.3-4)).
2. Solve the impedance problem. This step involves determining the impedance matrix $[X_{ff}]$ which is a complex stiffness matrix corresponding to interacting nodes in free-field soil medium. That is $\begin{bmatrix} X_{ii} & X_{iw} \\ X_{wi} & X_{ww} \end{bmatrix}$ in the flexible volume method and $[X_{ii}]$ in the substructure subtraction method. Methods used for impedance analysis are described in Chapter 4.
3. Form the load vector. For the seismic excitation, the load vector in Eq. (2.2-6) for the flexible volume method and in Eq. (2.3-3) for the subtraction method can be obtained from the solutions of Steps 1 and 2 in accordance with Eqs. (2.2-6) and (2.3-3), respectively. For the external force excitation, this step simply consists of forming the load vector in accordance with Eq. (2.2-7) for the flexible volume method or Eq. (2.3-4) for the subtraction method.

4. Form the complex stiffness matrix. This step, which is identical for the seismic or external force excitation involves forming the coefficient matrix in Eq. (2.2-6) or (2.2-7) for the flexible volume method, or in Eq. (2.3-3) or (2.3-4) for the subtraction method. The method used for computing the mass and stiffness matrices used in the coefficient matrix is described in Section 5.
5. Solve the system of linear equations of motion, Eq. (2.2-6) or (2.2-7) for the flexible volume method or Eq. (2.3-3) or (2.3-4) for substructure subtraction method. The methods used to compute the steady state response and transient responses are described in Chapter 6.

The flexible volume method and the substructure subtraction method described above have been extended to handle the SSI problems involving pile foundations. The methods used to model and analyze pile foundations are described in Chapter 5.

CHAPTER 3

SITE RESPONSE ANALYSIS

For seismic excitation, as shown in the equation of motion in Eqs. (2.2-6) and (2.3-3) the free-field motion at interacting nodes, $\{U_f'\}$, must be computed. For this computation, substructure (b) in Fig. 2.2 or Fig. 2.3 is used and the free-field motion is assumed to result from a combination of coherent plane wave fields which may include P-, SV-, and SH-body waves or Rayleigh and Love surface waves. The following sections describe the analytical model and the analysis methods used to solve the site response problem. The techniques used to simulate the halfspace boundary condition at base and to characterize the dynamic soil properties in the formulation are also presented.

3.1 SITE RESPONSE ANALYSIS MODEL

The original site before the soil excavation to accommodate the structure is assumed to consist of horizontal soil layers overlying either a rigid base or an elastic halfspace using the techniques to simulate the halfspace boundary condition at the base as described in Section 3.5. The soil material properties for the soil layer system are assumed to be viscoelastic with the complex modulus representation of the stiffness and damping properties of the soil layers. However, the stiffness and damping of each layer may be adjusted using the equivalent linear method to consider the strain-dependency of the properties, as will be described in Sections 3.6 and 3.7.

To solve the site response problem for surface waves, it is necessary to form and solve the eigenvalue problem for the site model. Furthermore, the submatrices computed from the properties of each layer to form the eigen equations are also used for body wave calculation. For these reasons, the eigenvalue problem for the site model is discussed first.

3.2 EIGENVALUE PROBLEM FOR SITE MODEL

Based on the horizontally layered site model described above and the assumption of linear variations of displacement within each layer, Waas (Ref. 33) formulated the eigenvalue problem for the system in the frequency domain. The eigenvalue problem can be subdivided into two uncoupled algebraic eigenvalue problems, one for generalized Rayleigh wave motion and another for generalized Love wave motions. A brief description of these two eigenequations, which are in effect a reduced form of the equation of motion for the site model, is presented as follows.

3.2.1 EIGENVALUE PROBLEM FOR GENERALIZED RAYLEIGH WAVE MOTION

Using the discretized soil model shown in Fig. 3.2-1(a), the eigenequation for generalized Rayleigh wave motion may be written as

$$([A]k^2 + i[B]k + [G] - \omega^2[M])\{V\} = 0 \quad (3.2-1)$$

In this model, there are 2 degrees-of-freedom associated with each layer interface, with a total of $2n$ degrees-of-freedom for an n layer system. In the above equation, ω is the circular frequency, which is the frequency at which the model is excited; k is the eigenvalue known as the wave number; and $\{V\}$ is the associated eigenvector with $2n$ components. The matrices $[A]$, $[B]$, $[G]$, and $[M]$ are of order $2n \times 2n$ and are assembled from submatrices for the soil layers according to the scheme shown in Fig. 3.2-2. Each submatrix corresponds to a soil layer. Denoting the thickness of the j^{th} layer from the top by h_j , the mass density by ρ_j , the shear modulus by G_j , and the Lamé's constant by λ_j , these layer submatrices are:

$$[A_j] = \frac{h_j}{6} \begin{bmatrix} 2(\lambda_j + 2G_j) & 0 & (\lambda_j + 2G_j) & 0 \\ 0 & 2G_j & 0 & G_j \\ (\lambda_j + 2G_j) & 0 & 2(\lambda_j + 2G_j) & 0 \\ 0 & G_j & 0 & 2G_j \end{bmatrix} \quad (3.2-2)$$

$$[B_j] = 1/2 \begin{bmatrix} 0 & -(\lambda_j - G_j) & 0 & (\lambda_j + G_j) \\ (\lambda_j - G_j) & 0 & (\lambda_j + G_j) & 0 \\ 0 & -(\lambda_j + G_j) & 0 & (\lambda_j - G_j) \\ -(\lambda_j + G_j) & 0 & -(\lambda_j - G_j) & 0 \end{bmatrix} \quad (3.2-3)$$

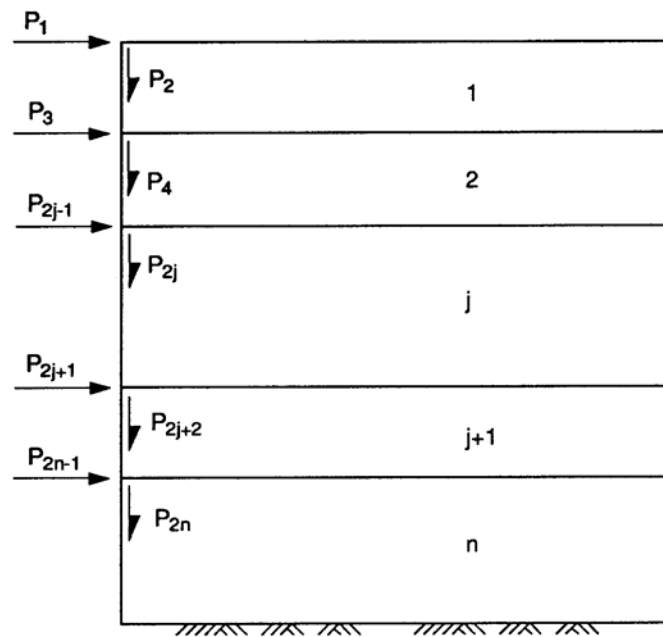
$$[G_j] = \frac{1}{h_j} \begin{bmatrix} G_j & 0 & -G_j & 0 \\ 0 & (\lambda_j + 2G_j) & 0 & -(\lambda_j + 2G_j) \\ -G_j & 0 & G_j & 0 \\ 0 & -(\lambda_j + 2G_j) & 0 & (\lambda_j + 2G_j) \end{bmatrix} \quad (3.2-4)$$

$$[M_j]^{(c)} = \frac{\rho_j h_j}{6} \begin{bmatrix} 2 & 0 & 1 & 0 \\ 0 & 2 & 0 & 1 \\ 1 & 0 & 2 & 0 \\ 0 & 1 & 0 & 2 \end{bmatrix} \quad (3.2-5a)$$

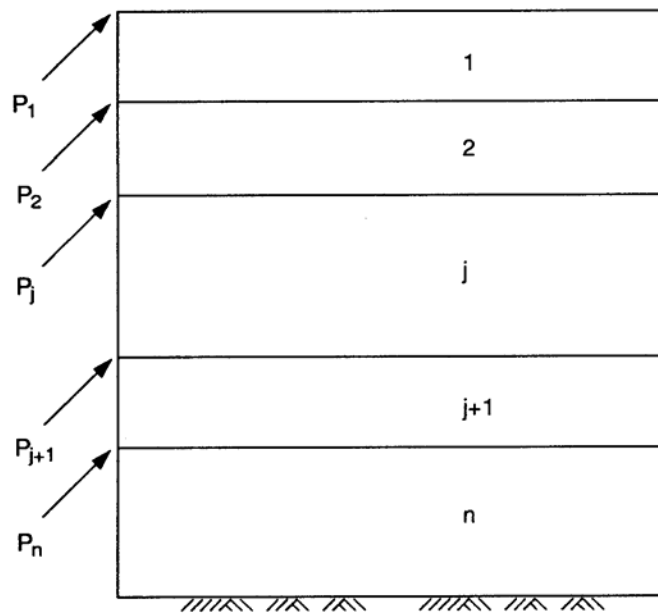
$$[M_j]^{(\ell)} = \frac{\rho_j h_j}{2} \begin{bmatrix} 1 & 0 & 0 & 0 \\ 0 & 1 & 0 & 0 \\ 0 & 0 & 1 & 0 \\ 0 & 0 & 0 & 1 \end{bmatrix} \quad (3.2-5b)$$

The matrices $[M_j]^{(c)}$ and $[M_j]^{(\ell)}$ are the consistent and lump mass matrices, respectively. The mass matrix used in Eq. (3.2-1) is a combination of one-half lump mass matrix and one-half consistent mass matrix (see Section 5.4 for further description). Using the numerical techniques developed by Waas (Ref. 33), the eigenvalue in Eq. (3.2-1) can be solved. The solution yields $2n$ Rayleigh modes and $2n$ wave numbers, which will be

used in computing the transmitting boundary condition for the wave motions moving in the plane of the site model.



(a)



(b)

Figure 3.2–1. Degrees of Freedom: (a) Rayleigh Wave, and (b) Love Wave

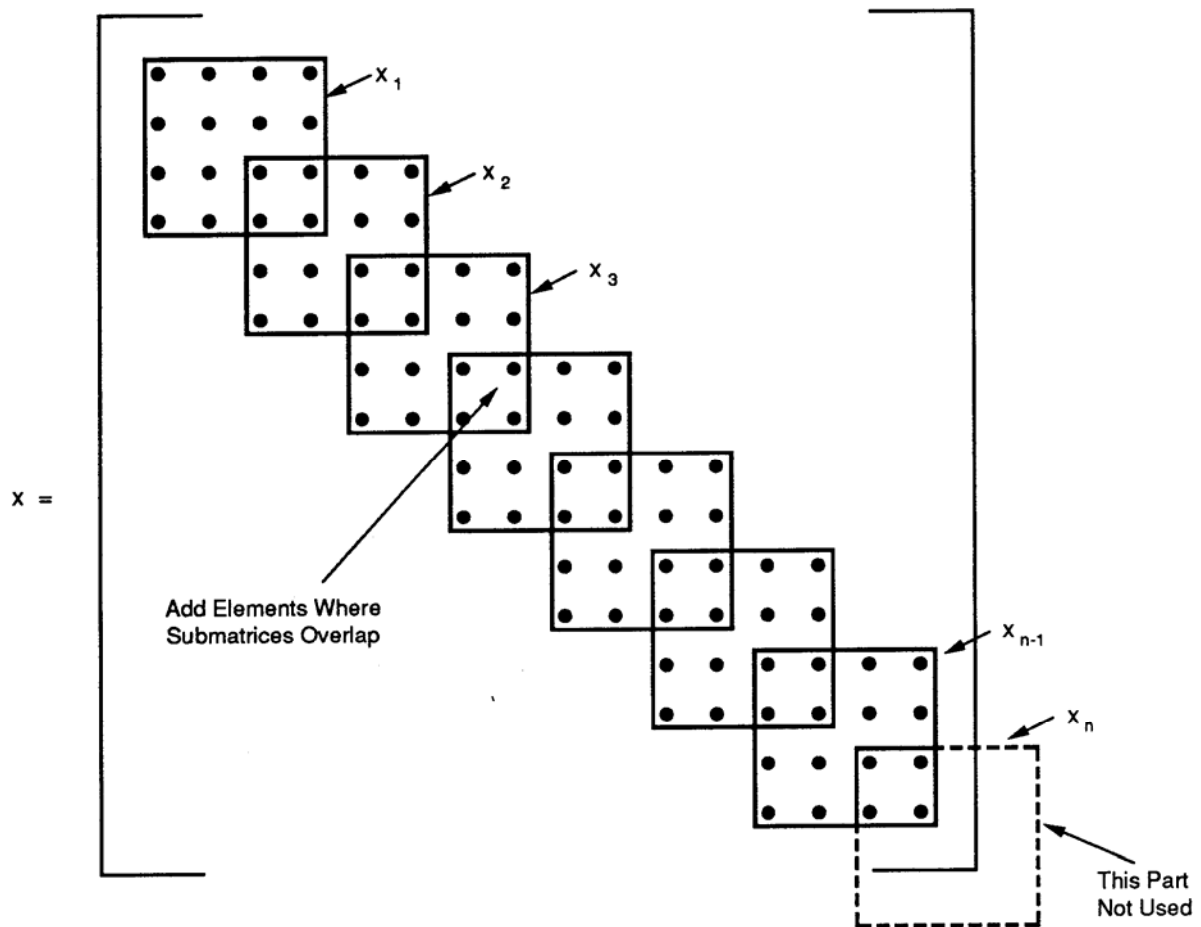


Figure 3.2–2. Assembling Submatrices of Each Layer

3.2.2 EIGENVALUE PROBLEM FOR GENERALIZED LOVE WAVE MOTION

Based on the n horizontally layered soil model shown in Fig. 3.2-1(b), the eigenvalue problem for generalized Love wave motion may be written in the form

$$([A]k^2 + [G] - \omega^2[M]) \{V\} = 0 \quad (3.2-6)$$

In this wave mode, only one degree-of-freedom associated with each layer interface is required. The matrices [A], [B], [G], and [M] in Eq. (3.2-6) are assembled in a similar manner from the 2 x 2 layer submatrices defined below.

$$[A_j] = h_j G_j \begin{bmatrix} 1/3 & 1/6 \\ 1/6 & 1/3 \end{bmatrix} \quad (3.2-7)$$

$$[G_j] = \frac{G_j}{h_j} \begin{bmatrix} 1 & -1 \\ -1 & 1 \end{bmatrix} \quad (3.2-8)$$

$$[M_j]^{(c)} = \frac{\rho_j h_j}{6} \begin{bmatrix} 2 & 1 \\ 1 & 2 \end{bmatrix} \quad (3.2-9a)$$

$$[M_j]^{(\ell)} = \frac{\rho_j h_j}{2} \begin{bmatrix} 1 & 0 \\ 0 & 1 \end{bmatrix} \quad (3.2-9b)$$

The mass matrix used in Eq. (3.2-6) is similarly a combination of one-half lump mass matrix and one-half consistent mass matrix. The solution of the eigenequation of Eq. (3.2-6) yields n Love wave mode shapes with the associated wave numbers which will be used in computing the transmitting boundary condition for the wave motions moving out of the plane of the site model.

3.3 TRANSMITTING BOUNDARY MATRICES

Transmitting boundaries are formulated by using exact analytical solution in the horizontal direction and a displacement function consistent with the finite element representation in the vertical direction. These boundaries accurately transmit energy in horizontal directions. Development of these boundaries is central to the development of the impedance matrix which is presented in Chapter 4. Formulation of these boundary matrices for two-dimensional and axisymmetric problems is separately described in the following subsections.

3.3.1 TRANSMITTING BOUNDARY MATRIX FOR TWO-DIMENSIONAL PROBLEMS

Using the eigenvalues and eigenvectors obtained for the generalized Rayleigh wave motion, and using the stress-strain relationship in each layer, Waas (Ref. 33) formulated the force-displacement relationship in the frequency domain for the layered system as follows:

$$\{P\} = [R] \{U\} \quad (3.3-1)$$

where $\{U\}$ is the vector of $2n$ displacement and $\{P\}$ are the associated forces and $[R]$ is the dynamic stiffness of the semi-infinite layered region that can be obtained from

$$[R] = i[A] [V] [K] [V]^{-1} + [D] \quad (3.3-2)$$

In the above equation all matrices are of order $2n \times 2n$, matrix $[A]$ is defined in Section 3.2.1, matrix $[V]$ is the matrix containing all $2n$ mode shapes, matrix $[K]$ is the diagonal matrix containing the wave numbers (eigenvalues) of the generalized Rayleigh wave motion, and matrix $[D]$ is assembled from the properties of each layer in the same manner as that described in Section 3.2.1. The matrix for the j^{th} layer can be written as:

$$[D_j] = \frac{1}{2} \begin{bmatrix} 0 & \lambda_j & 0 & -\lambda_j \\ G_j & 0 & -G_j & 0 \\ 0 & \lambda_j & 0 & -\lambda_j \\ G_j & 0 & -G_j & 0 \end{bmatrix} \quad (3.3-3)$$

where G_j and λ_j are the shear modulus and Lamé's constant as defined previously in Section 3.2. Matrix $[R]$ is a symmetric full matrix and will be used in Section 4.1 for computation of the compliance matrix to solve for the impedance problem.

3.3.2 TRANSMITTING BOUNDARY MATRIX FOR AXISYMMETRIC PROBLEMS

Using the generalized Rayleigh and Love waves eigen solutions described in Sections 3.2.1 and 3.2.2 and the Fourier expansion techniques, the force-displacement relationship for the axisymmetric soil model shown in Fig. 3.3-1 may be written in the form:

$$\{P\}_m = [R]_m \{U\}_m \quad (3.3-4)$$

where vectors $\{P\}_m$ and $\{U\}_m$ are the force and associated displacement shown in Fig. 3.3-1 of the order $3n \times 1$ and matrix $[R]$ is the $3n \times 3n$ axisymmetric dynamic stiffness of the layered system. The subscript m refers to the order of the Fourier expansion. The dynamic stiffness matrix $[R]$ can be obtained using the relation

$$[R]_m = r_o \left\{ \begin{aligned} & [A][\psi]_m [K^2] + ([D] - [E] + m[N])(\phi)_m [K] \\ & - m \left(\frac{m+1}{m} [L] + [Q] \right) [\psi]_m \end{aligned} \right\} [W(r_o)]^{-1} \quad (3.3-5)$$

where r_o is the radial distance from the central axis to the transmitting boundary. The matrices $[K]$ and $[K^2]$ are simple diagonal matrices which contain the wave numbers k_s and k_s^2 , respectively, on their diagonals in the same order as the columns of $[W(r_o)]$. The wave numbers are obtained from the eigenvalues of the site model as shown in Eqs. (3.2-1) and (3.2-6). The $3n \times 3n$ matrix $[W(r_o)]_m$ has the general elements

$$w_{is} = \begin{cases} H'_m(k_s r_o) v_{is} + \frac{m}{r_o} H_m(k_s r_o) v_{i+2s} & \text{for } i = 1, 4, \dots, 3n - 2 \\ H_m(k_s r_o) k_s v_{is} & \text{for } i = 2, 5, \dots, 3n - 1 \\ \frac{m}{r} H_m[k_s r_o] v_{i-2s} + H'_m(k_s r_o) v_{is} & \text{for } i = 3, 6, \dots, 3n \end{cases} \quad (3.3-6)$$

where v_{is} is the i^{th} component of mode shape s , H_m is the Hankel function of order m of the second kind, and H'_m is the derivative of this function.

The matrices $[A]$, $[D]$, $[E]$, $[N]$, $[L]$, and $[Q]$ are assembled from submatrices of the soil layers according to the scheme shown in Fig. 3.2-2. The submatrices for the j^{th} soil layer are defined as follows:

$$[A_j] = \frac{h_j}{6} \begin{bmatrix} 2(\lambda_j + 2G_j) & 0 & 0 & (\lambda_j + 2G_j) & 0 & 0 \\ 0 & 2G_j & 0 & 0 & G_j & 0 \\ 0 & 0 & 2G_j & 0 & 0 & G_j \\ 2(\lambda_j + 2G_j) & 0 & 0 & (\lambda_j + 2G_j) & 0 & 0 \\ 0 & G_j & 0 & 0 & 2G_j & 0 \\ 0 & 0 & G_j & 0 & 0 & 2G_j \end{bmatrix} \quad (3.2-7)$$

which is related to the matrix defined by Eq. (3.2-2).

$$[D_j] = 1/2 \begin{bmatrix} 0 & \lambda_j & 0 & 0 & -\lambda_j & 0 \\ -G_j & 0 & 0 & G_j & 0 & 0 \\ 0 & 0 & 0 & 0 & 0 & 0 \\ 0 & \lambda_j & 0 & 0 & -\lambda_j & 0 \\ -G_j & 0 & 0 & G_j & 0 & 0 \\ 0 & 0 & 0 & 0 & 0 & 0 \end{bmatrix} \quad (3.3-8)$$

$$[E_j] = \frac{G_j h_j}{3r_o} \begin{bmatrix} 2 & 0 & 0 & 1 & 0 & 0 \\ 0 & 0 & 0 & 0 & 0 & 0 \\ 0 & 0 & 2 & 0 & 0 & 1 \\ 1 & 0 & 0 & 2 & 0 & 0 \\ 0 & 0 & 0 & 0 & 0 & 0 \\ 0 & 0 & 1 & 0 & 0 & 2 \end{bmatrix} \quad (3.3-9)$$

$$[N_j] = \frac{G_j h_j}{6r_o} \begin{bmatrix} 0 & 0 & 4 & 0 & 0 & 2 \\ 0 & 2 & 0 & 0 & 1 & 0 \\ 4 & 0 & 0 & 2 & 0 & 0 \\ 0 & 0 & 2 & 0 & 0 & 4 \\ 0 & 1 & 0 & 0 & 2 & 0 \\ 2 & 0 & 0 & 4 & 0 & 2 \end{bmatrix} \quad (3.3-10)$$

$$[L_j] = \frac{2}{3} \frac{G_j h_j}{r_o^2} \begin{bmatrix} 2 & 0 & -2 & 1 & 0 & 2 \\ 0 & 0 & 0 & 0 & 1 & 0 \\ -2 & 0 & 2 & -1 & 0 & 1 \\ 1 & 0 & -1 & 2 & 0 & -2 \\ 0 & 0 & 0 & 0 & 0 & 0 \\ -1 & 0 & 1 & -2 & 0 & 2 \end{bmatrix} \quad (3.3-11)$$

$$[Q_j] = \frac{G_j}{2r_o} \begin{bmatrix} 0 & 0 & 0 & 0 & 0 & 0 \\ 1 & 0 & -1 & -1 & 0 & 1 \\ 0 & 0 & 0 & 0 & 0 & 0 \\ 0 & 0 & 0 & 0 & 0 & 0 \\ 1 & 0 & -1 & -1 & 0 & 1 \\ 0 & 0 & 0 & 0 & 0 & 0 \end{bmatrix} \quad (3.3-12)$$

The $3n \times 3n$ matrices $[\psi]_m$ and $[\phi]_m$ are related to the mode shape vectors $\{V\}_s$. They have the elements:

$$\psi_{is} = \begin{cases} H_m(k_s r_o) v_{is} & , \text{ for } i = 1, 4, \dots, 3n - 2 \\ -H_{m-1}(k_s r_o) v_{is} & , \text{ for } i = 2, 5, \dots, 3n - 1 \\ H_m(k_s r_o) v_{is} & , \text{ for } i = 3, 6, \dots, 3n \end{cases} \quad (3.3-13)$$

$$\phi_{is} = \begin{cases} H_m(k_s r_o) v_{is} & , \text{ for } i = 1, 4, \dots, 3n - 2 \\ -H_{m-1}(k_s r_o) v_{is} & , \text{ for } i = 2, 5, \dots, 3n - 1 \\ H_m(k_s r_o) v_{is} & , \text{ for } i = 3, 6, \dots, 3n \end{cases} \quad (3.3-14)$$

The axisymmetric transmitting boundary matrix, $[R]_m$, is used in Section 4.2 for computation of the compliance matrix for three-dimensional problems.

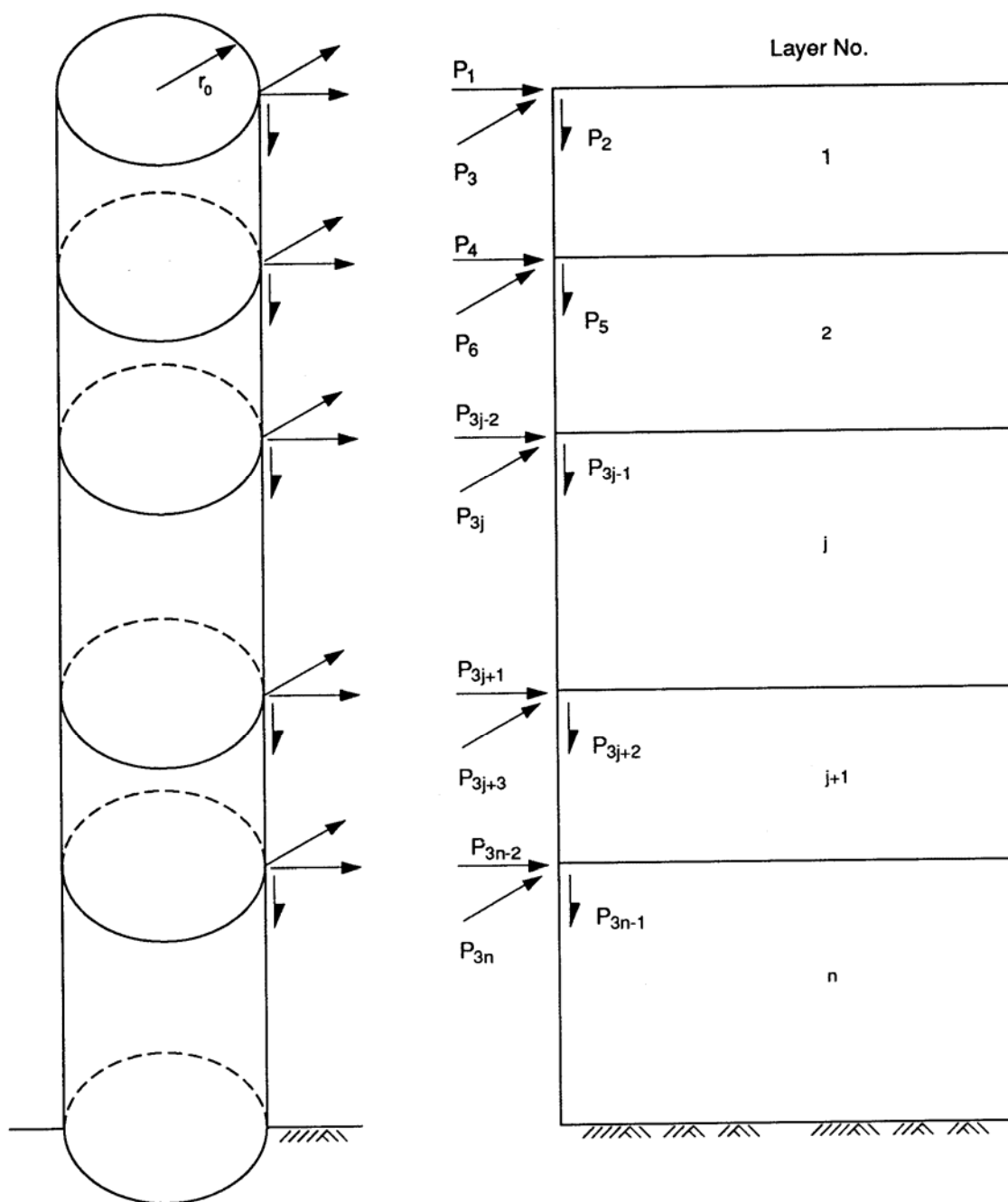


Figure 3.3-1. Degrees of Freedom on Axisymmetric Transmitting Boundary

3.4 FREE-FIELD MOTION

Using the site response model, the techniques used for computing the site response for inclined body waves and surface waves are described.

3.4.1 INCLINED SV- AND P-WAVES

Using the n layer soil system shown in Fig. 3.4-1, Chen (Ref. 4) formulated the equation of motion for incident SV- and P-waves. Note that only the case of incident SV-wave is shown in this figure. The techniques, however, is applicable to both SV- and P-waves. The equation of motion to the soil system subjected to inclined P- and/or SV-wave can be written in the form:

$$([A]k^2 + [\bar{B}]k + [G] - \omega^2[M]) \{U\} = \begin{Bmatrix} 0 \\ P_b \end{Bmatrix} \quad (3.4-1)$$

The matrices [A], [G], and [M] are assembled from the submatrices [A_j], [G_j], and [M_j] defined in Eqs. (3.2-2), (3.2-4), (3.2-5a), and (3.2-5b) following the scheme shown in Fig.

3.2-2. The matrix [B] is assembled from submatrices $\begin{bmatrix} \bar{B}_j \end{bmatrix}$ defined by:

$$[\bar{B}_j] = 1/2 \begin{bmatrix} 0 & (3G_j - M_j) & 0 & -(G_j - M_j) \\ (3G_j - M_j) & 0 & (G_j - M_j) & 0 \\ 0 & (G_j - M_j) & 0 & (G_j - M_j) \\ -(G_j - M_j) & 0 & (3G_j - M_j) & 0 \end{bmatrix} \quad (3.4-2)$$

where M_j and G_j are the constrained and shear modulus of layer j. Note that the matrices in Eq. (3.4-1) are of order (2n+2n) x (2n+2) corresponding to degrees-of-freedom shown in Fig. 3.4-1. The vector {P_b} is a vector with 2 components and defines the load vector at the base. Depending on the angle of incidence of the wave and nature of the wave field (SV or P or combined SV + P) the load vector P_b and the wave number k are obtained (see Ref. 4).

Solution to Eq. (3.4-1) yields the displacement vector $\{U\}$. For vertically propagating waves Eq. (3.4-1) reduces to much simpler equation (Ref. 4). The free-field motion at any distance x can be obtained from the solution using the relation

$$\left\{ U(x) \right\} = \delta \cdot \{U\} \exp(-ikx) \quad (3.4-3)$$

where δ is the mode participation factor which is obtained from the input control motion at control point at the frequency of analysis. Note that Eq. (3.4-3) defines the motion at any horizontal distance x and for all the points on layer interfaces within the soil model. Once the location of control point is selected, the horizontal distance x can be obtained for all the interaction nodes in Substructures (b) in Fig. 2.2-1. The free-field motion $\{U_f\}$ used in Eq. (2.2-6) or Eq. (2.3-3) can thus be obtained from Eq. (3.4-3) for all the interacting nodes for the case of SV and/or P incident waves.

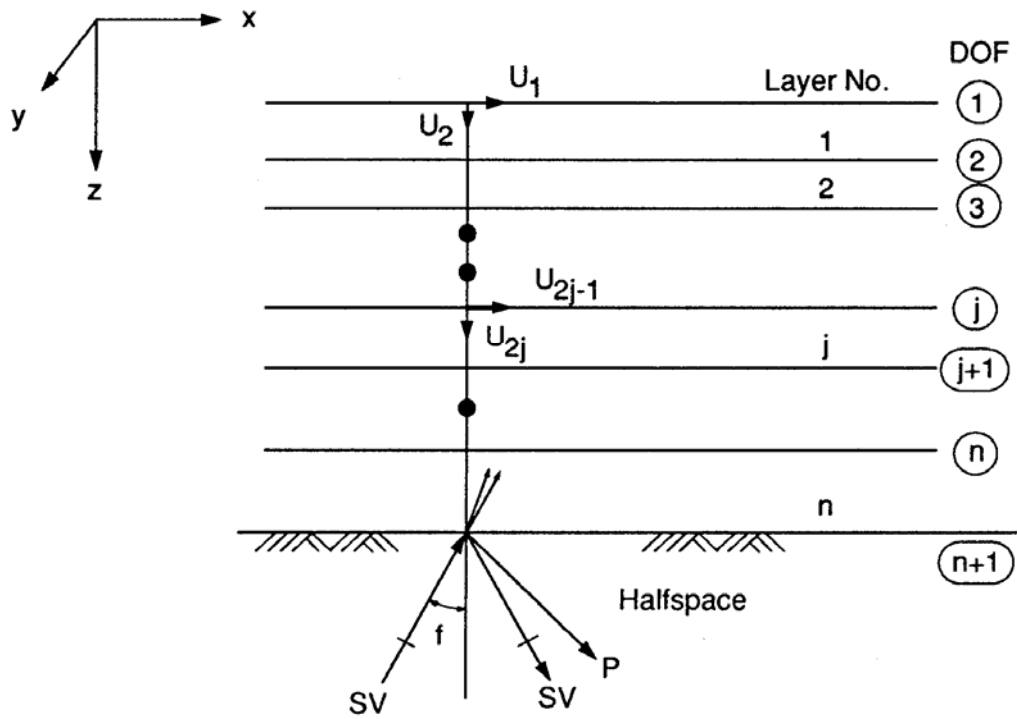


Figure 3.4–1. Model of Plane SV-Wave Incidence

3.4.2 INCLINED SH-WAVE

A similar technique has been developed for inclined SH-waves. The corresponding site model is shown in Fig. 3.4-2. For this model, the equation of motion for SH incident waves may be written in the form

$$([A]k^2 + [G] - \omega^2[M]) \{U\} = \begin{Bmatrix} 0 \\ P_b \end{Bmatrix} \quad (3.4-4)$$

The matrices $[A]$, $[G]$, and $[M]$ are assembled from the submatrices $[A_j]$, $[G_j]$, and $[M_j]$ defined in Eqs. (3.2-7), (3.2-8), and (3.2-9a) and (3.2-9b), respectively. Note the assembled matrices are of the order $(n+1) \times (n+1)$. The wave number k and the load vector P_b (single component) are obtained from the angle of incidence and properties of the halfspace (see Ref. 4). Solution of Eq. (3.4-4) yields to the free-field motion of the site model subjected to inclined SH-wave. For vertically propagating SH-wave, Eq. (3.4-4) reduces to a much simpler equation (Ref. 4). Similarly, the free-field motion at any distance x from the control point can be computed using the relation of Eq. (3.4-3) to compute the free-field motion $\{U'_f\}$ for inclined SH-waves.

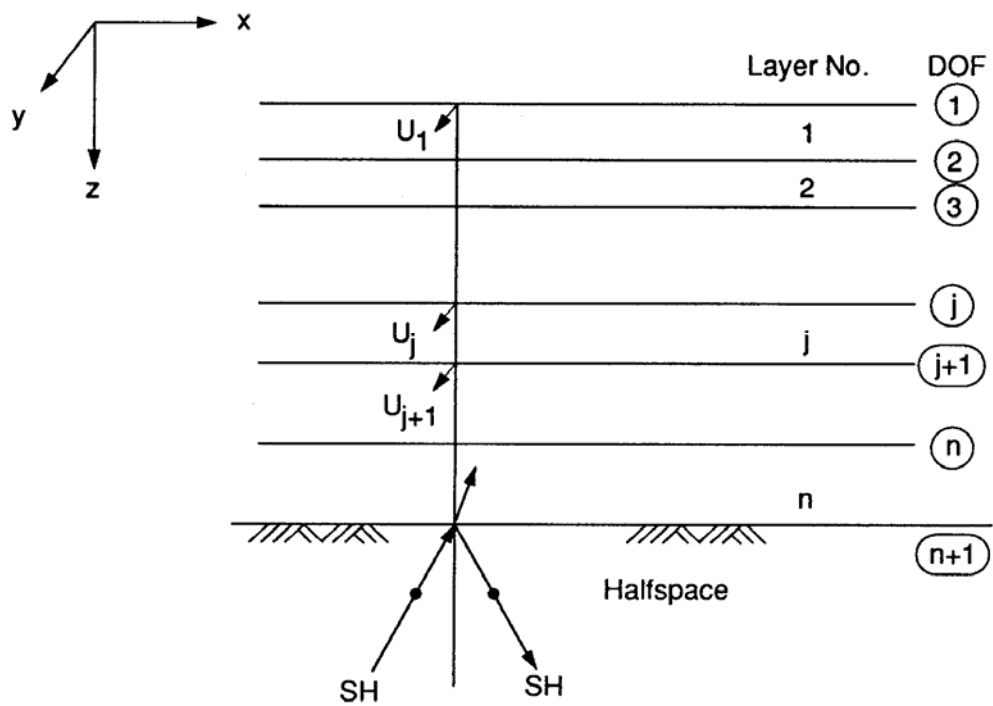


Figure 3.4-2. Model of Plane SH-Wave Incidence

3.4.3 RAYLEIGH WAVE

The equation of motion for the site model subjected to Rayleigh wave is the same equation as defined by Eq. (3.2-1) and described in Section 3.2.1. From the solution to this equation $2n$ mode shape vectors $\{V\}$ and $2n$ wave numbers k are selected for an n layer soil system. It should be noted, however, that in the engineering application, the input motion is defined in terms of the location of the control point and time history of the control motion which in effect defines the time history of a particular component of the mode shapes. While this information is sufficient to define the wave field for the case of body waves consisting of single mode for each frequency, it is not adequate to define the wave field for the case of surface waves since multiple modes may exist for the same frequency. On the other hand since surface waves are highly dissipative it can be assumed that only fundamental mode travels with distance. As a result, the selection of fundamental mode for Rayleigh wave is based on the study of the characteristic of generalized Rayleigh wave modes to select the most appropriate mode from the set of $2n$ modes.

Depending on the soil profile model, one of the following two methods may be used. Once the fundamental mode is selected, computation of free-field motion at interacting nodes, $\{U_f'\}$, follows the same procedures as described for body waves.

3.4.3.1 The Least-Decay Method

Consider a typical Rayleigh wave mode with wave number $k = k_r + ik_i$ where k_r and k_i are the real and imaginary components of the wave number. This mode has the wave length $2\pi/k_r$ and attenuates as $\exp(k_i x)$ with distance x . Hence, the decay factor per wave length is $\exp(2\pi k_i/k_r)$. The ratio $(-k_i/k_r)$ is thus a measure for how fast the wave mode decays. It is expected that the fundamental mode, which does not decay in the undamped case, will have a very small attenuation for damped cases. Therefore, for damped case, the mode with smallest $(-k_i/k_r)$ ratio is selected as the least-decay mode.

Study of the Rayleigh mode using the least-decay method for different soil profiles (see Ref. 4) shows while the method produces reasonable mode shapes in many cases it

does not yield to most realistic mode for sites with a soft highly damped surface layer overlaying a stiff halfspace with low damping. The method, in this case, tends to select a mode which corresponds to the classical Rayleigh mode in the halfspace without the surface layer (Ref. 4).

3.4.3.2 The Shortest Wave Length Method

In this method a mode with shortest wave length is selected. For undamped soil systems this mode is the one with the largest wave number k (hence shortest wave length and lowest phase velocity). This definition coincides with that used by seismologists.

However, actual sites cannot be modeled by undamped materials. It has been found (Ref. 4) that with the magnitude of the damping which are used in practical problems, the changes in the numerical values of wave numbers and mode shapes from the corresponding values obtained from undamped system are not very large. Based on this observation the following steps are taken to compute the fundamental mode.

1. Compute the undamped natural frequencies of the system by setting $k = 0$ in Eq. (3.2-1).
2. Determine m , the number of natural modes below the frequency of excitation
3. Sort the modes in order of magnitude of the imaginary part of the wave number
4. Select from the first m modes of step 3, the mode whose wave number k has the largest real part. It has been shown (Ref. 4) that this method leads to a mode shape with the usual characteristics of fundamental Rayleigh wave, i.e., decay with depth, simple mode shape, and low phase and group velocities. Furthermore, for the undamped system, the definition coincides with that used by seismologists.

However, in practical application, only a small percentage of the Rayleigh wave, if any, is present in the control motion. Nevertheless, it is prudent to study the fundamental

modes selected by both methods described above and select a mode which is appropriate for the site considered.

3.4.4 LOVE WAVE MOTION

Equation of motion for the site model subjected to Love wave motion is the same equation as defined by Eq. (3.2-6) and described in Section 3.2.2. For reasons similar to the case of Rayleigh wave, from the set of n mode shapes obtained from Eq. (3.2-6), one mode is selected as the fundamental mode. The method used is based on the shortest wave length method. Following the selection of the mode, the free-field motion at interacting nodes, $\{U_f'\}$, can similarly be computed.

3.5 MODELLING OF SEMI-INFINITE HALFSPACE AT BASE

The approach described above was originally developed for layered sites resting on a rigid base. In many practical cases the site is a layered system which extends to such great depth that it becomes necessary to introduce an artificial rigid boundary at some depth. This boundary will reflect some energy back into the system and will cause the site to have some erroneous natural frequencies which will affect the overall response. This becomes especially critical for sites with low material damping.

To remedy this problem, the two techniques as described in the following two subsections are used in the SASSI program to simulate the semi-infinite halfspace at the soil layer base.

3.5.1 THE VARIABLE DEPTH METHOD

In this method n extra layers which represent the halfspace are added to the base of the top soil layers (see Fig. 3.6-1). The total depth H of the added layers varies with frequency and is set to

$$H = 1.5 \frac{V_s}{f} \quad (3.6-1)$$

where f is the frequency of analysis in Hz, and V_s in the shear wave velocity of halfspace. The choice of this depth is based on the observation that fundamental mode Rayleigh waves in a halfspace decay rapidly with depth and essentially vanish at a depth corresponding to one and a half wave length. Only a minimal error is therefore introduced by placing a rigid base at this depth.

Assuming the thickness of the last top layer to be h_0 , and this layer has the same properties as the halfspace, the thickness of the j^{th} layer in the simulated halfspace is set to

$$h_j = \alpha^j h_0 \quad (3.6-2)$$

where α is a constant coefficient. This coefficient is determined as follows:

The total thickness of the n layers is

$$H = h_0 + \alpha h_0 + \dots + \alpha^n h_0 = \frac{(\alpha^n - 1) h_0}{\alpha - 1} \quad (3.6-3)$$

Hence

$$\frac{(\alpha^n - 1)}{\alpha - 1} = \frac{H}{h_0} \quad (3.6-4)$$

Eq. (3.5-4), in which the right-hand side is known at each frequency, is solved by the Newton iteration method to determine α . The number of layers, n , used to represent the halfspace is usually chosen such that $\alpha > 1$ for the highest frequency of analysis.

Based on the above method of subdivision the layer thicknesses will increase with depth and decrease with frequency. This is the desired characteristic of the model since surface wave mode shapes decrease exponentially with depth and since their depth of

penetration increases with decreasing frequency. The fact that the layer thickness becomes very large at low frequencies is acceptable since the thickness remains small as compared to the wave length. The choice of $n = 10$ has been found to be adequate for all practical problems (Ref. 2).

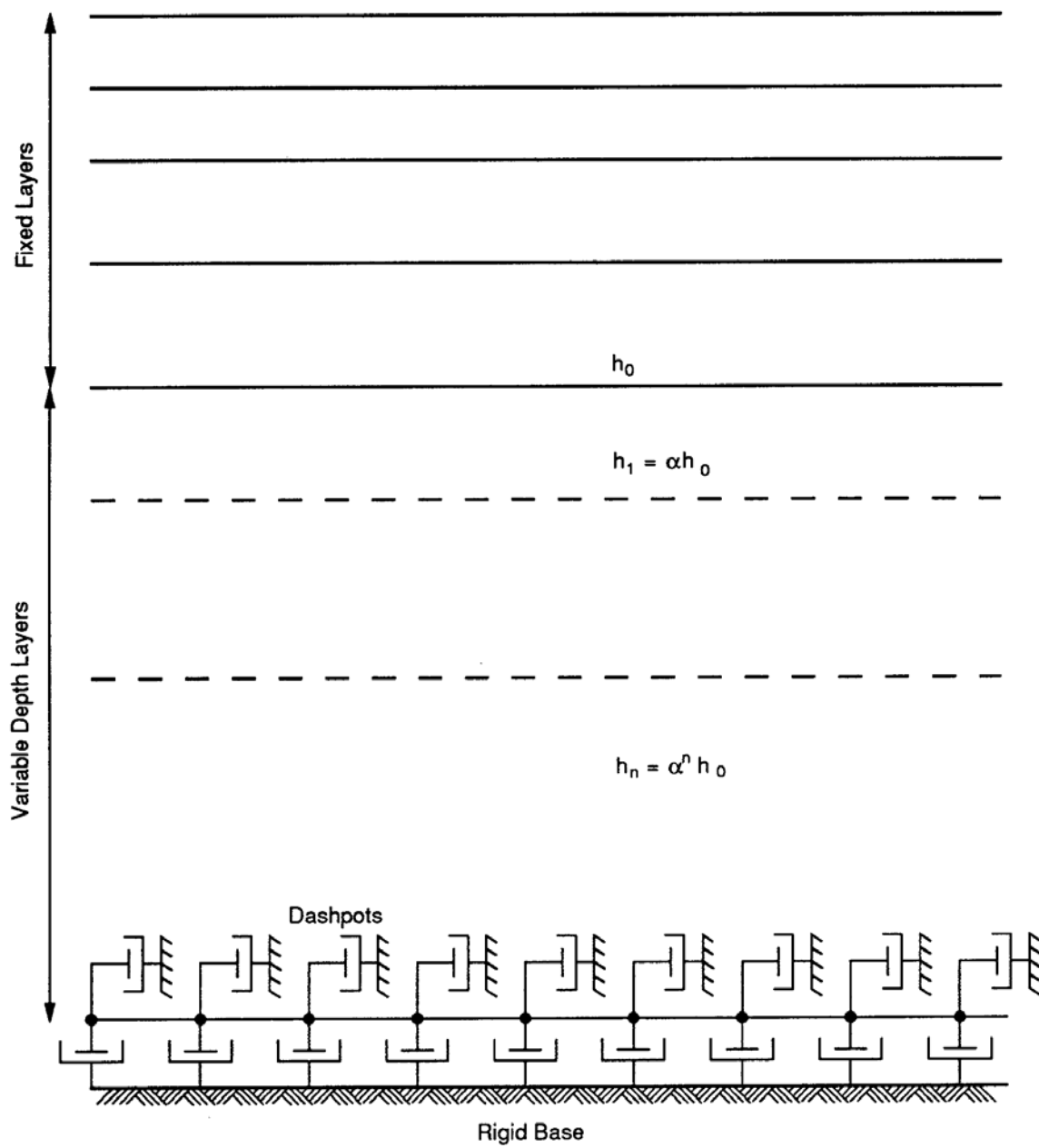


Figure 3.5-1. Simulation of Halfspace

3.5.2 VISCOUS BOUNDARY AT BASE

The site model may be further improved by replacing the rigid boundary with a viscous boundary, as shown in Fig. 3.6-1. This boundary which was developed by Lysmer and Kuhlemeyer (Ref. 7) consists of two dashpots per unit area of the boundary. The dashpots have the damping coefficients

$$\text{Vertical dashpot: } C_p = \rho V_p \quad (3.5-5a)$$

$$\text{Horizontal dashpot: } C_s = \rho V_s \quad (3.5-5b)$$

where ρ is the mass density and V_p and V_s are the P- and S-wave velocities, respectively, of the halfspace below the boundary of the model. Thus the boundary condition is

$$\sigma(X, t) = V_p \dot{U}_z(x, t) \quad (3.5-6a)$$

$$\tau(X, t) = V_s \dot{U}_x(x, t) \quad (3.5-6b)$$

where σ , τ , \dot{U}_z , and \dot{U}_x are the normal stress, the shear stress, the normal velocity, and the tangential velocity, respectively, at the boundary. The boundary condition in Eq. (3.5-6) is the exact boundary condition for the (downward) vertically propagating P and S plane waves in a perfect elastic halfspace. Thus the dashpots exactly simulate the halfspace impedances below the base of the model for the special load cases shown in Fig. 3.6-2. In fact, all of the three models shown in Figs. 3.6-2(a) and 3.6-2(b) will result in the same surface response.

The inclusion of dashpots in the site model also greatly improves the accuracy of the impedance calculations to be discussed in Chapter 4. Thus, for the simulation of halfspace the site model as shown in Fig. 3.6-1 which combines both the variable depth

method and the viscous boundary condition should be used when applying the SASSI program.

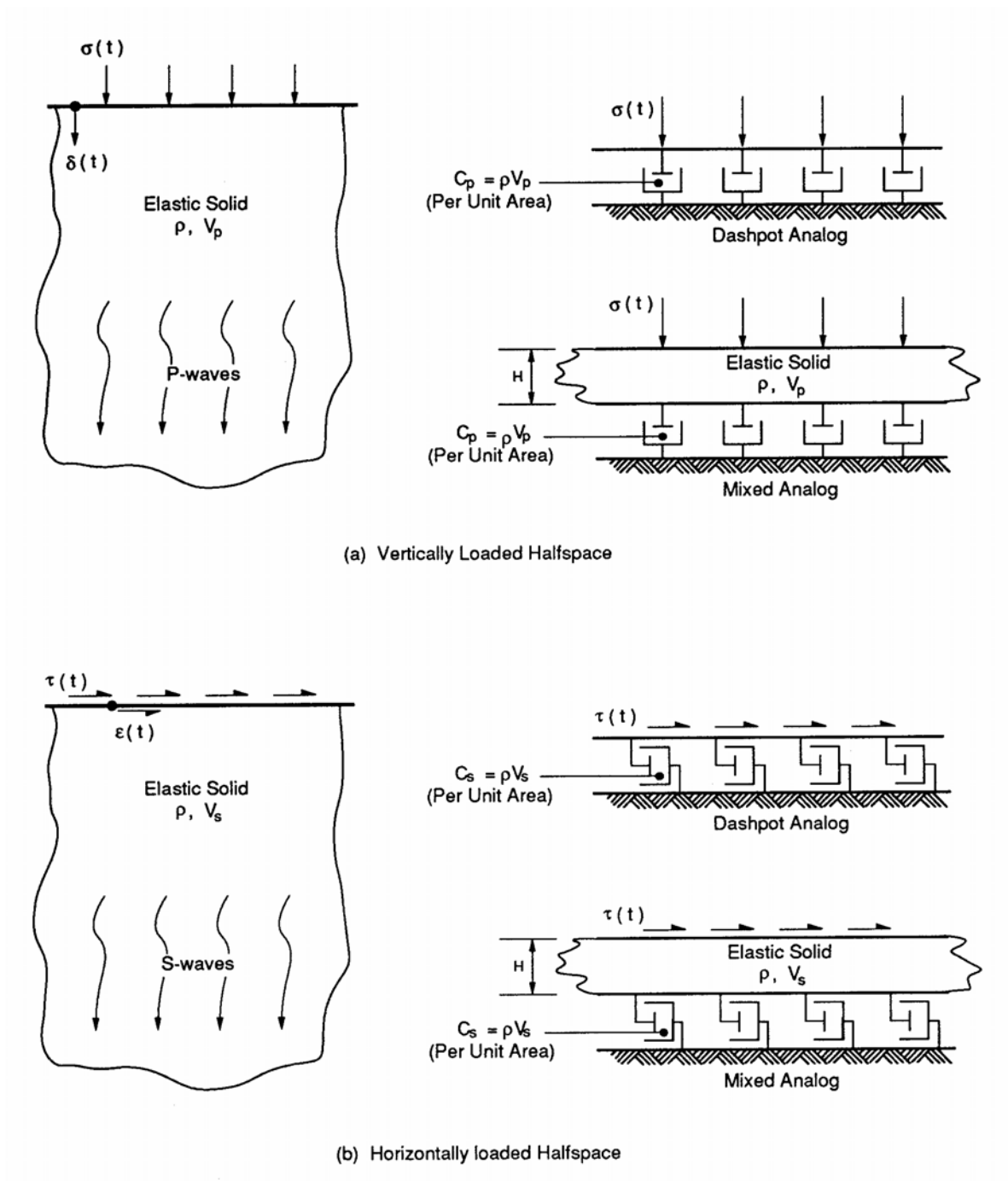


Figure 3.5-2. Halfspace Simulation by Viscous Dashpots

3.6 DYNAMIC SOIL PROPERTIES AND EQUIVALENT LINEAR METHOD

The substructure methods used by SASSI is valid only for linear analyses. It is well known, however, that the response of soils to dynamic loading exhibits strain-dependent nonlinear behavior. The nonlinear behavior of the soil is considered approximately in SASSI using the equivalent linear method proposed by Seed and Idriss (Ref. 28). Using this method, the nonlinear properties of the soil are approximated by equivalent linear properties consisting of the equivalent linear shear modulus and damping ratio for the soil which are compatible with the induced strain amplitudes in the soil medium.

An extensive summary of data on strain compatible moduli and damping ratios for clays and sands has been presented by Seed and Idriss (Ref. 29). Additional data have been presented by Hardin and Drnevich (Ref. 7). Recently more data has been published that shows the effect of overburden pressure on soil nonlinear behavior. The data are presented in the form of curves shown in Fig. 3.7-1. These curves show the effective dynamic shear moduli and damping ratios for clays and sands subjected to cyclic excitation at different strain amplitudes. The curves provide the essential data for the equivalent linear method which proceeds as follows: A linear analysis is performed with estimated soil properties. This analysis provides approximate values of the effective strain amplitude developed in each soil layer and these are used to estimate better soil properties from the curves for a second linear analysis. The process is continued until compatibility is obtained between soil properties and strain amplitudes and the results of the last linear analysis is assumed to represent the nonlinear response.

The effect of nonlinear soil behavior under seismic excitations can be considered in two parts: the primary nonlinearity attributed to the nonlinearity induced by the seismic excitation in the free field, and the secondary nonlinearity due to soil-structure interaction only. The primary nonlinearity is usually considered using Computer Program SHAKE (Ref. 27). The iterated soil properties obtained from SHAKE analysis are used for SASSI analysis.

The secondary nonlinearity, which occurs at soil elements adjacent to the structure, may also arise from separation or debonding between the soil and the structure and the

subsequent closing of the gaps or sliding of the structure. The stress and strain in the soil elements near the structure can also be computed by SASSI. If need be, the properties of these elements are adjusted using the iterated equivalent linear soil properties and the analysis can be restarted with adjusted soil properties.

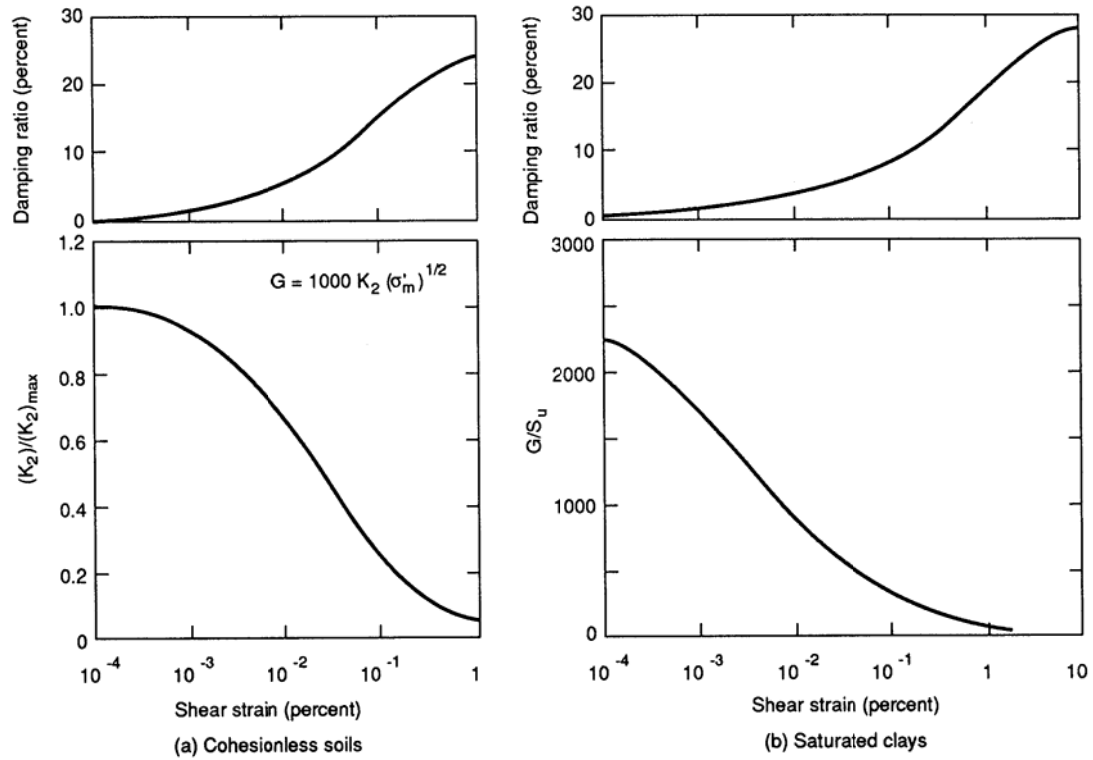


Figure 3.6-1. Average Shear Moduli and Damping Characteristics of Soils

3.7 COMPLEX RESPONSE METHOD

In SASSI, the soil material properties are represented by the complex shear, G^* , and complex constrained moduli, M^* , defined by the following equations:

$$G^* = G \left(1 - 2\beta_s^2 + 2i\beta_s \sqrt{1 - 2\beta_s^2} \right) \cong G \left(1 + 2i\beta_s \right) \quad (3.8-1a)$$

$$M^* = M \left(1 - 2\beta_p^2 + 2i\beta_p \sqrt{1 - 2\beta_p^2} \right) \cong M \left(1 + 2i\beta_p \right) \quad (3.8-1b)$$

where G and M are real numbers corresponding to the shear and constrained moduli, respectively, and β_s and β_p are the critical damping ratios associated with S-wave and P-waves, respectively. Currently only limited data are available on the ratio between β_s and β_p and these quantities are therefore usually chosen to be equal, in which case the subscripts are dropped and the corresponding Poisson's ratio becomes real number.

Using the complex modulus described above, the spatial variation of damping can be included in the analysis. This is particularly important for SSI systems in which the material damping in the soil and structure is significantly different.

CHAPTER 4

IMPEDANCE ANALYSIS

The equations of motion of the SSI system based on the flexible volume and the subtraction substructuring methods used by SASSI include the impedance matrix $[X_{if}]$ as shown in Eqs. (2.2-6), (2.2-7), (2.3-3) and (2.3-4). In the flexible volume method, the impedance matrix needs to be computed for all the interacting nodes in the flexible volume, i.e., the excavated soil volume (i and w nodes in Fig. 2.2-1.) In the subtraction method, the impedance matrix needs to be computed only for the exterior boundary nodes (the i nodes in Fig. 2.3-1.) The calculation of the impedance matrix is achieved by inverting the dynamic flexibility (compliance) matrix for each frequency of analysis. The methods and analytical models used to compute the compliance matrix based on the model of substructure (b) shown in Fig. 2.2-1 (or Fig. 2.3-1) for two- and three-dimensional problems are described in Sections 4.1 and 4.2, respectively. In the flexible volume method, two methods, namely, the direct method and the skin method, are used in SASSI for the impedance analysis. Depending on which method is used, the compliance matrix is computed for all or part of the interacting nodes. The direct and skin methods of impedance analysis are described in Sections 4.3 and 4.4, respectively. For the subtraction method, the impedance matrix is computed following the procedure for the direct method but limited to the nodes for which the impedance matrix is needed in accordance with the equation of motion in Section 2.3.

4.1 COMPLIANCE MATRIX FOR TWO-DIMENSIONAL PROBLEMS

By definition of the compliance matrix, the components of the i^{th} column of the matrix are the dynamic displacements of the interacting degrees-of-freedom caused by a harmonic force of unit amplitude acting at the i^{th} degree-of-freedom. Thus, the problem of determining the compliance matrix for two-dimensional problems is that of finding the harmonic response displacements of a layered halfspace to a harmonic line load.

Fig. 4.1-1 shows a layered system and the interaction nodes for which the matrix is to be

determined. To obtain the compliance matrix, the basic problem is to determine the displacement responses of all the nodes subject to unit loads placed successively at one column of nodes shown as heavy dots in Fig. 4.1-1. Once this problem has been solved, solution corresponding to other nodes can be obtained simply by a shift of the horizontal coordinates.

The basic solution is obtained using a model which consists of a single column of plane-strain rectangular elements. This model, which takes advantage of symmetry, is shown in Fig. 4.1-2 and is solved with different boundary conditions at the axis of symmetry depending on the direction of the applied forces at the loaded nodes. The existence of the semi-infinite layered region is simulated by applying the consistent transmitting boundary impedances as described in Section 3.3 on the nodes numbered $n+1$ to $2n$, where n is the number of layers. The lower boundary may be fixed or a halfspace simulated using the variable depth method and the viscous boundary at base as discussed in Section 3.5.

The equations of motion for the model are

$$\begin{bmatrix} C_{cc} & C_c \\ C_{\ell\ell} & C_{\ell\ell} + R \end{bmatrix} \begin{Bmatrix} U_c \\ U_\ell \end{Bmatrix} = \begin{Bmatrix} Q_c \\ 0 \end{Bmatrix} \quad (4.1-1)$$

where C indicates a dynamic stiffness matrix of the form ($C = k - \omega^2 M$) and R is the transmitting boundary impedance matrix described in Section 3.3.1. The indices c and ℓ refer to degrees of freedom on the center line and the lateral boundary, respectively; and U_c and U_ℓ are the corresponding displacements. The load vector for each load case has only one non-zero element corresponding to a load of unit amplitude. Since the matrix in Eq. (4.1-1) is the same for all horizontal load cases (Fig. 4.1-2a), only a single triangulation is required to find the solution vectors for these cases.

The unit horizontal harmonic loads are applied at the interacting nodes on the center line of the model (see Fig. 4.1-2a) successively. Solution to Eq. (4.1-1) yields displacement

responses on the center line and on the boundary of the model for each loading case. To compute the components of the flexibility matrix at interacting nodes outside the boundary of the model, the following relationship applicable to layered halfspace is used.

$$\{U\} = \sum_{s=1}^{2n} \alpha_s \{V\}_s \exp(-ik_s x) \quad (4.1-2)$$

In this equation, x is the horizontal distance, $\{V\}_s$, α_s , and k_s are the mode shapes, mode participation factors, and wave number associated with the soil layered system, respectively. As discussed in Section 3.2, there are $2n$ modes for a n layer soil system. The mode shapes and the associated wave numbers are obtained from the solution of the eigenvalue problem of a layered system as discussed in Chapter 3. The mode participation factors are computed from Eq. (4.1-2) by letting $x=0$ and using the solution of Eq. (4.1-1) at the boundary nodes. Thus, by knowing the horizontal distance between the loaded nodes on the center line and the interacting nodes outside the boundary, the displacements at all other nodes are computed from Eq. (4.1-2).

A similar technique is used for the vertical loading case. In this case the model shown in Fig. 4.1-2b is used and the solution is obtained in a similar manner. Eq. (4.1-2) is then used to compute the displacement at other interacting nodes.

It should be noted, however, that the analytical models shown in Figs. 4.1-2a and 4.1-2b are analyzed only for one column of the interacting nodes as shown in Fig. 4.1-1. The same solution is successfully used for the remaining columns of interacting nodes and only the horizontal distance x in Eq. (4.1-2) needs to be computed to measure the horizontal distance between the new set of loaded nodes and the remaining interacting nodes.

Using the technique described above, a $2i \times 2i$ compliance matrix associated with total of i interacting nodes is computed for each frequency of analysis.

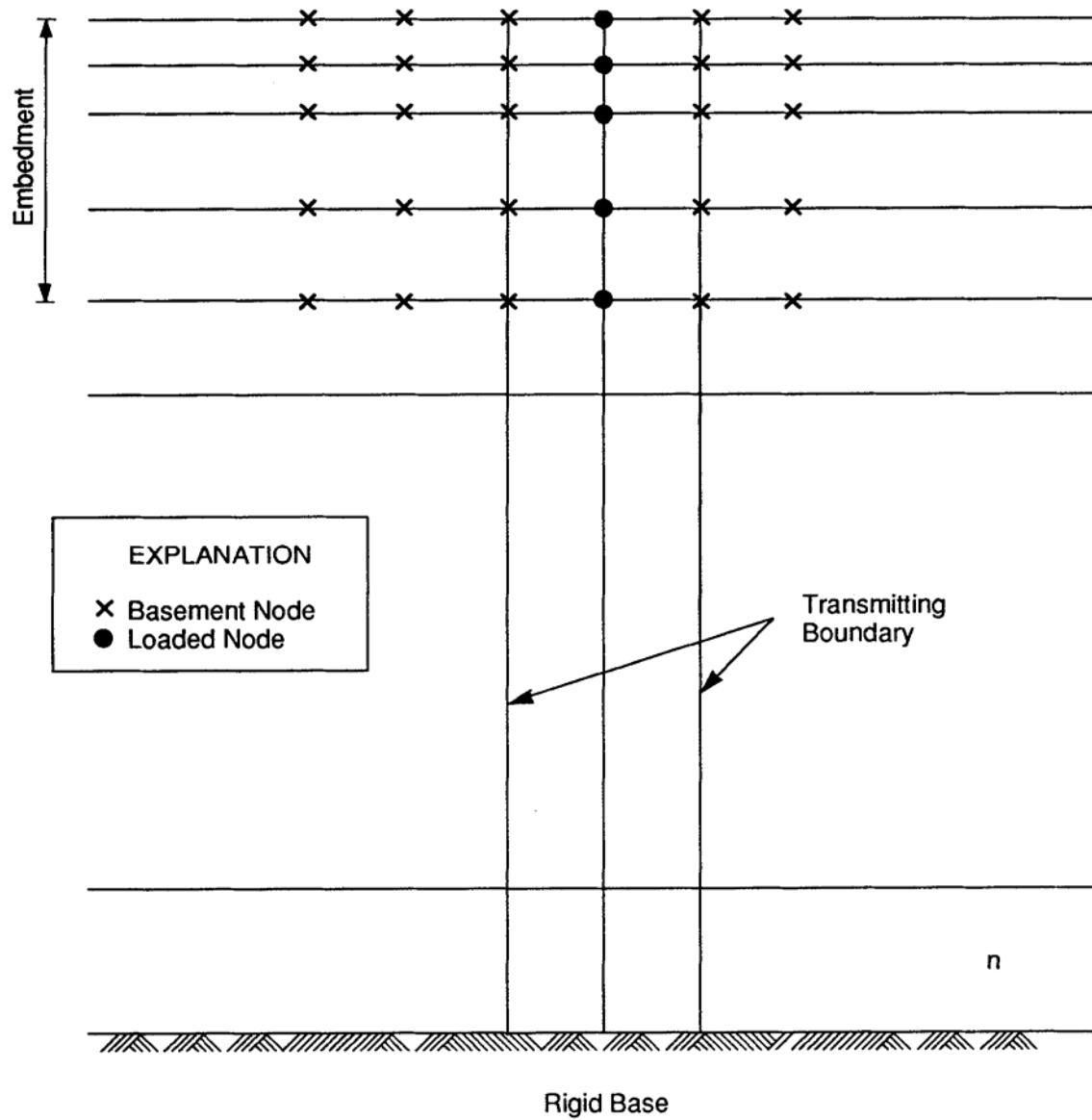
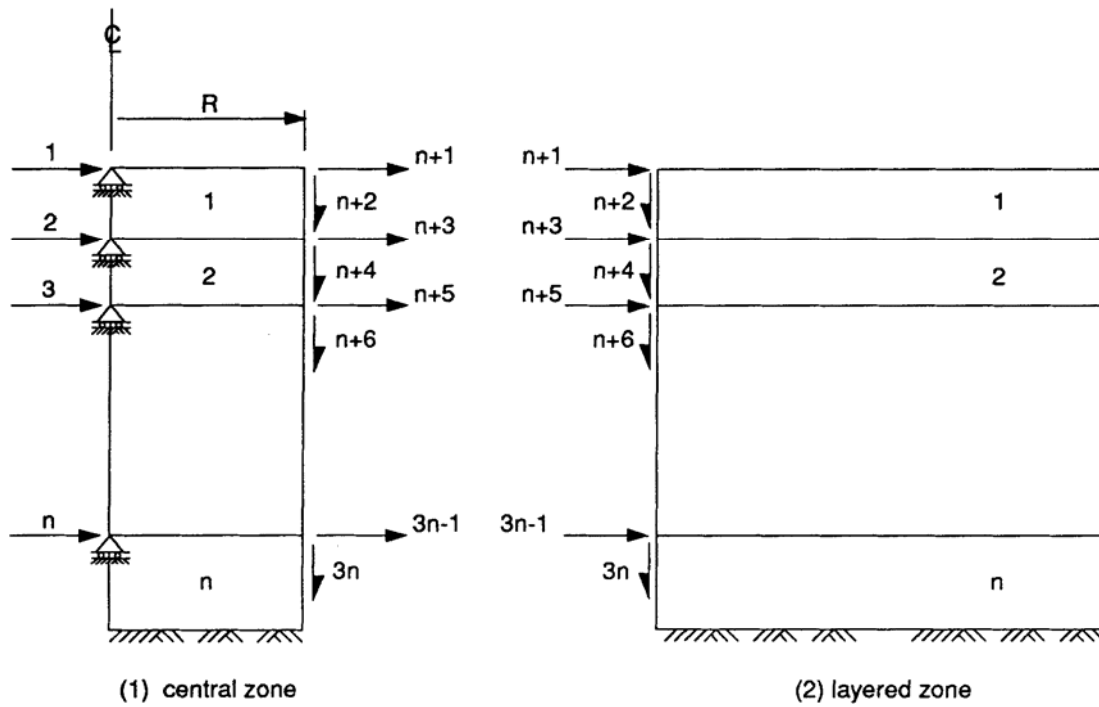
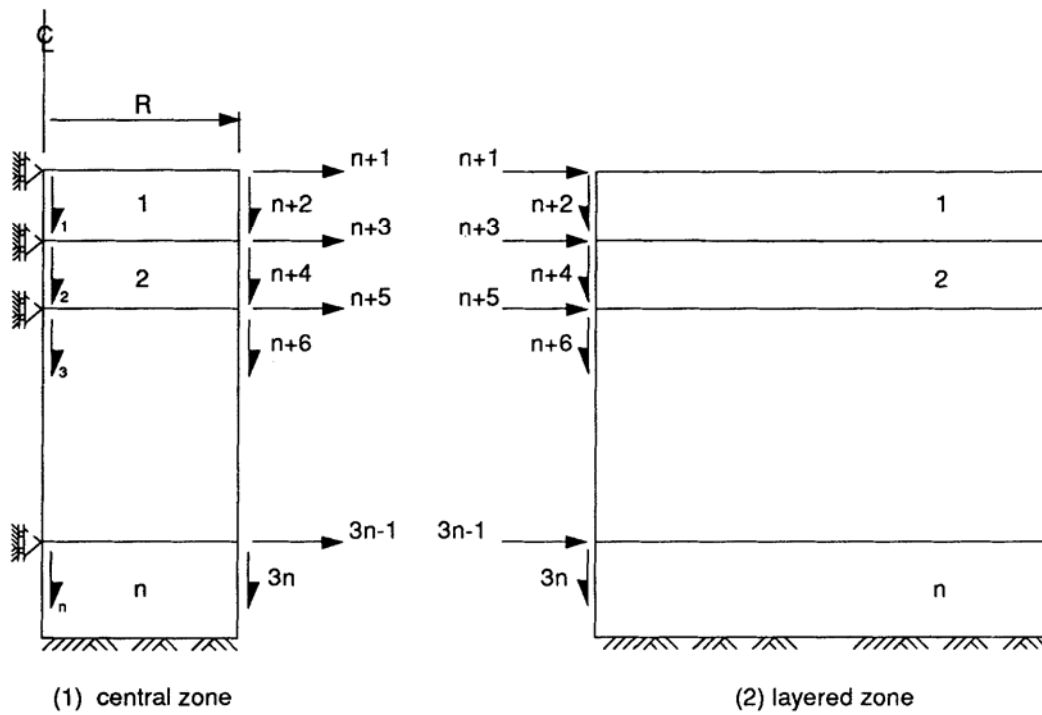


Figure 4.1-1. Plane-Strain Model for Impedance Analysis



(a) Boundary Conditions for Horizontal Loading



(b) Boundary Conditions for Vertical Loading

Figure 4.1-2. Boundary Conditions

4.2 COMPLIANCE MATRIX FOR THREE-DIMENSIONAL PROBLEMS

Similar to the 2-D case, the problem of evaluating the dynamic flexibility matrix for a three-dimensional case reduces to the problem of finding the response of a horizontally layered system to point loads at the layer interfaces. This problem, however, is an axisymmetric problem and can be solved using the axisymmetric model shown in Fig. 4.2-1. The model consists of a central zone with radius r_o of cylindrical elements enclosed by an axisymmetric transmitting boundary. As for the two-dimensional case, the lower boundary can either be fixed or halfspace simulated using the variable depth and viscous boundary methods. Taking advantage of symmetry and antisymmetry boundary conditions, the models shown in Figs. 4.2-2a and 4.2-2b are used for vertical and horizontal loading cases, respectively.

The mass and stiffness matrices of the elements in these models are computed in cylindrical coordinates system. Fourier harmonics are used to expand the displacement field within each element in tangential direction. In the model used for horizontal loading (Fig. 4.2-2b), up to 1st Fourier expansion terms are used. In the model used for vertical loading (Fig. 4.2-2a), only zero harmonic terms are needed since the model and the loading are symmetric. Following the computation of element mass and stiffness matrices, the equation of motion is assembled in the following form:

$$\begin{bmatrix} C_{cc} & C_{cp} \\ C_{pc} & C_{pp} + R \end{bmatrix} \begin{Bmatrix} U_c \\ U_p \end{Bmatrix} = \begin{Bmatrix} Q_c \\ 0 \end{Bmatrix} \quad (4.2-1)$$

where C indicates the dynamic stiffness matrix ($C = k - \omega^2 M$) and R is the axisymmetric transmitting boundary impedance matrix described in Section 3.3.2. The indices c and p refer to degrees of freedom on the center line and perimeter of the model, respectively, and U_c and U_p are the corresponding displacement amplitudes. The displacements of the nodes outside the model ($r > r_o$) may be obtained from

$$\{U(r)\}_m = [W(r)]_m \{\Delta\}_m \quad (4.2-2)$$

where the subscript m refers to Fourier harmonic order (zero or one) and

$$\{\Delta\}_m^T = \langle \alpha_1, \alpha_2, \dots, \alpha_{3n} \rangle \quad (4.2-3)$$

is the modal participation factors associated with 3n modes of the n layer soil system. The 3n x 3n matrix $[W(r)]_m$ has the general elements defined in Eq. (3.3-6).

The displacement of the nodes on the perimeter of the model ($r=r_o$) obtained from Eq. (4.2-1) are used in Eq. (4.2-2) to compute the mode participation vector $\{\Delta\}_m$. Knowing the mode participation vector, Eq. (4.2-2) can be used to compute the displacement at any point with radius of r from the axis of the model. These displacements are in cylindrical coordinates. The displacement components at each node are transformed into Cartesian coordinates and used to construct the compliance matrix.

Using the technique described above, a 3i x 3i flexibility matrix is computed for a system with i interacting nodes in the free-field soil medium for each frequency of analysis.

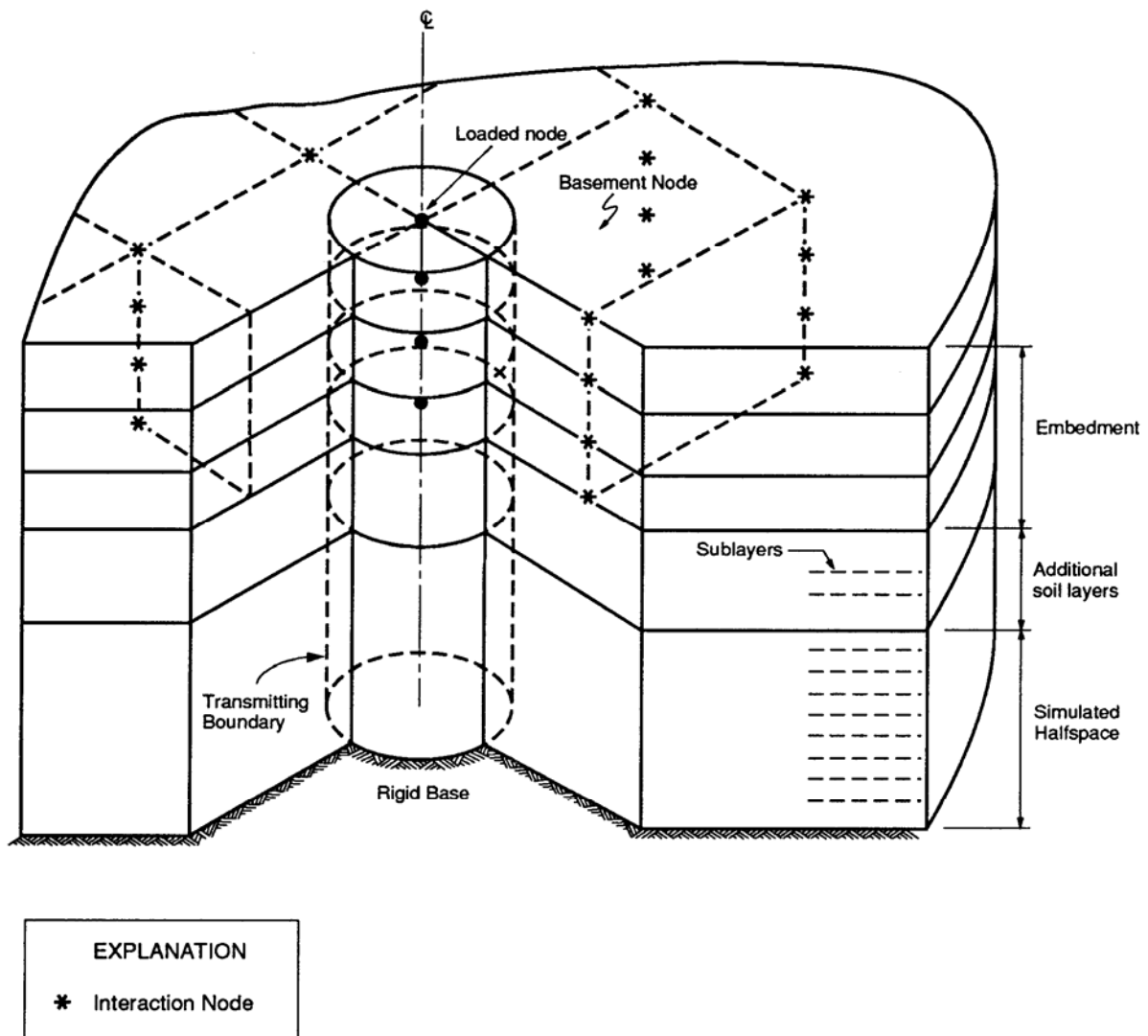
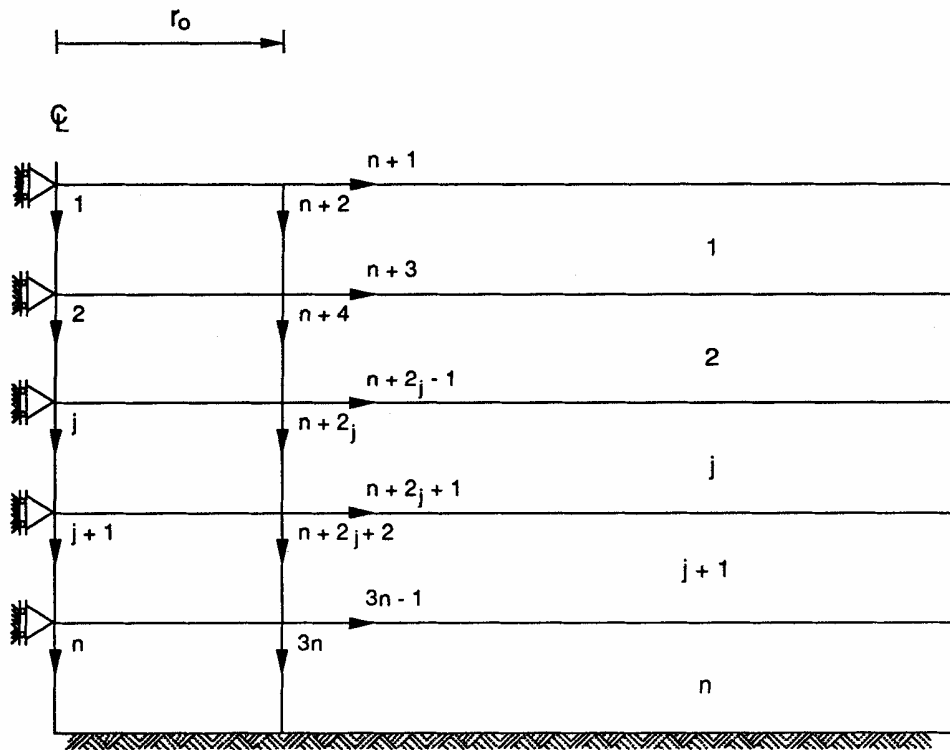
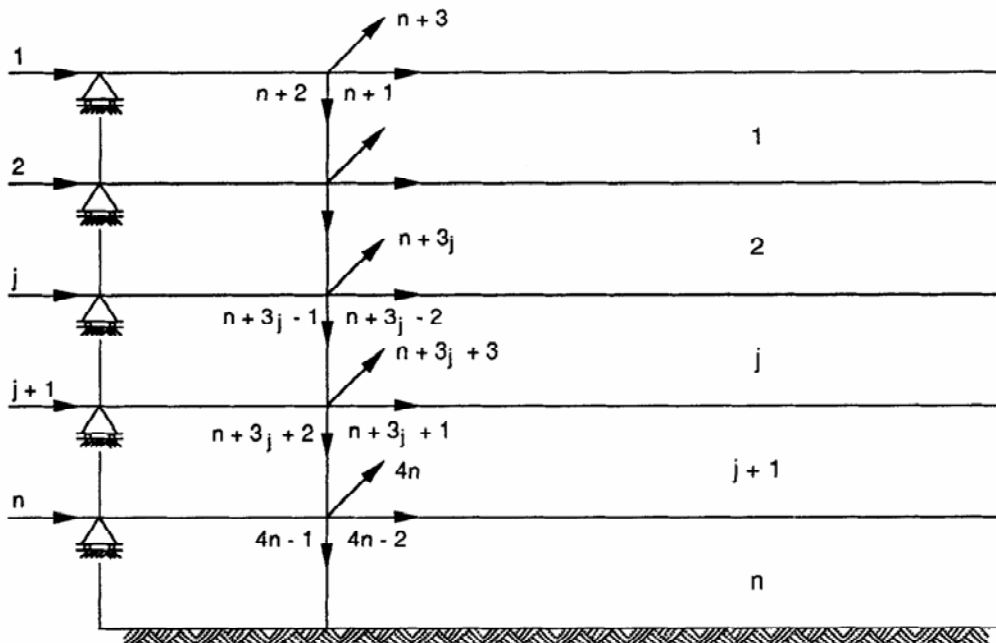


Figure 4.2-1. Axisymmetric Model for Impedance Analysis



(a) Boundary Conditions for Vertical Loading



(b) Boundary Conditions for Horizontal Loading

Figure 4.2-2. Boundary Conditions

4.3 DIRECT METHOD OF IMPEDANCE ANALYSIS

In this method, the compliance matrix $[F_{ff}]$ needs to be computed for all the interacting nodes using the methods described above. The impedance matrix $[X_{ff}]$ is obtained by inverting the compliance matrix, i.e.,

$$[X_{ff}] = [F_{ff}]^{-1} \quad (4.3-1)$$

The impedance matrix as obtained is subsequently used in the assemblage of the equations of motion as described in Section 2.2. The inversion of the matrix is computer CPU intensive and needs to be performed for every frequency of analysis. An efficient in-place inversion routine is used to invert the flexibility matrix which is a full matrix in the direct method of analysis. For a total number of i interacting nodes, the resultant impedance matrix is of the order of $2i \times 2i$ or $3i \times 3i$ for two- and three-dimensional problems, respectively.

4.4 SKIN METHOD OF IMPEDANCE ANALYSIS

According to this method, the interacting nodes are grouped into three groups, defined as skin, intermediate, and internal nodes. These groups are shown in Fig. 4.4-1. By definition, skin nodes are those located along the physical boundary between the structure basement and the soil region (labeled by digit 1 in Fig. 4.4-1). Intermediate nodes are defined as those interaction nodes within the flexible volume which are directly connected to the skin nodes (labeled by digit 2 in Fig. 4.4-1). The remaining interaction nodes, which are not connected to skin nodes, are internal nodes (labeled by digit 3 in Fig. 4.4-1).

According to the above definition, the impedance and compliance matrices are partitioned as follows:

$$\begin{bmatrix} X_{11} & X_{12} & X_{13} \\ X_{21} & X_{22} & X_{23} \\ X_{31} & X_{32} & X_{33} \end{bmatrix} = \begin{bmatrix} F_{11} & F_{12} & F_{13} \\ F_{21} & F_{22} & F_{23} \\ F_{31} & F_{32} & F_{33} \end{bmatrix}^{-1} \quad (4.4-1)$$

Consider the embedment region separated from the surrounding environment as shown in Fig. 4.4-1b. The dynamic stiffness matrix of this region is identical to the matrix C_{ff} in Eq. (2.2-6) and has the form

$$[C_{ff}] = \begin{bmatrix} C_{11} & C_{12} & 0 \\ C_{21} & C_{22} & C_{23} \\ 0 & C_{32} & C_{33} \end{bmatrix} \quad (4.4-2)$$

where $C = K - \omega^2 M$ are formed from the mass and stiffness properties of the "excavated" soil.

By the definition of a stiffness matrix, the elements of X and C are the forces at all degrees of freedom when a particular degree of freedom is given a unit displacement while all other nodes remain fixed. By this definition the following relations are obtained:

$$X_{12} = C_{12} \quad (4.4-3a)$$

$$X_{22} = C_{22} \quad (4.4-3b)$$

$$X_{32} = C_{32} \quad (4.4-3c)$$

$$X_{13} = 0 \quad (4.4-3d)$$

$$X_{23} = C_{23} \quad (4.4-3e)$$

$$X_{33} = C_{33} \quad (4.4-3f)$$

These relations are exact if the same displacement fields are used in the layered site and in modeling the excavated soil. In actual analysis, plane strain or brick elements with linear displacement fields are used to model the excavated soil while continuum formulation (see Eqs. [4.1-2] and [4.2-2]) are used to compute the displacements in layered site with respect to horizontal distance. Therefore, the above equations are only

approximately satisfied. However, the errors introduced by assuming Eqs. (4.4-3) are acceptable for practical purposes.

Multiplication of the impedance matrix, X , with the flexibility matrix, F , yields the identity matrix. Hence, substituting for elements of X from the above equations,

$$\begin{bmatrix} F_{11} & F_{12} & F_{13} \\ F_{21} & F_{22} & F_{23} \\ F_{31} & F_{32} & F_{33} \end{bmatrix} \begin{bmatrix} X_{11} & C_{12} & 0 \\ C_{21} & C_{22} & C_{23} \\ 0 & C_{32} & C_{33} \end{bmatrix} = \begin{bmatrix} I & 0 & 0 \\ 0 & I & 0 \\ 0 & 0 & I \end{bmatrix} \quad (4.4-4)$$

X_{11} is obtained from the first set of equations and is

$$X_{11} = F_{11}^{-1} \cdot (I - F_{12} \cdot C_{12}^T) \quad (4.4-5)$$

The entire impedance matrix is now of the form

$$[X_{ff}] = \begin{bmatrix} F_{11}^{-1}(I - F_{12} \cdot C_{12}^T) & C_{12} & 0 \\ C_{21} & C_{22} & C_{23} \\ 0 & C_{32} & C_{33} \end{bmatrix} \quad (4.4-6)$$

As is evident from Eq. (4.4-6), only F_{11} and F_{12} of the total flexibility matrix need to be formed and only F_{11} needs to be inverted. The efficiency of the skin method is clearly highest when the number of skin nodes is small compared to the total number of interaction nodes. This will usually be the case for deep foundations.

Following the computation of the impedance matrix, this matrix is used in the equation of motion as described in Section 2.2.

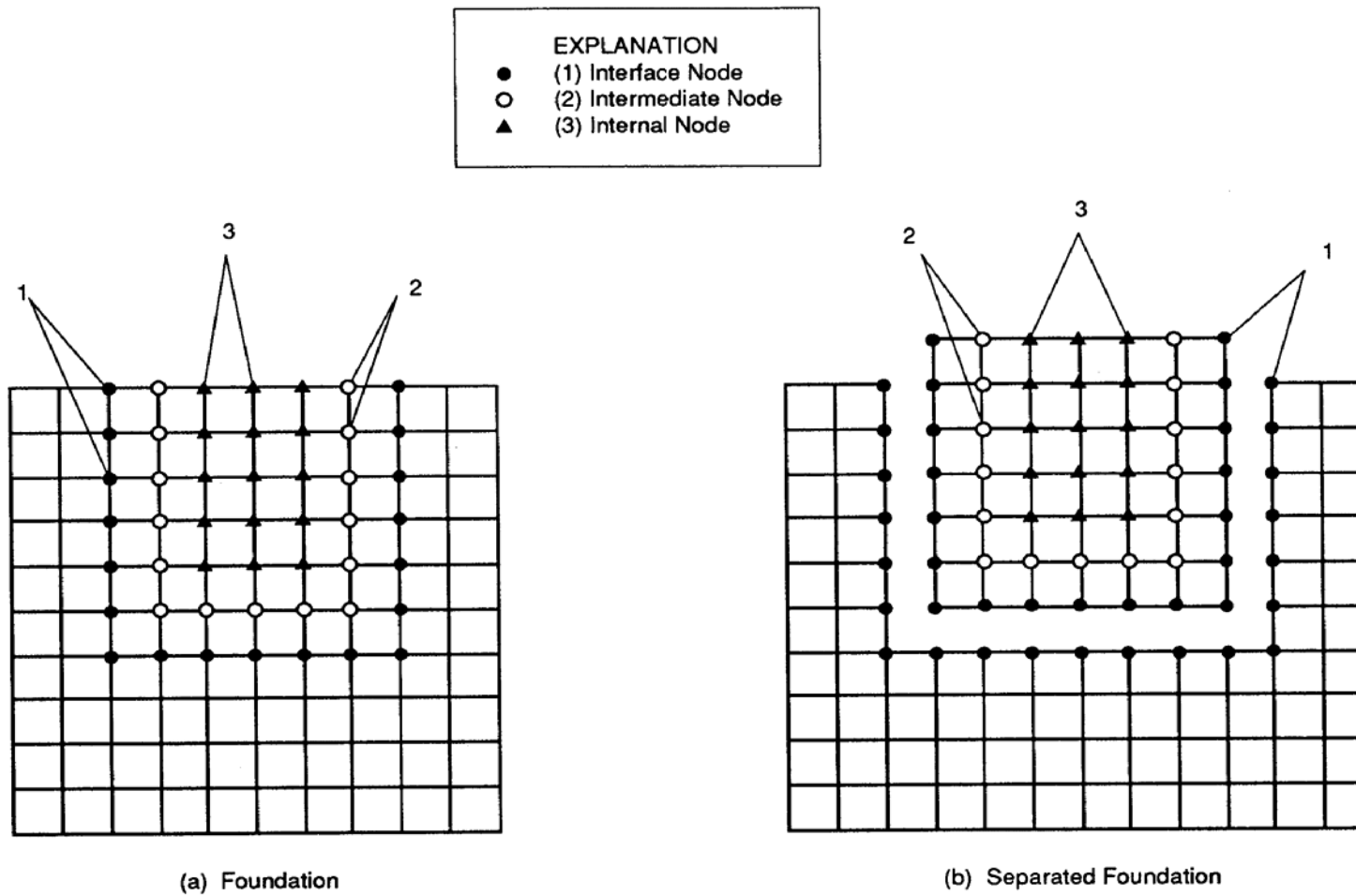


Figure 4.4-1. Foundation System for Skin Method

4.5 IMPEDANCE ANALYSIS IN SUBTRACTION METHOD

In the subtraction method the procedures for computing the flexibility matrix and inverting the matrix to obtain the impedance matrix are the same as those used in the direct method. The difference is in the number of the interaction nodes for which the impedance matrix needs to be computed. As described in Section 2.3, in the subtraction method the interaction nodes are limited to the outer boundary of the basement nodes (nodes i in Fig. 2.3-1). For this reason, the CPU time spent to obtain the impedance matrix in the subtraction method is significantly less than the direct method and the efficiency increases as the embedment depth increases.

4.6 IMPEDANCE MATRICES FOR SYMMETRIC AND ANTISYMMETRIC SYSTEMS

For SSI systems with symmetric properties and symmetric or antisymmetric loading, the model size and cost of analysis can be reduced by using one-half or one-fourth of the model. This requires calculation of the impedance matrix for the symmetric systems. Using the direct method as described In Section 4.3, the symmetric impedance matrix X_{ff} can be determined as the inverse of the corresponding symmetric dynamic flexibility matrix F_{ff} using

$$[X_{ff}] = [F_{ff}]^{-1} \quad (4.6-1)$$

The elements of the symmetric flexibility matrix f_{ij}^s represent the displacement at degree-of-freedom i due to unit harmonic loads acting at degree-of-freedom j and degree-of-freedom j' which is the mirror image of j relative to the axis of symmetry. The displacements are computed using the methods described in Sections 4.1 and 4.2.

Similarly for SSI systems with antisymmetric loading, the antisymmetric compliance matrix can be computed with the exception that the unit harmonic load at degree-of-freedom j' takes the opposite direction.

CHAPTER 5

PILE FOUNDATIONS

5.1 INTRODUCTION

Piles are structural members of small cross-sectional areas compared to their lengths. The piles are connected to the superstructure either directly or by a foundation block. The function of the piles is to carry the load from the superstructure into the ground.

Static pile behavior has been a subject of research for many years. Problems such as the effects of installation of piles, ultimate load capacity, settlement analysis and load deflection for laterally loaded piles are a few of these research topics. Conventionally, the theory of elasticity is used for evaluation of deformations of piles and soils at the working load condition. The ultimate bearing capacity is evaluated from formulas based on limit equilibrium. Among all the methods used to analyze static pile behavior only those relating to the present work will be referred to.

The fundamental elastic solutions used in static soil-pile interaction analysis were derived by Mindlin [Ref. 49]. He formulated a set of equations for the stresses and displacements throughout an elastic half-space subjected to a horizontal or a vertical point load acting at a point beneath the surface. The response can be integrated in such a way that the displacements of the pile and soil are compatible.

Among the early studies of static pile group behavior using Mindlin's equations are those of Poulos and Aust [Ref. 57], Poulos [Refs. 58 to 59], and Butterfield and Banerjee [Ref. 42]. Their analysis of static pile group behavior reflected the important effect of pile-soil-pile interaction in the response in terms of displacements and the distribution of the loads among the piles. The influence of factors such as spacing, number of piles and the configuration of the pile group were highlighted.

Most current procedures for designing pile foundations are based on static methods. However, for critical structures such as nuclear power plants and offshore oil production

platforms it is often necessary to consider dynamic effects due to seismic action and/or impact loads. Dynamic effects must also be considered for heavy piloted machine foundations. Such foundations will often have resonance frequencies which fall in the operating range of the machinery, and it becomes very important to be able to predict these frequencies so that remedial measures, like stiffening of the foundations, can be taken. In view of the above problems there clearly exists a need to develop rational design procedures which take into account the dynamic behavior of pile foundations.

The current methods for analyzing dynamic soil-pile interaction can be divided into three main groups:

- 1) Beam-on-Winkler-foundation methods
- 2) Continuum methods
- 3) Finite element methods.

These methods will be discussed briefly below.

5.1.1 BEAM-ON-WINKLER-FOUNDATION METHODS

With this method the soil response is modeled by a series of springs acting independently on the pile. The advantage of this method is that it is possible to allow for nonlinear soil behavior by using nonlinear springs. Major disadvantages of the method are as follows:

- 1) There is no coupling between the springs. This assumption in fact neglects the continuity of the soil medium.
- 2) There is no appropriate way to incorporate the inertia and damping effects of the soil media into the model.

Penzien et. al [Ref. 56], in the analysis of bridge pile foundations, proposed a method for approximating the constants of an equivalent Winkler foundation by using Mindlin's equations. The addition of some lumped masses and dashpots was also recommended to allow for inertia and damping effects. Based on test results, Matlock [Ref. 48] and Reese, Cox and Koop [Ref.63] have suggested some nonlinear spring characteristics

which, incorporated in the P-Y and T-Z curves, are widely used in the design of offshore structures. Novak [Ref. 52] analyzed the case of a single pile with a fixed tip condition. In his method the soil is modeled by a set of independent infinitesimally thin horizontal layers. This model can be viewed as a generalized Winkler model which possesses inertia and the capability to dissipate energy. Using the same method, Novak [Ref.53] extended his work to the case of vertical vibrations of floating piles. The reaction at the tip was approximated by the response of a half-space to a rigid circular disk on its surface. As was expected, the motion of the tip reduces the stiffness and increases the damping of the system. The seismic response of end-bearing piles has recently been investigated by Flores and Whitman [Ref. 44] using this method.

5.1.2 CONTINUUM METHODS

Two basic approaches have been used to develop dynamic continuum solutions for single piles:

- 1) In the first approach the equation of motion of the soil-pile system and that of the free field in cylindrical coordinates are considered. By making some assumptions which depend on the mode of vibration, pile displacements can be represented in terms of mode shapes of the free field. This method was used by Tajimi [Ref. 65] to study the seismic response of rigid and flexible embedded foundations. Nogami [Ref. 50] analyzed the vertical vibration of piles. Later, Nogami and Novak [Ref. 51] extended the method to horizontally vibrating piles.
- 2) In the second approach the soil-pile system is analyzed in two steps. First the soil reaction is obtained by vibrating an infinitely long rigid cylinder in the soil medium allowing for only horizontally propagating waves. Having obtained the impedance in this manner, it can be incorporated into the equation of motion for the pile. This method can be extended to the case of layered media. Novak and Howell [Ref. 54] and Novak and Aboul-Ella [Ref. 55] have studied dynamic pile behavior in homogeneous and layered media using the same approach. It should be noted that with the above method the

stiffness of the soil-pile system vanishes at low frequencies. This error is due to the assumptions that are made.

5.1.3 FINITE ELEMENT METHODS

Since the finite element method is able to consider an inhomogeneous soil medium as well as nonlinearities in the soil, this method has been widely used to analyze the dynamic behavior of single piles.

Blaney et al [Ref. 41] used a discretized model near the pile and a consistent boundary matrix to obtain the stiffness of the soil-pile system. Kuhlemeyer [Ref. 47] has used axisymmetric finite elements to analyze laterally loaded-piles for both static and dynamic cases. Kagawa et al [Ref. 45] attempted to obtain dynamic P-Y curves to be used in the Beam-on-Winkler-foundation method. The effect of soil nonlinearity has also been investigated by, among others, Angelides et al [Ref. 39]. Some simple expressions for the horizontal stiffness and damping of single piles have been obtained by Dobry et al [Ref. 43], who used both the finite element and the Beam-on-Winkler-foundation method.

5.1.4 PILE GROUPS

Although there are numerous methods for characterizing the dynamic response of single piles, only a few of these methods are applicable to pile groups. Wolf and Von Arx [Ref. 60] used the finite element method to analyze pile groups. In their method the flexibility matrix is obtained from a model in which the soil is discretized by toroidal elements and a Fourier expansion is used in the circumferential direction. The impedance matrix of the soil-pile system is determined as the inverse of the dynamic flexibility matrix. A special technique may be used to correct the flexibility matrix for the effects of the soil volume displaced by piles. In the above papers the authors present results which indicate significant group effects and uneven distribution of loads between the piles. Nogami [Ref. 50] analyzed the vertical vibration of a pile group using a model that had been developed earlier by Nogami and Novak [Ref. 51]. The work was extended by Nogami [Ref. 50] to the case of an inhomogeneous soil medium. Novak has also analyzed the vertical vibration of a pile group using a fictitious layer around each pile to allow for soil nonlinearity. A more complete study of dynamic stiffness and seismic

response of a pile group was done by Kaynia [Ref. 46]. In his model the piles are discretized into small segments. The flexibility is obtained from the displacements caused by loads distributed over each pile segment using a method proposed by Apsel [Ref. 40]. Kaynia's study indicates that pile spacing and the size of the pile group have pronounced effects on the frequency response of the group.

It is important to remember, however, that all of the above methods are linear. Less significant pile-soil-pile interaction and concentration of forces may occur in real pile foundations due to nonlinear soil behavior.

5.1.5 MODELING OF PILE FOUNDATION IN SASSI

Two methods for modeling of pile foundations have been implemented in SASSI.

The first method is based on specially-derived two and three-dimensional elements. These elements can model closely spaced or sparsely spaced piles and take into account pile-to-pile interaction. The elements can be used for seismic as well as external direct loading. The elements can be used to evaluate this effect of soil non linearity for soil material adjacent to the piles using the equivalent linear method. Battered piles can be modeled. The 2nd method, called the pile impedance method, capable of computing the frequency dependent impedance functions for pile groups. The piles are assumed to be vertical. This method is described in Section 5.5.

5.2 SPECIAL ELEMENTS FOR PILE GROUPS IN THREE DIMENSIONS

A special element which enables one to discretize and analyze soil-pile systems in three dimensions is defined in the following section. In subsequent sections procedures are presented for evaluating the stiffness and mass matrices of this element.

5.2.1 DEFINITION OF THE ELEMENT

The basic idea of the new method is to model the piles in two parts. One part is a beam element with no dimension perpendicular to the pile axis. This part models only the stiffness and the mass of the pile. The other part, the inter-pile element, models the dimension perpendicular to the pile axis and the soil between the piles. The inter-pile elements must be designed such that they can model a general configuration of a pile group such as the one shown in Figure 5.2-1.

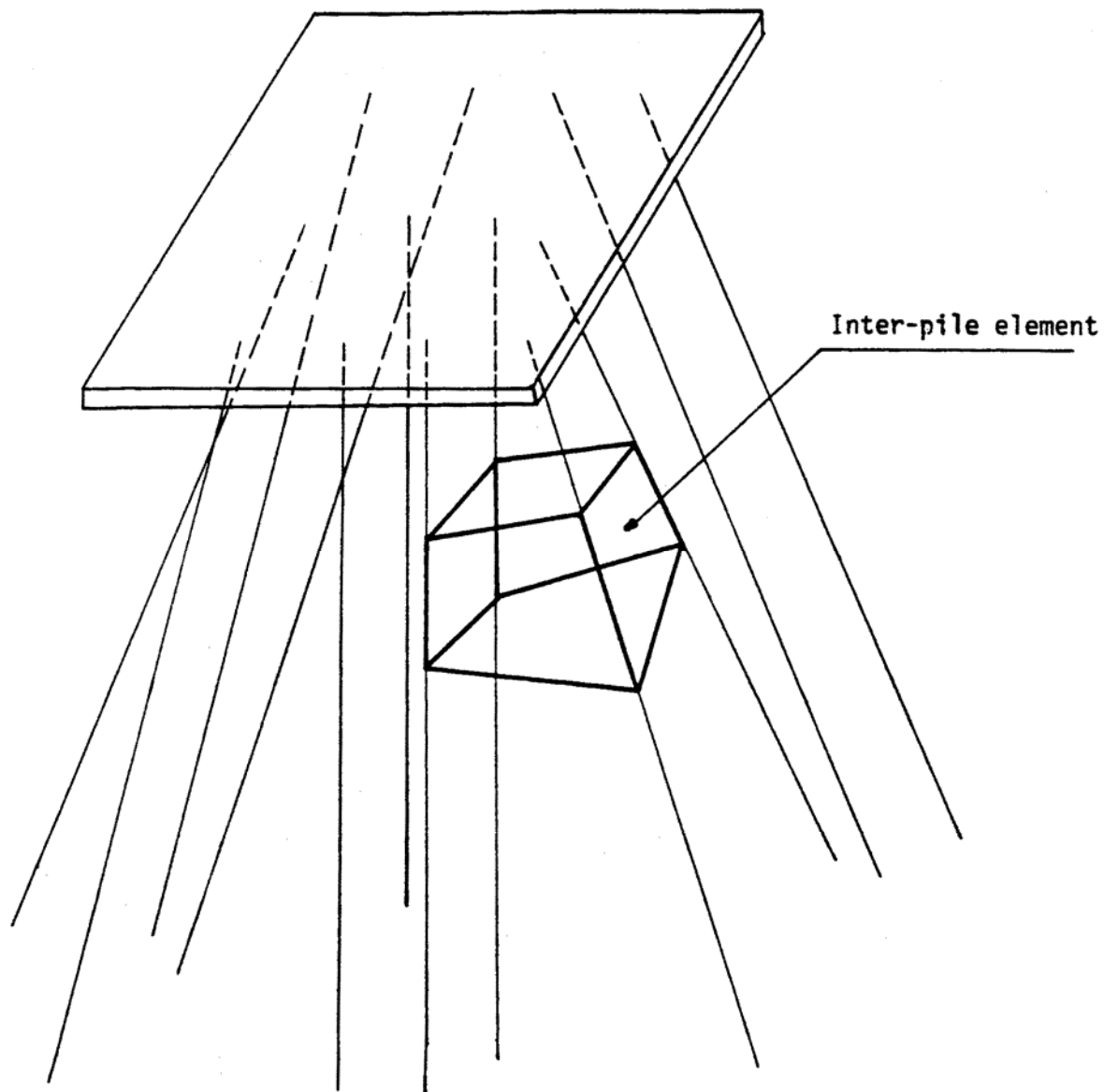


Figure 5.2-1. General Configuration of a Pile Group

The procedures for determining the mass and stiffness matrices of the pile are standard and are presented in Section 5.2.8. The special techniques used to obtain the mass and stiffness matrices of the inter-pile element are new and are discussed following the definition of the inter-pile element.

5.2.2 DEFINITION AND GEOMETRY OF THE INTER-PILE ELEMENT

The geometry of the general inter-pile element is shown in Figure 5.2-2. The element consists of nine parts: Four pile volume zones, each of which represents only part of a pile volume, and five soil parts. An "exploded" view of these parts is shown in Figure 5.2-2. The soil parts of the element behave like solid elements with properties of the soil. The pile volume zones of the element do not have mass and stiffness. They behave in such a manner that planes perpendicular to the pile axes remain plane during the deformation (Navier hypothesis in beam theory). This property, as will be seen, is used to transfer the mass and stiffness matrices of the soil parts of the element to the degrees of freedom defined on the pile axes such that complete compatibility is retained between the pile volume zones and the soil parts of the element.

The basic geometry of the inter-pile element is defined by the coordinates of the eight global corner nodes and the intersection areas of the pile volume zones. The top (t-plane) and bottom (b-plane) of the element are parallel. The detailed geometry of the element is determined as follows:

- 1) Figure 5.2-3 (a) shows a view of the t-plane of a typical element. In this figure, t_1 , t_5 , t_9 and t_{13} are global nodes in the t-plane and the ellipses represent intersection areas of round piles with the t-planes. For each inter-pile element only the shaded areas shown in the figure are considered. These areas must be provided as data and can be determined from the pile cross-sections (which are not necessarily circular) the pile inclinations, and from the angles of the element in the t-plane.

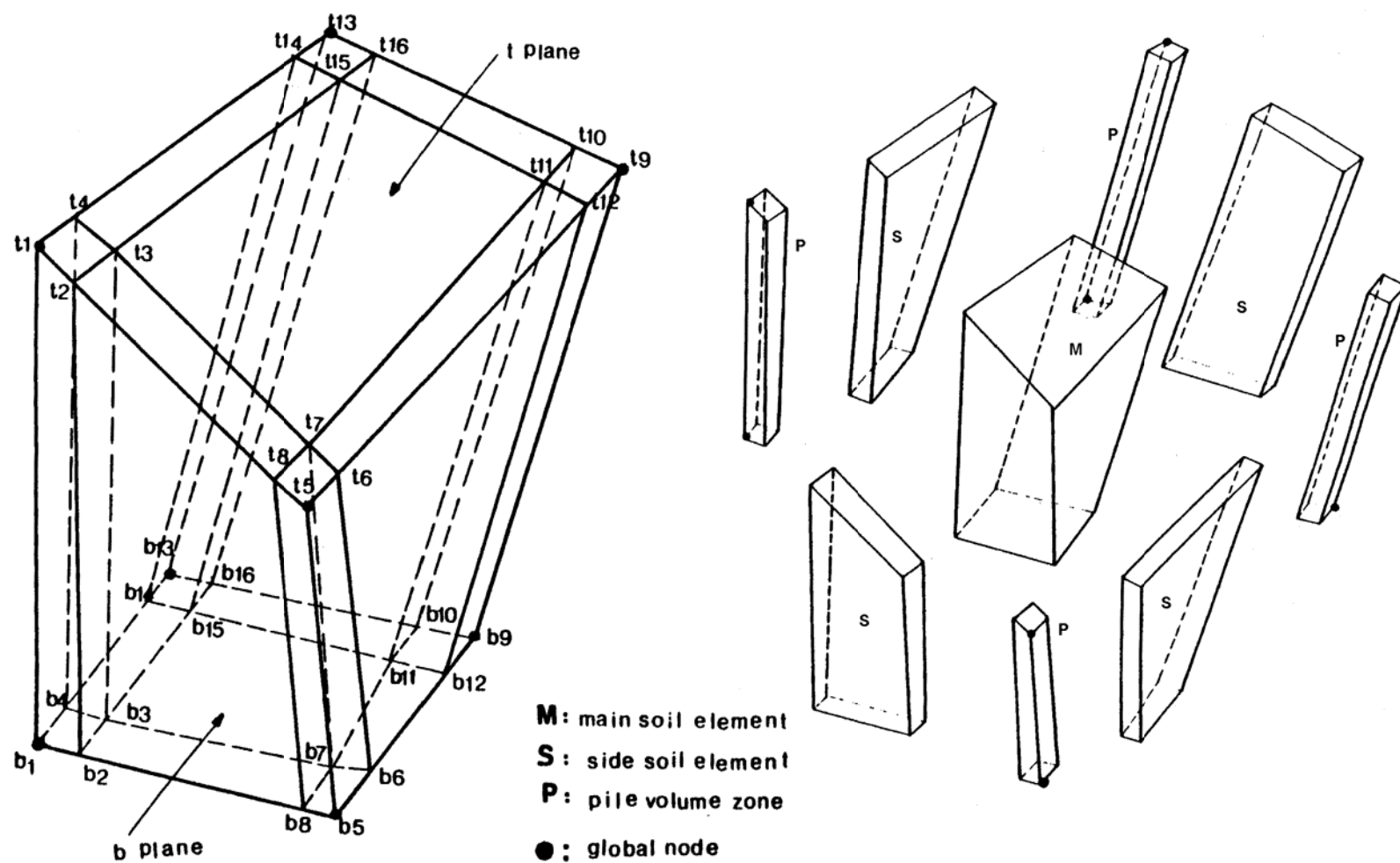


Figure 5.2-2. Three-dimensional Inter-pile Element

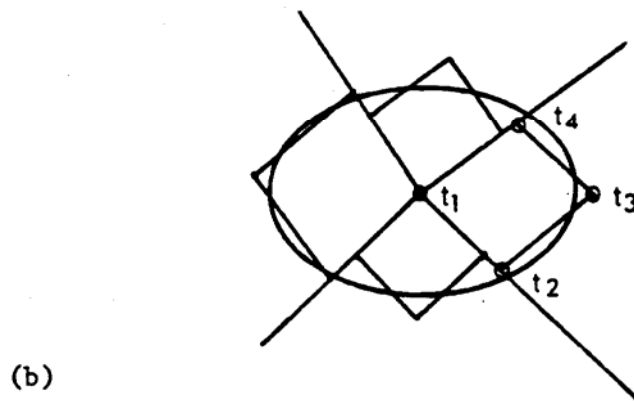
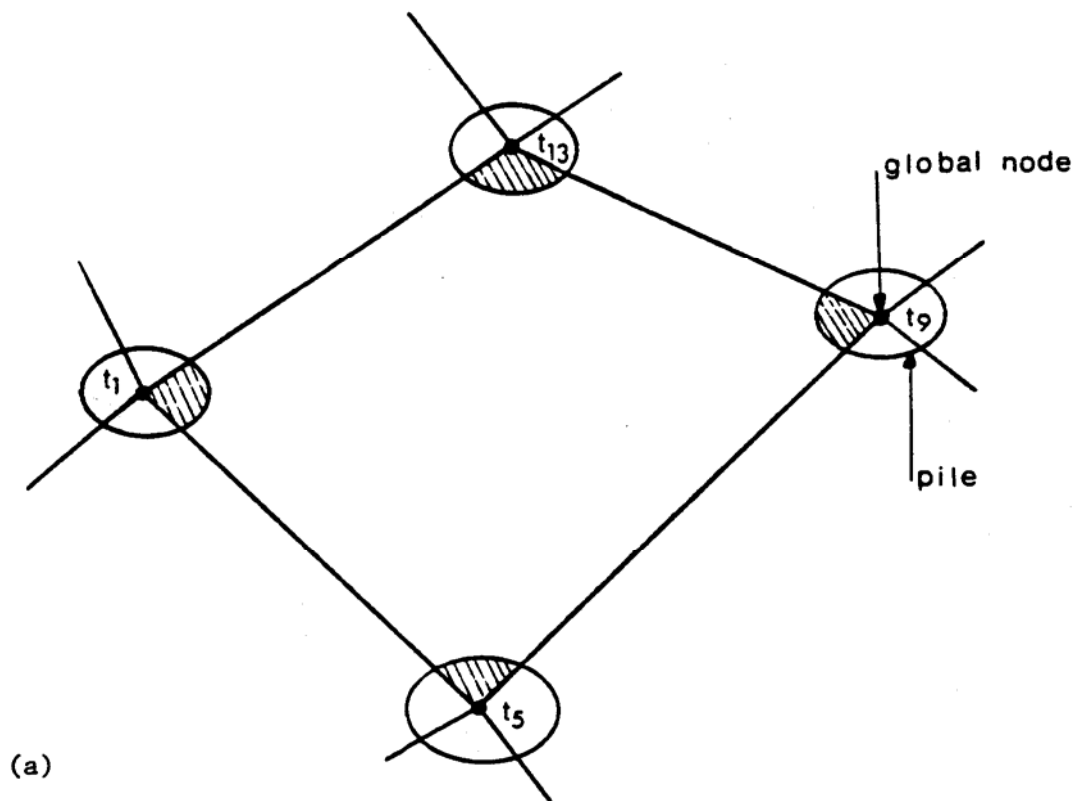


Figure 5.2-3. (a) Plane View of the t-plane, (b) Pile Intersection at Node t_1

- 2) At each global node in the t-plane the intersection area is transformed into an equivalent rhombic area with the sides parallel to the sides of the element. Figure 5.2-3 (b) shows this transformation for the intersection area near Node t_1 . As can be seen from Figure 5.2-3 (b), which also shows the transformation in neighboring elements, the procedure may in some cases lead to a somewhat deformed cross-section. However, for nearly vertical piles and not too distorted element shapes, the transformation will in general lead to only small distortions of the original intersection areas. For regular pile groups with vertical square piles the transformation is an identity transformation, i.e. no distortion is introduced by the transformation. The transformation defines the location of the internal nodes t_2 , t_3 and t_4 . The same procedure is used at the other global nodes in the t-plane and in the b-plane. The whole procedure defines the location of all nodes, t_1, \dots, t_{16} , b_1, \dots, b_{16} , shown in Figure 5.2-2.

- 3) Knowing the coordinates of Nodes b_1 to b_{16} and t_1 to t_{16} shown in Figure 5.2-2, the boundaries between the soil parts and pile volume zones are established. The soil parts of the element consist of one main soil element and four side soil elements. Connecting the nodes counterclockwise and from bottom to top the main soil element is $b_3 b_7 b_{11} b_{15} t_3 t_7 t_{11} t_{15}$ and the four side soil elements are $b_3 b_2 b_8 b_7 t_3 t_2 t_8 t_7$, $b_6 b_{12} b_{11} b_7 t_6 t_{12} t_{11} t_7$, $b_{10} b_{16} b_{15} b_{11} t_{10} t_{16} t_{15} t_{11}$ and $b_4 b_3 b_{15} b_{14} t_4 t_3 t_{15} t_{14}$.

In general the inter-pile element has eight global nodes. Each node may have up to six degrees of freedom (three translations and three rotations). Since the mass and stiffness of the piles is determined using beam theory, the combination of beam and inter-pile elements can model a pile group containing piles with different cross-sectional areas, inclinations, and stiff nesses.

In discretizing soil-pile systems, special configurations of the inter-pile elements, such as those shown in Figure 5.2-4, may occur. For these special cases the method for establishing the geometry of the element is similar to that used for the standard element. However, the number of side soil elements may be reduced depending on the number of pile volume zones of the element. Also, some of the soil elements may become wedge-shaped. The total number of degrees of freedom for these special cases becomes less than 48.

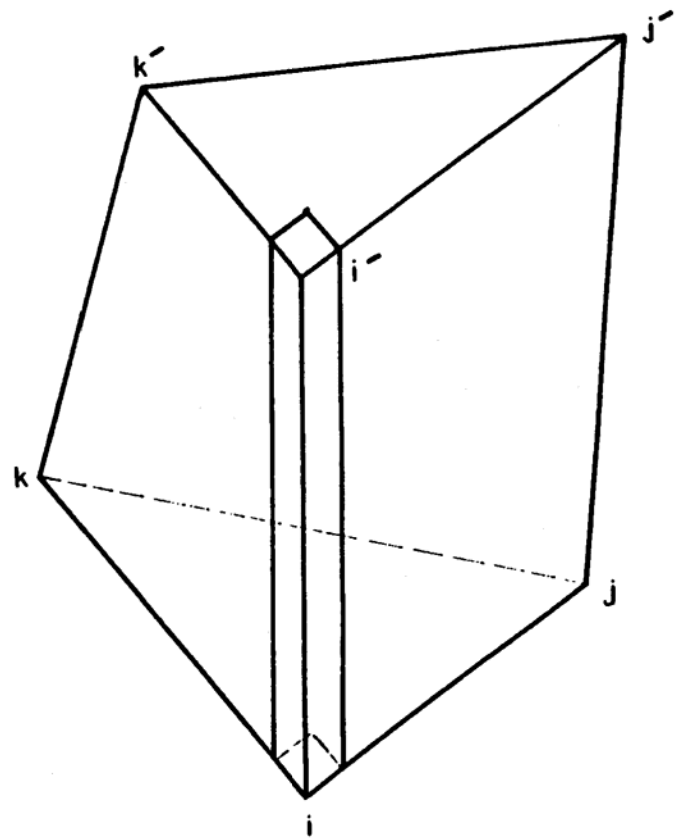
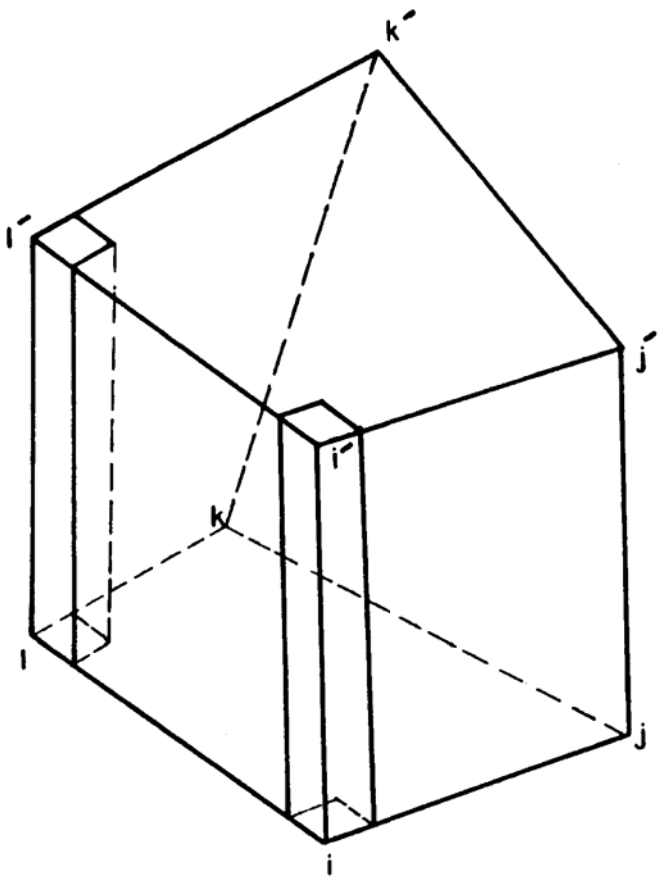


Figure 5.2-4. Special Configurations of the Inter-pile Element

5.2.3 STIFFNESS MATRIX FORMULATION

Piles behave essentially like beams in the ground. Therefore, it can be assumed that planes perpendicular to the pile axis remain rigid during deformation and that, between nodes, the displacements perpendicular to the pile axis vary as a third order polynomial.

In order to retain compatibility between the displacement fields in the pile volume zones and the soil parts of the element (the main and side soil elements), the displacement field in the soil elements must be able to follow the cubic order of variation along the interface to the pile volume zone. This is achieved by allowing four internal nodes on each side of the soil elements. The main and one side soil element with added internal nodes are shown in Figure 5.2-5 (a) and 5.2-5(b), respectively. The internal nodes are located at the corners and at the third-points of the sides of each soil element.

The following conventions are used with respect to the development of the mass and the stiffness matrices of the inter-pile element in three dimensions.

- 1) The global nodes of the element ($t_1, t_5, t_9, t_{13}, b_1, b_5, b_9$ and b_{13}) are indicated by the letters $i, j, k, \ell, i', j', k'$ and ℓ' . The global mass and stiffness matrices of the element will be determined at the degrees of freedom corresponding to these nodes, see Figure 5.2-2.
- 2) The internal nodes of the element are designated by numbers, see Figure 5.2-5. The degrees of freedom at these nodes are used to determine the mass and the stiffness matrices of the main and side soil element at the local level. In special cases such as those shown in Figure 5.2-4, some internal and global nodes coincide.
- 3) $u_x(x,y,z)$, $u_y(x,y,z)$ and $u_z(x,y,z)$ are the displacements of the point (x,y,z) in the x -, y - and z -directions.

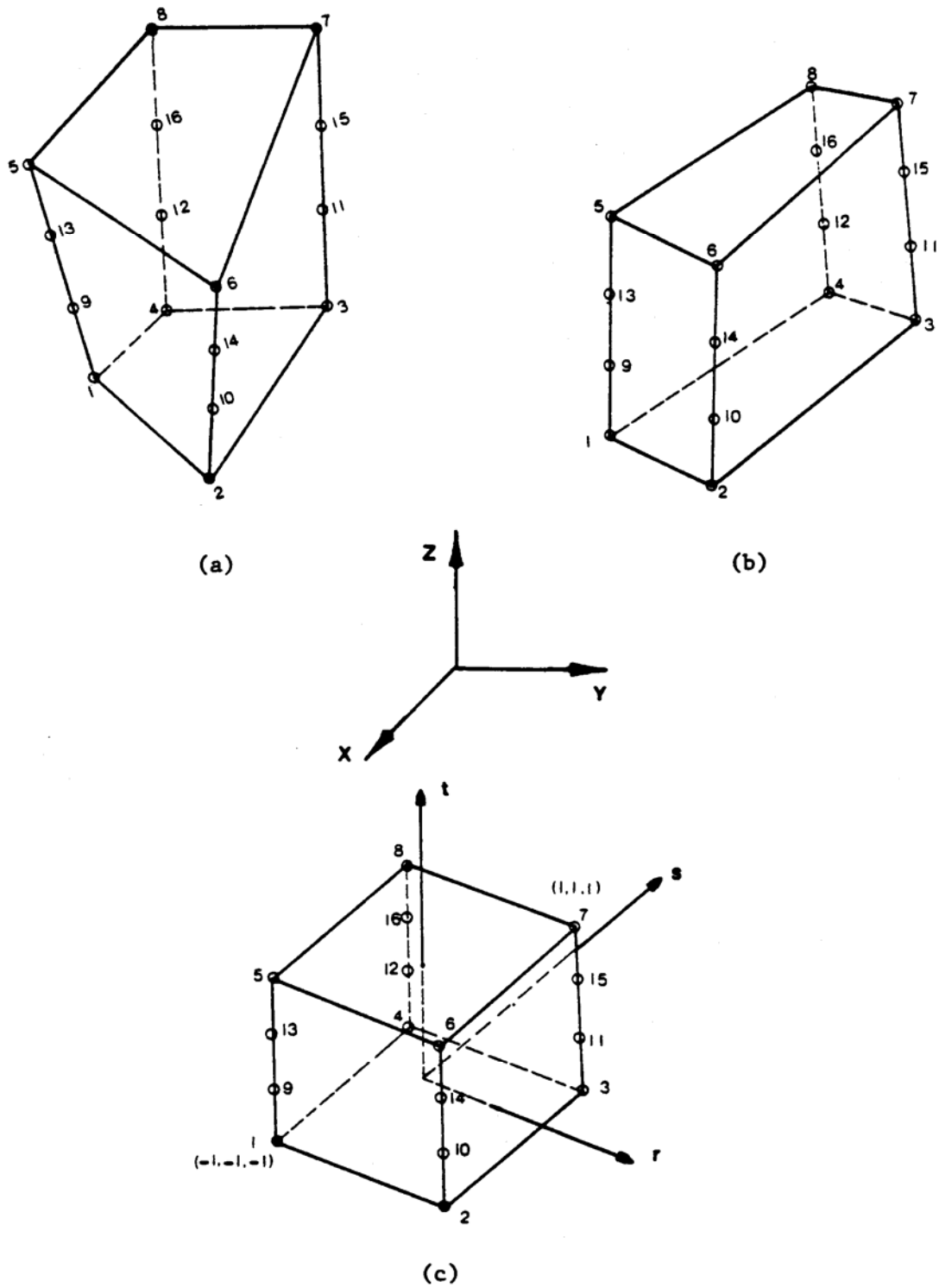


Figure 5.2-5. (a) Main, (b) Side Soil Element in Global Coordinate, and (c) Soil Element in Natural Coordinate System

- 4) u_{xi} , u_{yi} and u_{zi} are the displacements of the internal node i. The corresponding forces are P_{xi} , P_{yi} and P_{zi} .
- 5) U_{xi} , U_{yi} , U_{zi} are the displacements of the global node i in the x-, y- and z-directions, respectively. The corresponding rotations are $U_{\phi i}$, $U_{\eta i}$ and $U_{\theta i}$. The corresponding forces and moments are R_{xi} , R_{yi} , R_{zi} , $R_{\phi i}$, $R_{\eta i}$, and $R_{\theta i}$.

In Section 5.2.5 the relationship between the global displacements U , and the internal displacements u , will be established and the total mass and stiffness matrices will be expressed in terms of the global degrees of freedom.

a. Global and Natural Coordinate Systems

As was discussed earlier using displacement-based finite element analysis, the stiffness of an element can be obtained from the following equation.

$$[K]^m = \int_{V^{(m)}} [B]_{xyz}^{(m)T} [C]^{(m)} [B]_{xyz}^{(m)} dV \quad (5.1)$$

The matrix $[B]_{xyz}^{(m)}$ represents the strain-displacement relationship in Element m. $[C]$ is the matrix which relates stresses to strains. The operations in this equation are performed in a natural coordinate system in which the main and all the side soil elements have the same dimensions. Figure 5.2-5(c) shows a soil element in the natural coordinate system.

The relationship between the two sets of coordinate systems, the global (x, y, z) system, and the natural (r, s, t) system, is defined by

$$x = \sum_{i=1}^8 Q_i(r, s, t) x_i \quad (5.2a)$$

$$y = \sum_{i=1}^8 Q_i(r, s, t) y_i \quad (5.2b)$$

$$x = \sum_{i=1}^8 Q_i(r, s, t) z_i \quad (5.2c)$$

In these equations x_i , y_i and z_i are the coordinates of Node i in the (xyz) systems and

$$Q(1) = 1/8 (1-r) (1-s) (1-t) \quad (5.3a)$$

$$Q(2) = 1/8 (1+r) (1-s) (1-t) \quad (5.3b)$$

$$Q(3) = 1/8 (1+r) (1+s) (1-t) \quad (5.3c)$$

$$Q(4) = 1/8 (1-r) (1+s) (1-t) \quad (5.3d)$$

$$Q(5) = 1/8 (1-r) (1-s) (1+t) \quad (5.3e)$$

$$Q(6) = 1/8 (1+r) (1-s) (1+t) \quad (5.3f)$$

$$Q(7) = 1/8 (1+r) (1+s) (1+t) \quad (5.3g)$$

$$Q(8) = 1/8 (1-r) (1+s) (1+t) \quad (5.3h)$$

b. Displacement Field

Displacements in the (x,y,z) system, (u_x, u_y, u_z) , are related to the nodal displacements (u_{xi}, u_{yi}, u_{zi}) , through the following equations.

$$u_x(x, y, z) = \sum_{i=1}^{16} H_i(r, s, t) u_{xi} \quad (5.4a)$$

$$u_y(x, y, z) = \sum_{i=1}^{16} H_i(r, s, t) u_{yi} \quad (5.4b)$$

$$u_z(x, y, z) = \sum_{i=1}^{16} H_i(r, s, t) u_{zi} \quad (5.4c)$$

Using the numbering system shown in Figure 5.2-5, the mode shapes are defined in the (r, s, t) system as follows.

$$H(1) = Q(1) - 2/3 H(9) - 1/3 H(13) \quad (5.5a)$$

$$H(2) = Q(2) - 2/3 H(10) - 1/3 H(14) \quad (5.5b)$$

$$H(3) = Q(3) - 2/3 H(11) - 1/3 H(15) \quad (5.5c)$$

$$H(4) = Q(4) - 2/3 H(12) - 1/3 H(16) \quad (5.5d)$$

$$H(5) = Q(5) - 2/3 H(13) - 1/3 H(9) \quad (5.5e)$$

$$H(6) = Q(6) - 2/3 H(14) - 1/3 H(10) \quad (5.5f)$$

$$H(7) = Q(7) - 2/3 H(15) - 1/3 H(11) \quad (5.5g)$$

$$H(8) = Q(8) - 2/3 H(16) - 1/3 H(12) \quad (5.5h)$$

$$H(9) = 27/64 (1-r) (1-s) (1-t) (1+t) (1/3 - t) \quad (5.5i)$$

$$H(10) = 27/64 (1+r) (1-s) (1-t) (1+t) (1/3 - t) \quad (5.5j)$$

$$H(11) = 27/64 (1+r) (1+s) (1-t) (1+t) (1/3 - t) \quad (5.5k)$$

$$H(12) = 27/64 (1-r) (1+s) (1-t) (1+t) (1/3 - t) \quad (5.5l)$$

$$H(13) = 27/64 (1-r) (1-s) (1-t) (1+t) (1/3 + t) \quad (5.5m)$$

$$H(14) = 27/64 (1+r) (1-s) (1-t) (1+t) (1/3 + t) \quad (5.5n)$$

$$H(15) = 27/64 (1+r) (1+s) (1-t) (1+t) (1/3 + t) \quad (5.5o)$$

$$H(16) = 27/64 (1-r) (1+s) (1-t) (1+t) (1/3 + t) \quad (5.5p)$$

In the main and side soil elements, the special locations of the internal nodes on the straight sides of the element make it possible to use lower order functions, Q_i , for the transformation from (r, s, t) to (x, y, z) coordinates instead of the functions, H_i , used to define the displacement field. Thus the soil elements are 16-node subparametric elements of the serendipity type which satisfy the conditions of compatibility and completeness [Bathe and Wilson, 1976]. It can be shown that

$$\sum_{i=1}^{16} H_i(r, s, t) = 1 \quad (5.5q)$$

c. Strain-Displacement Relationship

The strain-displacement relationship in the three-dimensional case can be expressed as

$$\{\varepsilon\} = \begin{Bmatrix} \varepsilon_{xx} \\ \varepsilon_{yy} \\ \varepsilon_{zz} \\ \gamma_{xy} \\ \gamma_{xz} \\ \lambda_{yz} \end{Bmatrix} = \begin{bmatrix} \frac{\partial}{\partial x} & 0 & 0 \\ 0 & \frac{\partial}{\partial y} & 0 \\ 0 & 0 & \frac{\partial}{\partial z} \\ \frac{\partial}{\partial y} & \frac{\partial}{\partial x} & 0 \\ \frac{\partial}{\partial z} & 0 & \frac{\partial}{\partial x} \\ 0 & \frac{\partial}{\partial z} & \frac{\partial}{\partial y} \end{bmatrix} \begin{Bmatrix} u_x \\ u_y \\ u_z \end{Bmatrix} \quad (5.6)$$

In order to determine the displacement derivatives in this equation one needs to evaluate the Jacobian

$$[J] = \begin{bmatrix} \frac{\partial x}{\partial r} & \frac{\partial y}{\partial r} & \frac{\partial z}{\partial r} \\ \frac{\partial x}{\partial s} & \frac{\partial y}{\partial s} & \frac{\partial z}{\partial s} \\ \frac{\partial x}{\partial t} & \frac{\partial y}{\partial t} & \frac{\partial z}{\partial t} \end{bmatrix} \quad (5.7)$$

from Eqs. (5.2) and (5.3). The Jacobian satisfies the relation

$$\begin{Bmatrix} \frac{\partial}{\partial r} \\ \frac{\partial}{\partial s} \\ \frac{\partial}{\partial t} \end{Bmatrix} = [J] \begin{Bmatrix} \frac{\partial}{\partial x} \\ \frac{\partial}{\partial y} \\ \frac{\partial}{\partial z} \end{Bmatrix} \quad (5.8)$$

Hence

$$\begin{Bmatrix} \frac{\partial u_x}{\partial x} \\ \frac{\partial u_x}{\partial y} \\ \frac{\partial u_x}{\partial z} \end{Bmatrix} = [J]^{-1} \begin{bmatrix} \frac{\partial H_1}{\partial r} & 0 & 0 & \frac{\partial H_2}{\partial r} & \dots & \frac{\partial H_{16}}{\partial r} & 0 & 0 \\ \frac{\partial H_1}{\partial s} & 0 & 0 & \frac{\partial H_2}{\partial s} & \dots & \frac{\partial H_{16}}{\partial s} & 0 & 0 \\ \frac{\partial H_1}{\partial t} & 0 & 0 & \frac{\partial H_2}{\partial t} & \dots & \frac{\partial H_{16}}{\partial t} & 0 & 0 \end{bmatrix} \{u\} \quad (5.9a)$$

and

$$\begin{Bmatrix} \frac{\partial u_y}{\partial x} \\ \frac{\partial u_y}{\partial y} \\ \frac{\partial u_y}{\partial z} \end{Bmatrix} = [J]^{-1} \begin{bmatrix} 0 & \frac{\partial H_1}{\partial r} & 0 & 0 & \frac{\partial H_2}{\partial r} & \dots & 0 & \frac{\partial H_{16}}{\partial r} \\ 0 & \frac{\partial H_1}{\partial s} & 0 & 0 & \frac{\partial H_2}{\partial s} & \dots & 0 & \frac{\partial H_{16}}{\partial s} \\ 0 & \frac{\partial H_1}{\partial t} & 0 & 0 & \frac{\partial H_2}{\partial t} & \dots & 0 & \frac{\partial H_{16}}{\partial t} \end{bmatrix} \{u\} \quad (5.9b)$$

and

$$\begin{Bmatrix} \frac{\partial u_z}{\partial x} \\ \frac{\partial u_z}{\partial y} \\ \frac{\partial u_z}{\partial z} \end{Bmatrix} = [J]^{-1} \begin{bmatrix} 0 & 0 & \frac{\partial H_1}{\partial r} & 0 & 0 & \frac{\partial H_2}{\partial r} & \dots & 0 & 0 & \frac{\partial H_{16}}{\partial r} \\ 0 & 0 & \frac{\partial H_1}{\partial s} & 0 & 0 & \frac{\partial H_2}{\partial s} & \dots & 0 & 0 & \frac{\partial H_{16}}{\partial s} \\ 0 & 0 & \frac{\partial H_1}{\partial t} & 0 & 0 & \frac{\partial H_2}{\partial t} & \dots & 0 & 0 & \frac{\partial H_{16}}{\partial t} \end{bmatrix} \{u\} \quad (5.9c)$$

where $\{u\}$ is the nodal displacement vector defined as

$$\{u\}^T = \langle u_{x1}, u_{y1}, u_{z1}, u_{x2}, \dots, u_{x16}, u_{y16}, u_{z16} \rangle \quad (5.10)$$

By substitution of Eq. (5.9) into Eq. (5.6) the strains in the element can be expressed in the form

$$\{\varepsilon\} = [B]_{rst} \{u\} \quad (5.11)$$

where the coefficients of B_{rst} are functions of r , s and t . The volume element in Eq. (5.1) is $dV = \det J \, dr \, ds \, dt$. Hence, Eq. (5.1) can be evaluated from

$$[K]^{(m)} = \int_{-1}^1 \int_{-1}^1 \int_{-1}^1 [B]_{rst}^{(m)T} [C]^{(m)} [B]_{rst}^{(m)} \det J \, dt \quad (5.12)$$

where $\det J$ is the determinant of $[J]$.

d. Stress-Strain Relationship

The basic stress-strain relations are those of linear elasticity. For three-dimensional isotropic materials these relations can be expressed as follows:

$$\{\sigma\} = [C] \{\varepsilon\} \quad (5.13)$$

where

$$\{\sigma\}^T = \langle \sigma_{xx} \, \sigma_{yy} \, \sigma_{zz} \, \tau_{xy} \, \tau_{xz} \, \tau_{yz} \rangle \quad (5.14a)$$

$$\{\varepsilon\}^T = \langle \varepsilon_{xx} \, \varepsilon_{yy} \, \varepsilon_{zz} \, \gamma_{xy} \, \gamma_{xz} \, \gamma_{yz} \rangle \quad (5.14b)$$

and

$$[C] = \begin{bmatrix} M & M-2G & M-2G & 0 & 0 & 0 \\ M-2G & M & M-2G & 0 & 0 & 0 \\ M-2G & M-2G & M & 0 & 0 & 0 \\ 0 & 0 & 0 & G & 0 & 0 \\ 0 & 0 & 0 & 0 & G & 0 \\ 0 & 0 & 0 & 0 & 0 & G \end{bmatrix} \quad (5.14c)$$

For viscoelastic materials and harmonic motions M and G are the complex constrained and shear moduli, respectively (see Eq. (2.19)).

e. Numerical Integration

By using Gauss quadrature Eq. (5.12) can be reformulated as follows

$$[K]^{(m)} = \sum_{i=1}^{n_1} \sum_{j=1}^{n_1} \sum_{k=1}^{n_1} [B]_{ijk}^{(m)T} [C]^{(m)} [B]_{ijk}^{(m)} \det \mathbf{J}_{ijk} \alpha_{ijk} \quad (5.15)$$

where (i, j, k) is the Gauss point and α_{ijk} is the corresponding weighting factor. The indices i, j and k correspond to discretization in the r -, s - and t -directions, respectively. The basic idea in Gauss quadrature is that with n properly selected points in the interval of integration, an exact evaluation of the integral is achieved provided the integrand varies as a polynomial of order $(2n-1)$. The integrand in Eq. (5.15) is of higher order in t than in r and s . Hence, the number of points, n_1 , in the r - and s -directions can be chosen smaller than the number n_2 in the t -direction. It has been found that if the shape of the element is not too distorted choosing $n_1=2$ and $n_2=4$ leads to good results.

Following the computation of the stiffness matrix of the main soil element, the stiffness matrices of the four side elements are determined using the same method. Each

stiffness matrix has the dimensions 48 x 48 and has complex terms if soil damping is specified.

5.2.4 MASS MATRIX FORMULATION

It has been found that for most wave propagation analyses the best results are obtained by the use of a mixed mass matrix

$$[M]^{(m)} = \alpha [M^c]^{(m)} + (1 - \alpha) [M^L]^{(m)} \quad (5.16)$$

where $[M^c]^{(m)}$ and $[M^L]^{(m)}$ are the consistent and the lumped mass matrix, respectively. The coefficient α is usually chosen to be equal to 0.50. The consistent mass matrix has been defined by Eq. (2.11b) and it can be evaluated by Gauss-quadrature in a manner very similar to, but simpler, than the one presented for the stiffness matrix above. The lumped mass matrix is a simple diagonal matrix whose terms are obtained by distributing the total mass in proportion to the diagonal terms of the consistent mass matrix.

Following the computation of the mass matrix of the main soil element, the process is repeated for each side soil element. As for the stiffness matrices, all mass matrices for the soil elements have the dimension 48 x 48.

5.2.5 GLOBAL MAIN AND SIDE SOIL ELEMENT MASS AND STIFFNESS MATRICES

The stiffness matrix of the main soil element developed in the previous sections relates the forces $\{P_m\}$ and the displacements $\{u_m\}$ of the internal nodes shown in Figure 5.2-6. The relationship is

$$\{P_m\}_{48 \times 1} = [K_m]_{48 \times 48} \{u_m\}_{48 \times 1} \quad (5.17)$$

In order to develop a similar relationship between the corresponding forces $\{R\}$ and displacements $\{U\}$ at the global nodes i, j, k, l, i', j', k', and l' at the pile centers, a transformation matrix $[A]$ is introduced as follows

$$\{u\}_{96 \times 1} = [A]_{96 \times 48} \{U\}_{48 \times 1} \quad (5.18a)$$

and for the main element alone

$$\{u_m\}_{96 \times 1} = [A_m]_{48 \times 48} \{U\}_{48 \times 1} \quad (5.18b)$$

As will be seen in the following sections, the matrix $[A_m]$ is designed in such a manner that compatibility is retained between the displacements of the main soil element and the pile volume zones of the inter-pile element.

The force systems $\{P_m\}$ and $\{R_m\}$ must be statically equivalent. The equivalence can be expressed in terms of the principle of virtual work as follows

$$\{\bar{U}_m\}^T \cdot \{R_m\} = \{\bar{u}_m\}^T \cdot \{P_m\} \quad (5.19)$$

where $\{\bar{U}_m\}$ and $\{\bar{u}_m\}$ are virtual displacement vectors related through Eq. (5.18b).

Hence by this equation

$$\{\bar{U}_m\}^T \{R_m\} = \{\bar{u}_m\}^T [A_m]^T \{P_m\} \quad (5.20)$$

Since this identity must be true for any virtual displacement vector, $\{\bar{U}_m\}$, this implies, by a theorem from the calculus of variations, that

$$\{R_m\} = [A_m]^T \{P_m\} \quad (5.21)$$

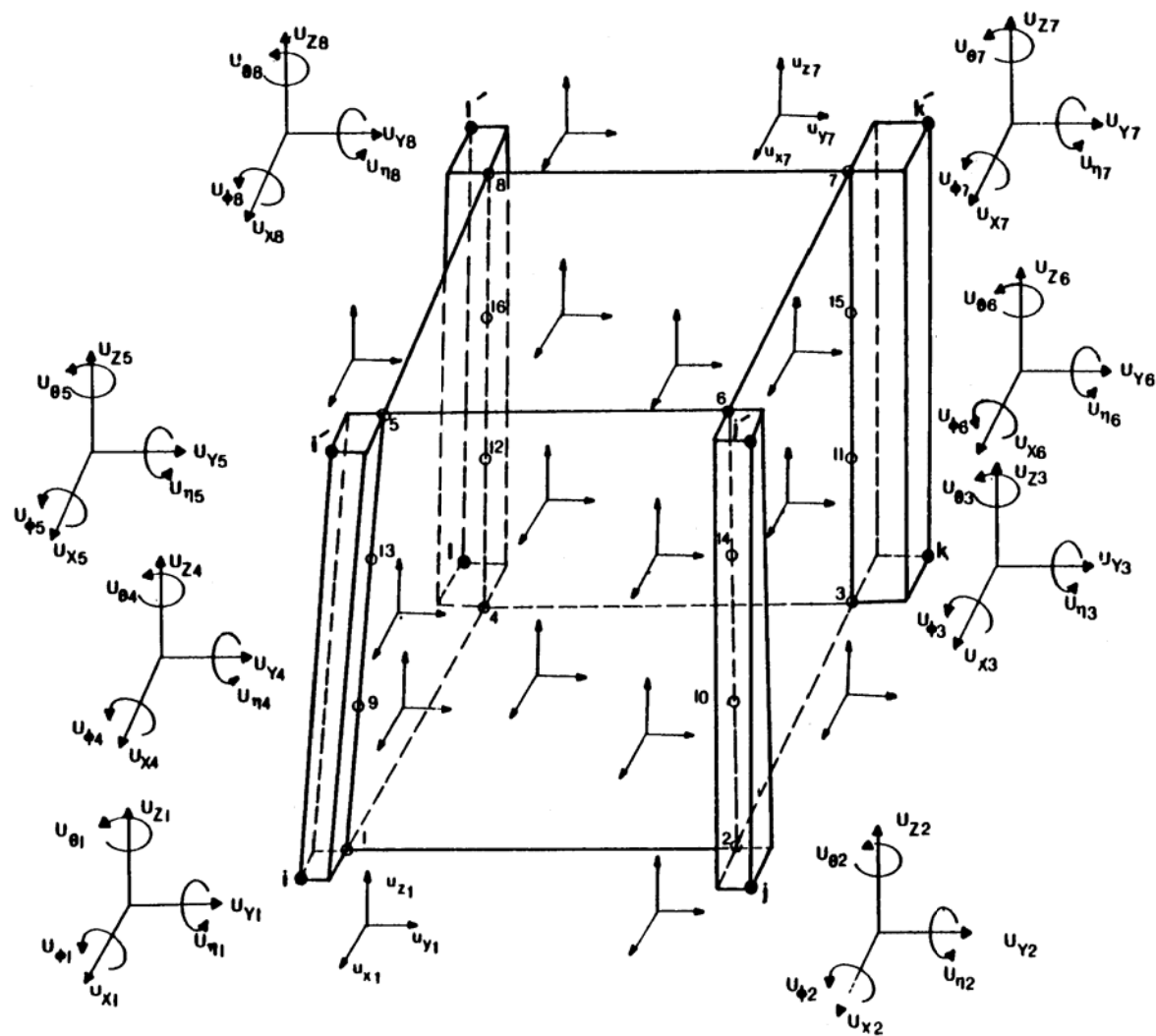


Figure 5.2-6. Degrees of Freedom of Internal and Global Nodes (Main Soil Element)

Substituting for $\{P_m\}$ using Eqs. (5.17) and (5.18b), the equation can be written in the following form

$$\{R_m\} = [K_m^g] \{U_m\} \quad (5.22)$$

where

$$[K_m^g]_{(48 \times 48)} = [A_m]_{(48 \times 48)}^T [K_m]_{(48 \times 48)} [A_m]_{(48 \times 48)} \quad (5.23)$$

The same procedure can be used for the set of accelerations and inertia forces at internal and global nodes of the main soil element to obtain the transferred mass matrix. The resulting mass matrix is

$$[M_m^g]_{(48 \times 48)} = [A_m]_{(48 \times 48)}^T [M_m]_{(48 \times 48)} [A_m]_{(48 \times 48)} \quad (5.24)$$

The procedure can also be used to transfer the mass and stiffness matrices of each side soil element to its global nodes at pile centers. Figure 5.2-7 shows one side soil element located between two pile volume zones with two sets of degrees of freedom in terms of the internal nodes and the global nodes i, j, i' and j' . The stiffness matrix of the side soil element i , $[K_{si}]$ relates the forces $\{P_{si}\}$ and the displacements $\{u_{si}\}$ as follows

$$\{P_{si}\}_{(48 \times 1)} = [K_{si}]_{(48 \times 48)} \{u_{si}\}_{(48 \times 1)} \quad (5.25)$$

The transformation matrix $[A_{si}]$ for the side soil element i is now defined such that the following relations hold:

$$\{U_{si}\}_{(48 \times 1)} = [A_{si}]_{(48 \times 24)} \{u_i\}_{(24 \times 1)} \quad (5.26)$$

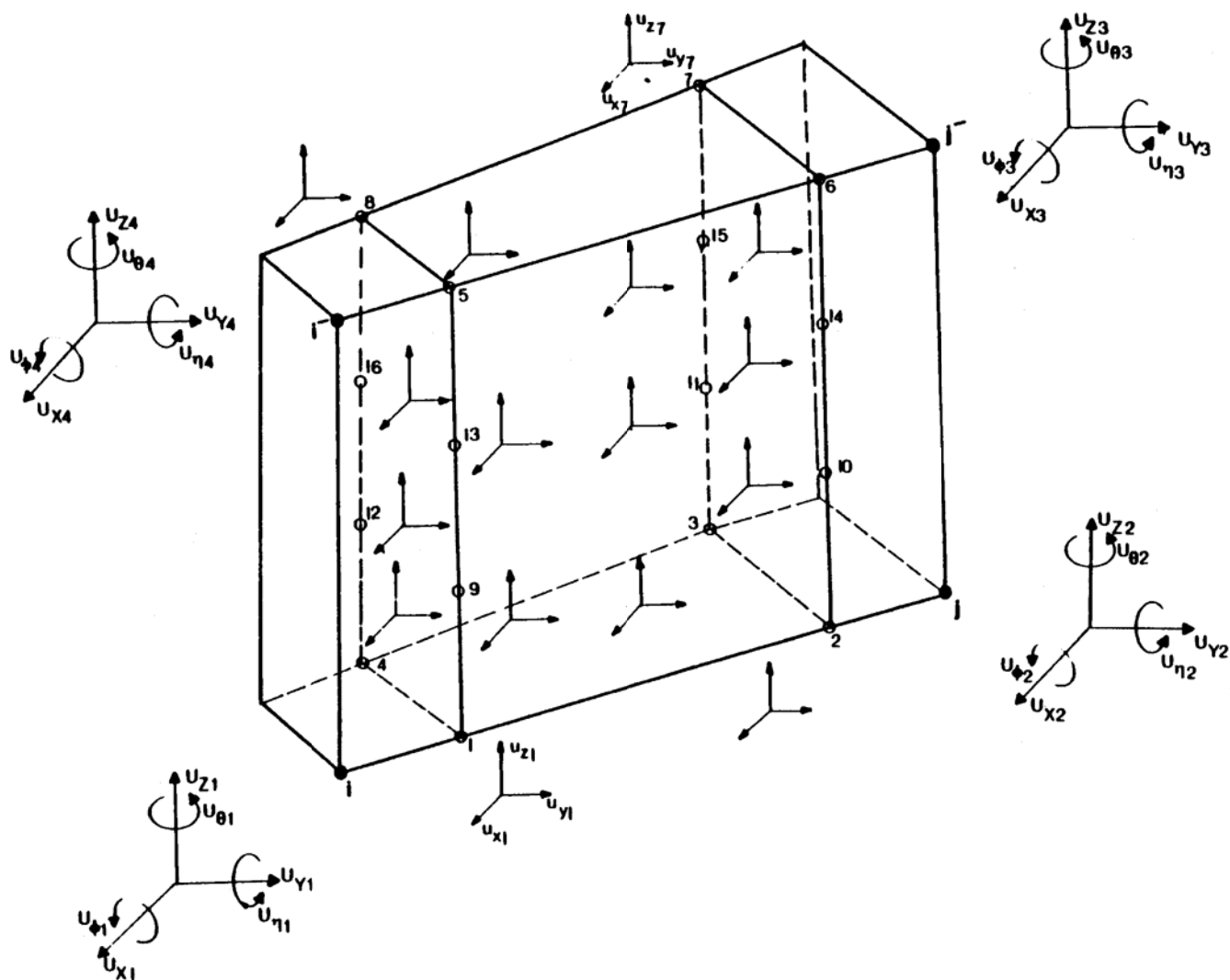


Figure 5.2-7. Degrees of Freedom of Internal and Global Nodes (Side Soil Element)

The displacements $\{U_i\}$ and the corresponding forces $\{R_i\}$ are parts of the global displacements $\{U\}$ and forces $\{R\}$, respectively, which correspond to the global nodes of the pile volume zones of the side soil element i . The relationship between two sets of forces is

$$\{R_i\}_{(24 \times 1)} = [A_{si}]_{(24 \times 48)}^T \{P_{si}\}_{(48 \times 1)} \quad (5.27)$$

Using the same steps discussed above one can write

$$\{R_i\} = [K_{si}^g] \{U_i\} \quad (5.28)$$

where

$$[K_{si}^g]_{(24 \times 24)} = [A_{si}]_{(24 \times 48)}^T [K_{si}]_{(48 \times 48)} [A_{si}]_{(48 \times 24)} \quad (5.29)$$

Similarly, the transferred mass matrix of the side soil element i is

$$[M_{si}^g]_{(24 \times 24)} = [A_{si}]_{(24 \times 48)}^T [M_{si}]_{(48 \times 48)} [A_{si}]_{(48 \times 24)} \quad (5.30)$$

The transferred mass and stiffness matrices of the side element i are assembled with the corresponding matrices of the main soil element. The computational steps discussed above are similarly repeated to consider all side soil elements.

The key factor in transferring the mass and stiffness matrices is the matrix A which is determined in the next section. However, the numerical operations in Eqs. (5.23), (5.24), (5.29) and (5.30) can be reduced significantly by performing these operations only on non-zero elements of the sparse matrix A . Thus only the non-zero elements of matrix A with an array to allocate their locations need to be stored.

5.2.6 DEVELOPMENT OF THE TRANSFORMATION MATRIX [A]

In order to retain compatibility between the displacement fields in the pile volume zones and soil parts of the inter-pile element, four internal nodes were introduced along each side of the soil element. With four nodes along the edge the soil elements can follow the cubic order of variation of displacements along the interface to the pile volume zone. Therefore, the transformation matrix [A] can be designed such that it is guaranteed that the internal nodes remain attached to the pile volume zones during deformations.

Equations (5.18) and (5.26) express the relations between the two sets of displacements defined at the internal and the global nodes. In order to determine the elements of matrix [A], e.g. the elements in Column i, the equations are rewritten in the following form:

$$\begin{Bmatrix} u_{x1} \\ u_{y1} \\ u_{z1} \\ \vdots \\ u_{x16} \\ u_{y16} \\ u_{z16} \end{Bmatrix} = \begin{bmatrix} A(1,1) & A(1,i) & A(1,j) \\ \cdot & \cdot & \cdot \\ \cdot & \cdot & \cdot \\ \cdot & \cdot & \cdot \\ \cdot & \cdot & \cdot \\ \cdot & \cdot & \cdot \\ \cdot & \cdot & \cdot \\ A(48,1) & A(48,i) & A(48,j) \end{bmatrix} \begin{Bmatrix} 0 \\ 0 \\ \vdots \\ 1 \\ 0 \\ \vdots \\ 0 \end{Bmatrix} \quad (5.31)$$

where j is 48 or 24 depending on the size of the transformation matrix (for the main and side soil element). Equation (5.31) simply states that the elements of Column i of matrix [A] are the displacements of the internal nodes created by a unit displacement of the global degree of freedom i while the remaining global degrees of freedom are kept fixed.

Hence, matrix [A] can be constructed- by successively imposing a unit displacement for every global degree of freedom and computing the displacements of the internal nodes.

Consider a pile volume zone of an element such as the one shown in Figure 5.2-8 with the two global nodes i and i'. The nodes b and t are located at the third points of the line ii' on the pile axis. A unit displacement of the global node (i or i') creates a known deformed shape of the axis of the pile (ii'). Since it is assumed that planes perpendicular to the pile axis remain rigid during the deformation, the displacements of the internal nodes on the pile volume zone perimeter can be determined from the knowledge of the deformed shape of the axis ii' and the distance of the internal nodes from the axis. It should be noted, however, that the global degrees of freedom at the global nodes are defined in the global (xyz) system and this system does not generally coincide with the principal axes of the pile. Thus, any unit displacement of a global degree of freedom needs to be considered in terms of its components along the principal axes of the pile.

Let the pile volume zone have the principal axes 1, 2 and 3, shown in Figure 5.2-8, and let

$$\hat{T}_s = \{T_{1s}, T_{2s}, T_{3s}\}, \quad s = 1, 2, 3 \quad (5.32)$$

be unit vectors on these axes. Then, according to a standard method, the relationship between displacements in the two coordinate systems is:

$$\{\delta_i\} = [T] \{U_i\} \quad (5.33)$$

where

$$\{\delta_i\}^T = \{\delta_{i'1}, \delta_{i'2}, \delta_{i'3}, \delta_{i'4}, \delta_{i'5}, \delta_{i'6}\} \quad (5.34)$$

are the displacements in the local (1,2,3) coordinate system and

$$\{U_i\}^T = \{U_{i'x}, U_{i'y}, U_{i'z}, U_{i'\phi}, U_{i'\eta}, U_{i'\theta}\} \quad (5.35)$$

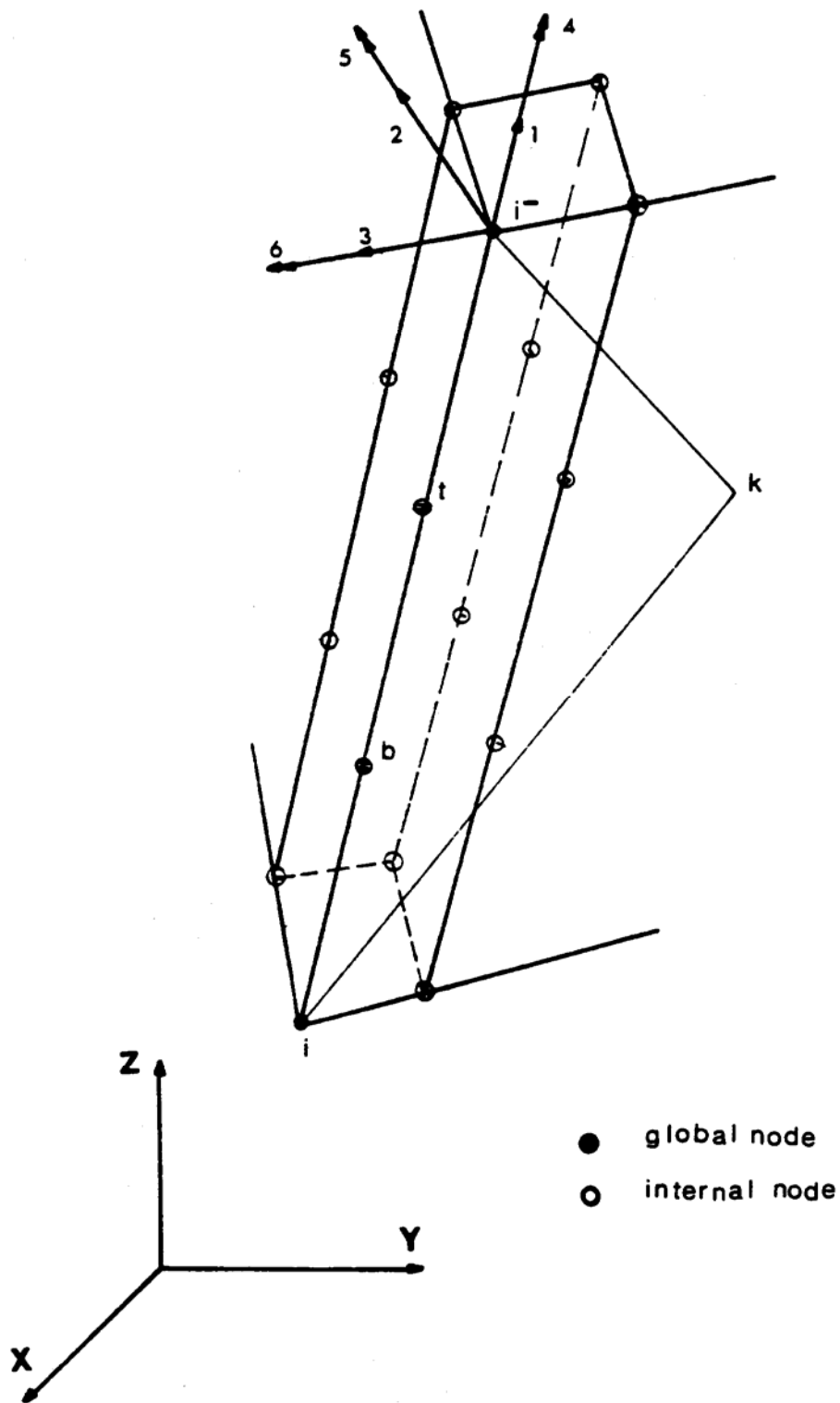


Figure 5.2-8. Pile Volume Zone, Principal Axes and Global Coordinate System

are the displacements in the global (x,y,z) coordinate system. In both Eq. (5.34) and Eq. (5.35) the first three components of the vector are translations and the last three are rotations. The above relations were written out only for Node i but are in fact valid for all nodes.

The transformation matrix $[T]$, which has the property $[T]^{-1} = [T]^T$, can be formed from the components of the unit vectors in Eq. (5.32) as follows:

$$[T] = \begin{bmatrix} T_{11} & T_{12} & T_{13} & 0 & 0 & 0 \\ T_{21} & T_{22} & T_{23} & 0 & 0 & 0 \\ T_{31} & T_{32} & T_{33} & 0 & 0 & 0 \\ 0 & 0 & 0 & T_{11} & T_{12} & T_{13} \\ 0 & 0 & 0 & T_{21} & T_{22} & T_{23} \\ 0 & 0 & 0 & T_{31} & T_{32} & T_{33} \end{bmatrix} \quad (5.36)$$

For computational convenience the principal axes of the pile volume zone are defined by introducing an auxiliary node k in the 1,3-plane (see Figure 5.2-8). Once this node has been defined (by entering its x,y,z coordinates as data), the unit vectors in Eq. (5.32) can be computed as follows:

$$\hat{T}_1 = \widehat{ii'} / |ii'| \quad (5.37a)$$

$$\hat{T}_2 = \widehat{ii' \times ik} / |ii' \times ik| \quad (5.37b)$$

$$\hat{T}_3 = \hat{T}_1 \times \hat{T}_2 \quad (5.37c)$$

Keeping Node i fixed and introducing the condition of third order variation of displacements along the pile axis, the local displacements of Node b can be shown to be

$$\{\delta_b\}_{(123)} = [C]_{bi'} \{\delta_{i'}\}_{(123)} \quad (5.38)$$

where

$$\{\delta_b\}^T = \langle \delta_{b1}, \delta_{b2}, \dots, \delta_{b6} \rangle \quad (5.39a)$$

$$\{\delta_{i'}\}^T = \langle \delta_{i'1}, \delta_{i'2}, \dots, \delta_{i'6} \rangle \quad (5.39b)$$

and

$$[C]_{bi'} = \begin{bmatrix} 1/3 & 0 & 0 & 0 & 0 & 0 \\ 0 & 7/27 & 0 & 0 & 0 & -4/27^\ell \\ 0 & 0 & 7/27 & 0 & 4/27^\ell & 0 \\ 0 & 0 & 0 & 1/3 & 0 & 0 \\ 0 & 0 & -2/3^\ell & 0 & -1/3 & 0 \\ 0 & 2/3^\ell & 0 & 0 & 0 & -1/3 \end{bmatrix} \quad (5.40)$$

where ℓ is the length ii'.

The expression for the displacements of Node t is similarly

$$\{\delta_t\}_{(123)} = [C]_{ti'} \{\delta_{i'}\}_{(123)} \quad (5.41)$$

where

$$[C]_{ti'} = \begin{bmatrix} 2/3 & 0 & 0 & 0 & 0 & 0 \\ 0 & 20/27 & 0 & 0 & 0 & -8/27 \ell \\ 0 & 0 & 20/27 & 0 & 8/27 \ell & 0 \\ 0 & 0 & 0 & 2/3 & 0 & 0 \\ 0 & 0 & -2/3 \ell & 0 & 0 & 0 \\ 0 & 2/3 \ell & 0 & 0 & 0 & 0 \end{bmatrix} \quad (5.42)$$

Substituting for $\{\delta_r\}$ from Eq. (5.33) into Eqs. (5.38) and (5.41) results in

$$\{\delta_b\}_{(123)} = [C]_{bi'} [T] \{u_r\}_{(xyz)} \quad (5.43)$$

$$\{\delta_t\}_{(123)} = [C]_{ti'} [T] \{u_r\}_{(xyz)} \quad (5.44)$$

Since Eq. (5.33) is in fact valid for all nodes, we can also write

$$\{\delta_b\}_{(123)} = [T] \{u_b\}_{(xyz)} \quad \text{or} \quad \{u_b\} = [T]^T \{\delta_b\} \quad (5.45)$$

$$\{\delta_t\}_{(123)} = [T] \{u_t\}_{(xyz)} \quad \text{or} \quad \{u_t\} = [T]^T \{\delta_t\} \quad (5.46)$$

Substituting for $\{\delta_b\}$ and $\{\delta_t\}$ from Eqs. (5.38) and (5.41) respectively, it follows that

$$\{u_b\}_{(xxz)} = [T]^T [C]_{bi'} [T] \{u_r\}_{(xyz)} \quad (5.47)$$

$$\{u_t\}_{(xzz)} = [T]^T [C]_{ti'} [T] \{u_r\}_{(xyz)} \quad (5.48)$$

Equations (5.47) and (5.48) express the relationship between the translations and the rotations of the nodes (b, i') and (t, i') in the global (xyz) system while Node i is kept fixed.

Similar expressions can be obtained for the nodes (b, i) and (t, i) while Node i' is kept fixed. These expressions are as follows.

$$\{u_b\}_{(xyz)} = [T]^T [C]_{bi} [T] \quad (5.49)$$

and

$$\{u_t\}_{(xyz)} = [T]^T [C]_{ti} [T] \quad (5.50)$$

where

$$[C]_{bi} = \begin{bmatrix} \frac{2}{3} & 0 & 0 & 0 & 0 & 0 \\ 0 & \frac{20}{27} & 0 & 0 & 0 & -\frac{8}{27}\ell \\ 0 & 0 & \frac{20}{27} & 0 & -\frac{8}{27}\ell & 0 \\ 0 & 0 & 0 & \frac{2}{3} & 0 & 0 \\ 0 & 0 & \frac{2}{3}\ell & 0 & 0 & 0 \\ 0 & -\frac{2}{3}\ell & 0 & 0 & 0 & 0 \end{bmatrix} \quad (5.51)$$

and

$$[C]_{ti} = \begin{bmatrix} 1/3 & 0 & 0 & 0 & 0 & 0 \\ 0 & 7/27 & 0 & 0 & 0 & 4/27 \ell \\ 0 & 0 & 7/27 & 0 & -4/27 \ell & 0 \\ 0 & 0 & 0 & 1/3 & 0 & 0 \\ 0 & 0 & 2/3 \ell & 0 & -1/3 & 0 \\ 0 & -2/3 \ell & 0 & 0 & 0 & -1/3 \end{bmatrix} \quad (5.52)$$

Using the method described above the displacements of the nodes i, i', b and t on the pile axis created by a unit displacement of each global degree of freedom may be computed.

Since the soil parts of the element are connected not to Nodes i, b, t and i' on the pile axis but to the internal nodes denoted by the numbers 1 to 16 in Figures 5.2-6 and 5.2-7, the translations of these nodes for unit displacements of the global nodes i and i' must be computed. This can be done by the formulas

$$u_x = \delta_{bx} + \eta_b(z - z_b) - \theta_b(y - y_b) \quad (5.53a)$$

$$u_y = \delta_{by} - \phi_b(z - z_b) + \theta_b(y - y_b) \quad (5.53b)$$

$$u_z = \delta_{bz} - \eta_b(x - x_b) + \theta_b(y - y_b) \quad (5.53c)$$

which imposes the condition that planes perpendicular to the pile axis remain plane during deformation. In these formulas (x_b, y_b, z_b) are the coordinates of Node b and δ_{bx} , δ_{by} , δ_{bz} , ϕ_b , η_b and θ_b are the displacements of that node. Similar formulas can be developed for the internal nodes in the plane containing Node t.

Following the above procedure the translations of all internal nodes of the element can be related to the displacements of the global nodes, i.e. the coefficients of the matrices $[A_m]$ and $[A_{si}]$ in Eqs. (5.23) and (5.29) can be computed.

5.2.7 MODIFICATION OF THE TRANSFORMATION MATRIX

The method for computing the stiffness and mass matrices of the main and side soil elements presented above is also used for the special configuration of the inter-pile element shown in Figure 5.2-4. Thus, internal nodes are also used along those sides of the element where no pile volume zone exists. The corresponding global nodes have only translational degrees of freedom and the variation of the displacement field between them is linear. Thus the matrices $[C]$ in Eqs. (5.40), (5.42), (5.51) and (5.52) can be determined by the condition that a unit displacement of a global degree of freedom must create a linear displacement along the side of the element. The rotational degrees of freedom at these nodes do not create any displacement. Modification of the matrices $[C]$ reflect the above results in new transformation matrices $[A_m]$ and $[A_{si}]$. The resulting transferred mass and stiffness matrices thus correspond to elements for which the displacement field varies linearly along edges where no pile volume zones are present and have a cubic variation along edges which are connected to a pile volume zone.

5.2.8 MASS AND STIFFNESS MATRICES OF THE PILE

As was discussed in Section 5.2.1, the mass and stiffness matrices of the piles are determined using beam theory. For the pile segment shown in Figure 5.2-9 these matrices are determined in the local (1,2,3) system from Eqs. (5.55) and (5.56), shown in Tables 5.1 and 5.2. In these equations ρ is the mass density, ℓ , is the length of the pile segment, A_1 is the axial area, and A_2 and A_3 are the shear areas associated with the principal directions 2 and 3, respectively. A_{11} , A_{22} and A_{33} are the moment of inertia in corresponding directions. E and G are the complex Young's and shear moduli, respectively, and

$$\psi_1 = \frac{GEA_{33}A_2}{\ell^2 G} \quad (3.54a)$$

$$\psi_2 = \frac{GEA_{22}A_3}{\ell^2 G} \quad (5.54b)$$

$[K_p]_{(123)}$ and $[M_p]_{(123)}$ are transferred to the global coordinate system using matrix $[T]$ in Eq. (5.36).

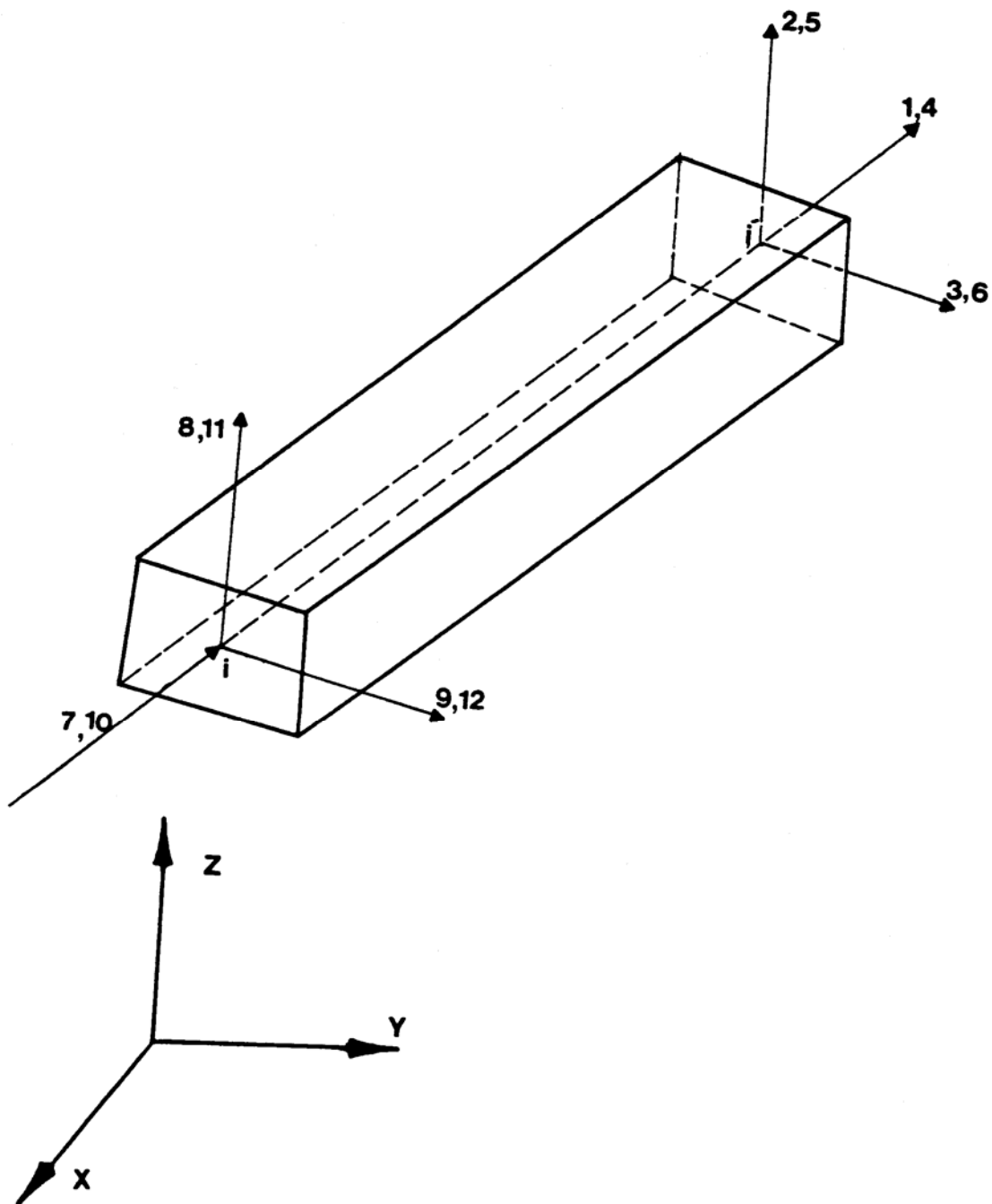


Figure 5.2-9. Pile Segment in Local Coordinate

$[M_p] =$

$\frac{\rho A_1 L}{3}$												
0	$\frac{12\rho A_1 L}{35} + \frac{12\rho A_{22}}{L}$											
0	0	$\frac{12\rho A_1 L}{105} + \frac{12\rho A_{22}}{L}$										
0	0	0	$\frac{\rho A_{11}}{3}$									
0	0	$\frac{12\rho A_1 L^2}{210} + \frac{\rho A_{22}}{10}$	0	$\frac{\rho A_1 L^3}{105} + \frac{\rho A_{22}}{7.5}$					SYMMETRIC			
0	$\frac{12\rho A_1 L^2}{210} + \frac{\rho A_{33}}{10}$	0	0	0	$\frac{\rho A_1 L^3}{105} + \frac{\rho A_{33}}{7.5}$							
$\frac{\rho A_1 L}{6}$	0	0	0	0	0	$\frac{\rho A_1 L}{3}$						
0	$\frac{\rho A_1 L}{70} - \frac{12\rho A_{33}}{L}$	0	0	0	$\frac{12\rho A_1 L^2}{420} - \frac{\rho A_{33}}{10}$	0	$\frac{12\rho A_1 L}{105} + \frac{12\rho A_{33}}{L}$					
0	0	$\frac{\rho A_1 L}{70} - \frac{12\rho A_{22}}{L}$	0	$\frac{12\rho A_1 L^2}{420} + \frac{\rho A_{22}}{10}$	0	0	0	$\frac{12\rho A_1 L}{105} + \frac{12\rho A_{22}}{L}$				
0	0	0	$\frac{\rho A_{11}}{6}$	0	0	0	0	0	$\frac{A_{11}}{3}$			
0	0	$\frac{12\rho A_1 L^2}{420} - \frac{\rho A_{22}}{10}$	0	$\frac{\rho A_1 L^3}{140} - \frac{\rho A_{22}}{30}$	0	0	0	$\frac{12\rho A_1 L^2}{210} + \frac{\rho A_{22}}{10}$	0	$\frac{\rho A_1 L^3}{105} + \frac{\rho A_{22}}{7.5}$		
0	$\frac{12\rho A_1 L^2}{420} + \frac{\rho A_{33}}{10}$	0	0	0	$\frac{\rho A_1 L^3}{140} + \frac{\rho A_{33}}{30}$	0	$\frac{12\rho A_1 L^2}{210} - \frac{\rho A_{33}}{10}$	0	0	0	$\frac{\rho A_1 L}{3}$	

Table 5-1. Equation (3.55)

$[K_p] =$

$\frac{EA_1}{L}$												
0	$\frac{12EA_{22}}{(1+2\phi_1)L^3}$											
0	0	$\frac{12EA_{22}}{(1+2\phi_2)L^3}$										
0	0	0	$\frac{GA_{11}}{L}$									
0	0	$\frac{6EA_{22}}{(1+2\phi_1)L^2}$	0	$\frac{4EA_{22}(1+.5\phi_2)}{(1+2\phi_2)L}$					SYMMETRIC			
0	$\frac{6EA_{22}}{(1+2\phi_1)L^2}$	0	0	0	$\frac{6EA_{22}(1+.5\phi_1)}{(1+2\phi_1)L}$							
$-\frac{EA_1}{L}$	0	0	0	0	0	$\frac{EA_1}{L}$						
0	$\frac{12EA_{22}}{(1+2\phi_1)L^3}$	0	0	0	$\frac{6EA_{22}(1+.5\phi_1)}{(1+2\phi_1)L}$	0	$\frac{12EA_{22}}{(1+2\phi_1)L^3}$					
0	0	$\frac{12EA_{22}}{(1+2\phi_2)L^3}$	0	$\frac{6EA_{22}}{(1+2\phi_2)L^2}$	0	0	0	$\frac{12EA_{22}}{(1+2\phi_2)L^3}$				
0	0	0	$-\frac{GA_{11}}{L}$	0	0	0	0	0	$\frac{GA_{11}}{L}$			
0	0	$\frac{6EA_{22}}{(1+2\phi_2)L^2}$	0	$\frac{4EA_{22}(1+.5\phi_1)}{(1+2\phi_1)L}$	0	0	0	$\frac{6EA_{22}}{(1+2\phi_2)L^2}$	0	$\frac{6EA_{22}(1+.5\phi_2)}{(1+2\phi_2)L}$		
0	$\frac{6EA_{22}}{(1+2\phi_1)L^2}$	0	0	0	$\frac{4EA_{22}(1+.5\phi_2)}{(1+2\phi_2)L}$	0	$\frac{6EA_{22}}{(1+2\phi_1)L^2}$	0	0	0	$\frac{6EA_{22}(1+.5\phi_1)}{(1+2\phi_1)L}$	

Table 5-2. Equation (3.56)

5.3 SPECIAL ELEMENTS FOR PILE GROUPS IN TWO DIMENSIONS

Certain pile groups may be analyzed in two dimensions by assuming that a pile row behaves like a continuous wall. The special finite element defined below facilitates this type of analysis. Procedures for evaluating the stiffness and mass matrices of the element are presented in subsequent sections.

5.3.1 DEFINITION OF THE ELEMENT

As for the three-dimensional case, the basic idea is to model the piles in two parts. One part is the beam element with no dimension perpendicular to the pile axis. This part models only the stiffness and the mass of the pile row. The other part, the inter-pile element, models the dimension perpendicular to the pile axis and the soil between the piles.

Since the procedure for computing the mass and stiffness of the piles in two dimensions is very similar to, but simpler than, the one presented in Section 5.2.8, they are not discussed for this case. The techniques employed to determine the mass and stiffness of the inter-pile element are explained following the definition of the element.

5.3.2 DEFINITION AND GEOMETRY OF THE INTER-PILE ELEMENT

The geometry of the general inter-pile element is shown in Figure 5.3-1. The element consists of three parts. Two pile area zones, each of which represents half of the pile width, and one soil part. As shown in Figure 5.3-1, the global nodes of the element are located at the pile axes. Each node may have up to three degrees of freedom (two translations and one rotation). The soil part of the element is in general a quadrilateral and behaves like a solid element with the properties of the soil. The pile area zones of the elements may have different widths and inclinations and they do not have mass and stiffness. As for the three-dimensional case, these parts behave in such a manner that planes perpendicular to the pile axes remain planes during the deformation. This property will similarly be used to transfer the mass and stiffness matrices of the soil part of the element to the degrees of freedom at the global nodes.

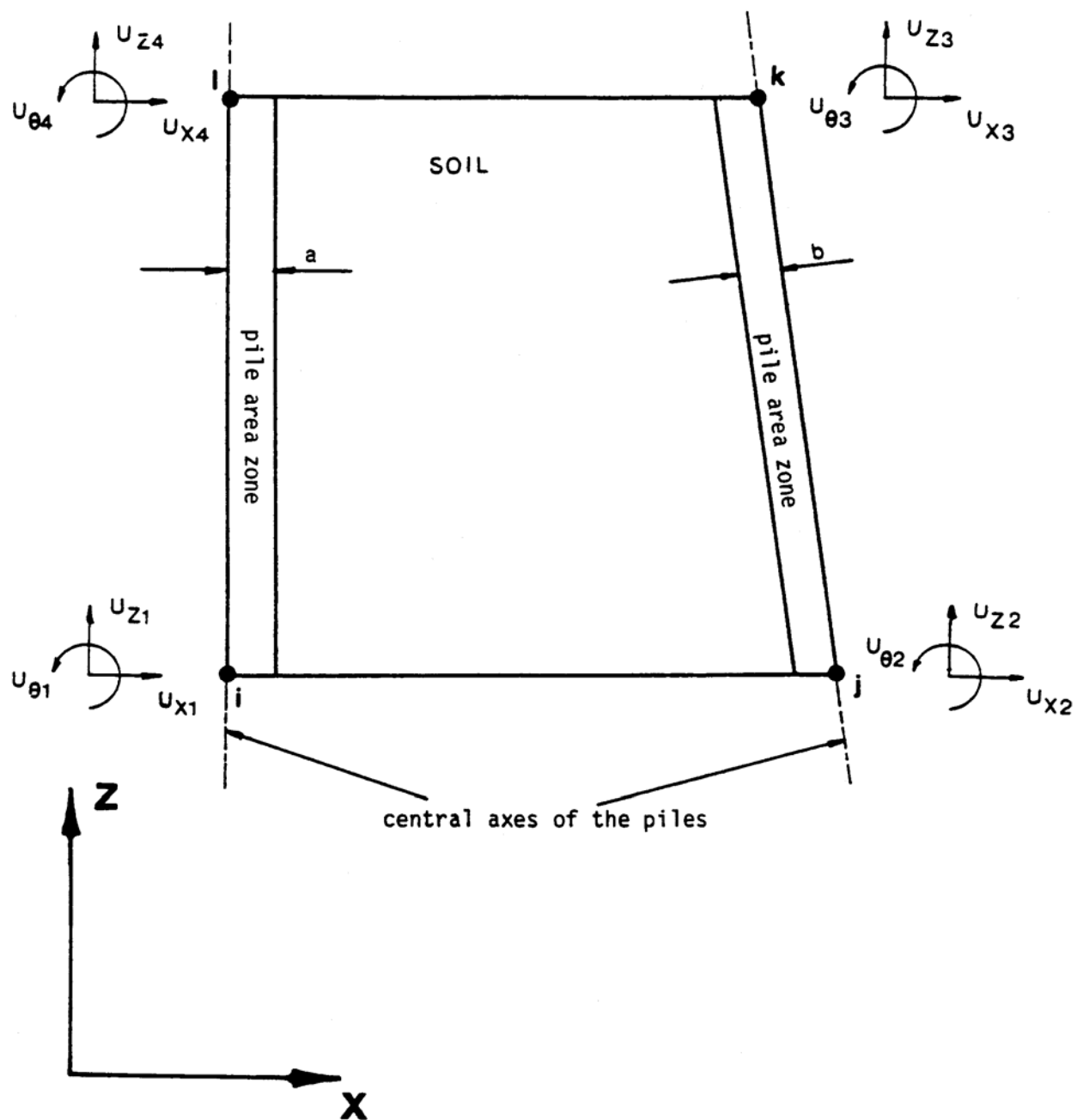


Figure 5.3-1. General Shape of the Two-dimensional Inter-pile Element

The inter-pile element behaves in such a manner that complete compatibility is retained on the boundaries between the pile area zones and the soil part of the element.

In general, the element will have 12 degrees of freedom. However, as shown in Figures 5.3-2(a) and (b), some special cases may occur in which the number of degrees of freedom are reduced to 10 and 8, respectively.

5.3.3 STIFFNESS MATRIX FORMULATION

Piles behave essentially as beams in the ground. Therefore, as was discussed in connection with the development of the three-dimensional element, it can be assumed that planes perpendicular to the pile axis remain rigid during deformation and that, between nodes, the displacements perpendicular to the pile axis vary as a third order polynomial.

In order to retain the compatibility between the displacement fields in the pile area zones and the soil part of the element, the displacement field in the soil element must be able to follow the cubic order of variation along the interface to the pile. This is achieved by allowing four internal nodes on each side of the soil element. The internal nodes are numbered as shown in Figure 5.3-3. Nodes 5 to 8 are located at the third points at the sides of the soil element. Figure 5.3-4 similarly shows the soil element (with internal nodes) used for the special cases previously shown in Figure 5.3-2.

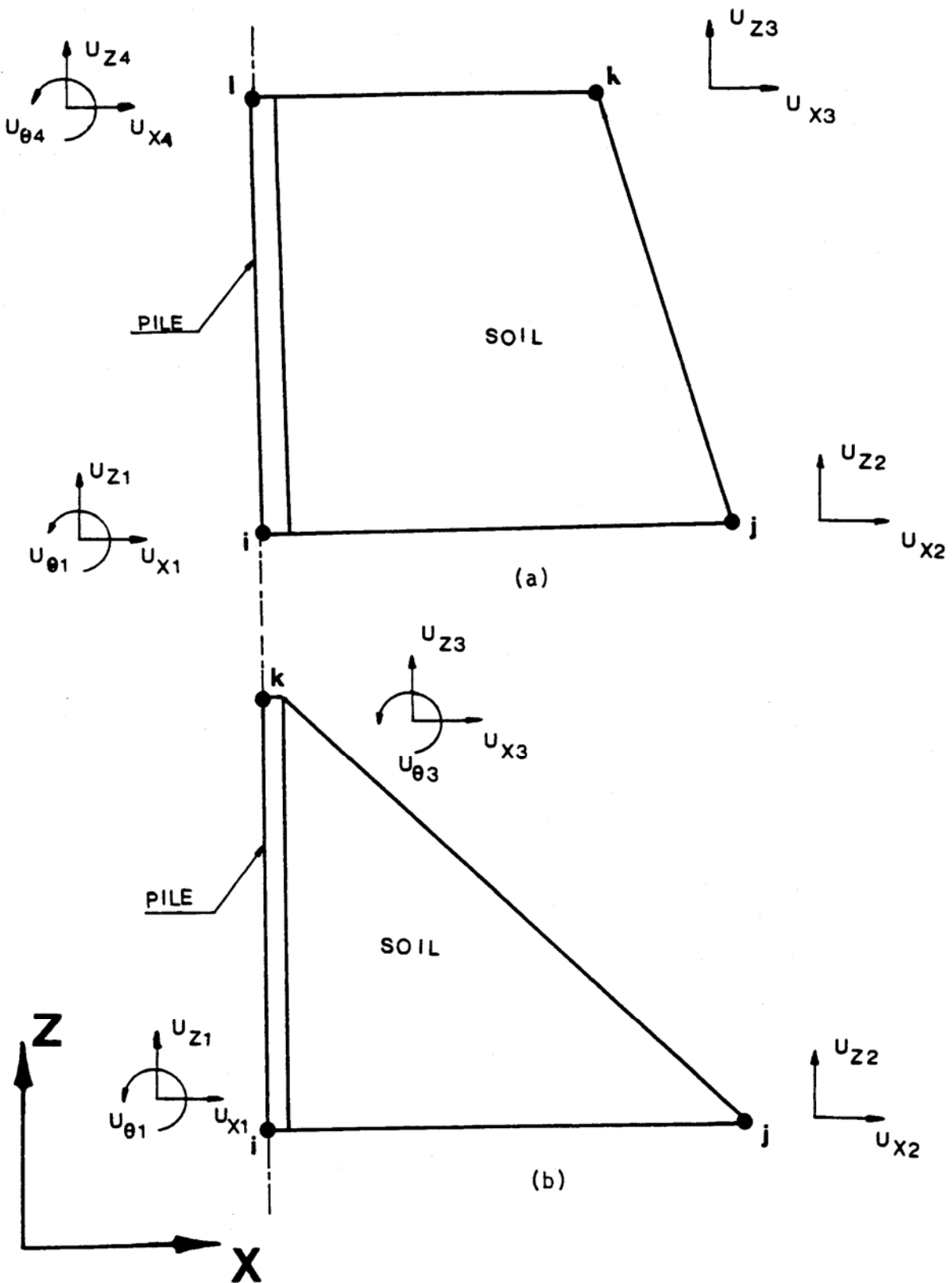


Figure 5.3-2. Special Cases of the 2-D Inter-pile Element

The following conventions are used with respect to the development of the mass and the stiffness matrices of the inter-pile element.

- 1) The global nodes of the element are indicated by the letters i, j, k and ℓ .
The global mass and stiffness matrices of the element will be determined at the degrees of freedom corresponding to these nodes.
- 2) Internal nodes of the element are designated by the numbers 1 to 8. The degrees of freedom at these nodes are used to determine the mass and stiffness matrices of the soil element at the local level.

In some special cases, such as those shown in Figure 5.3-4, some internal and global nodes coincide.

The conventions used for displacements and forces are as follows:

- $u_x(x, z)$ and $u_z(x, z)$ are the displacements of the point (x, z) in the x - and z -directions, respectively.
- u_{xi} and u_{zi} are the displacements of the internal node i ($i = 1, \dots, 8$) in the x - and z -directions. The corresponding forces are P_{xi} and P_{zi} .
- U_{xi} , U_{zi} and $U_{\theta i}$ are the displacements of the global node i ($i = i, j, k, \ell$). The corresponding forces and moment are R_{xi} , R_{zi} and $R_{\theta i}$.

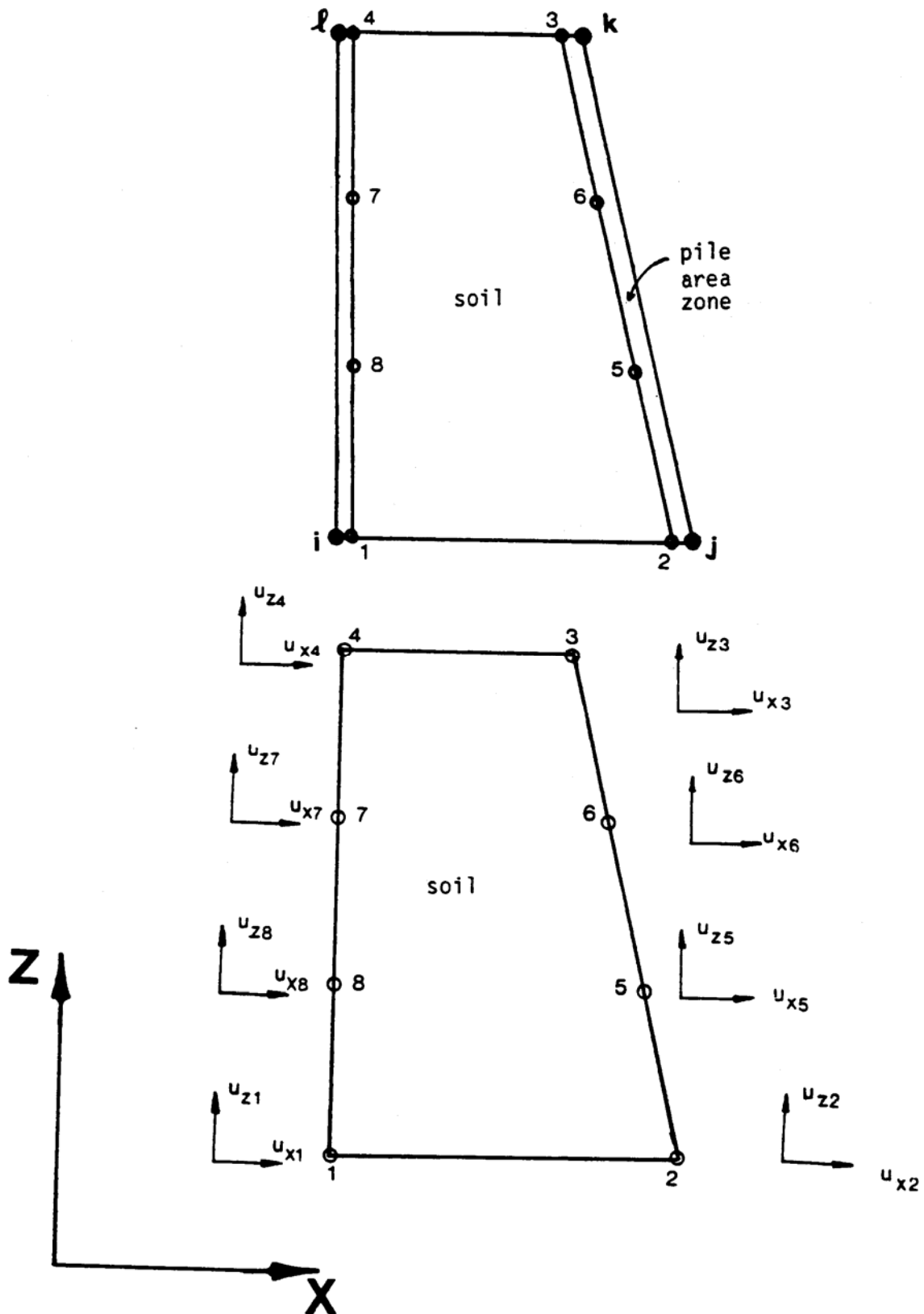


Figure 5.3-3. Soil Element with Internal Nodes (Two-dimensional Case)

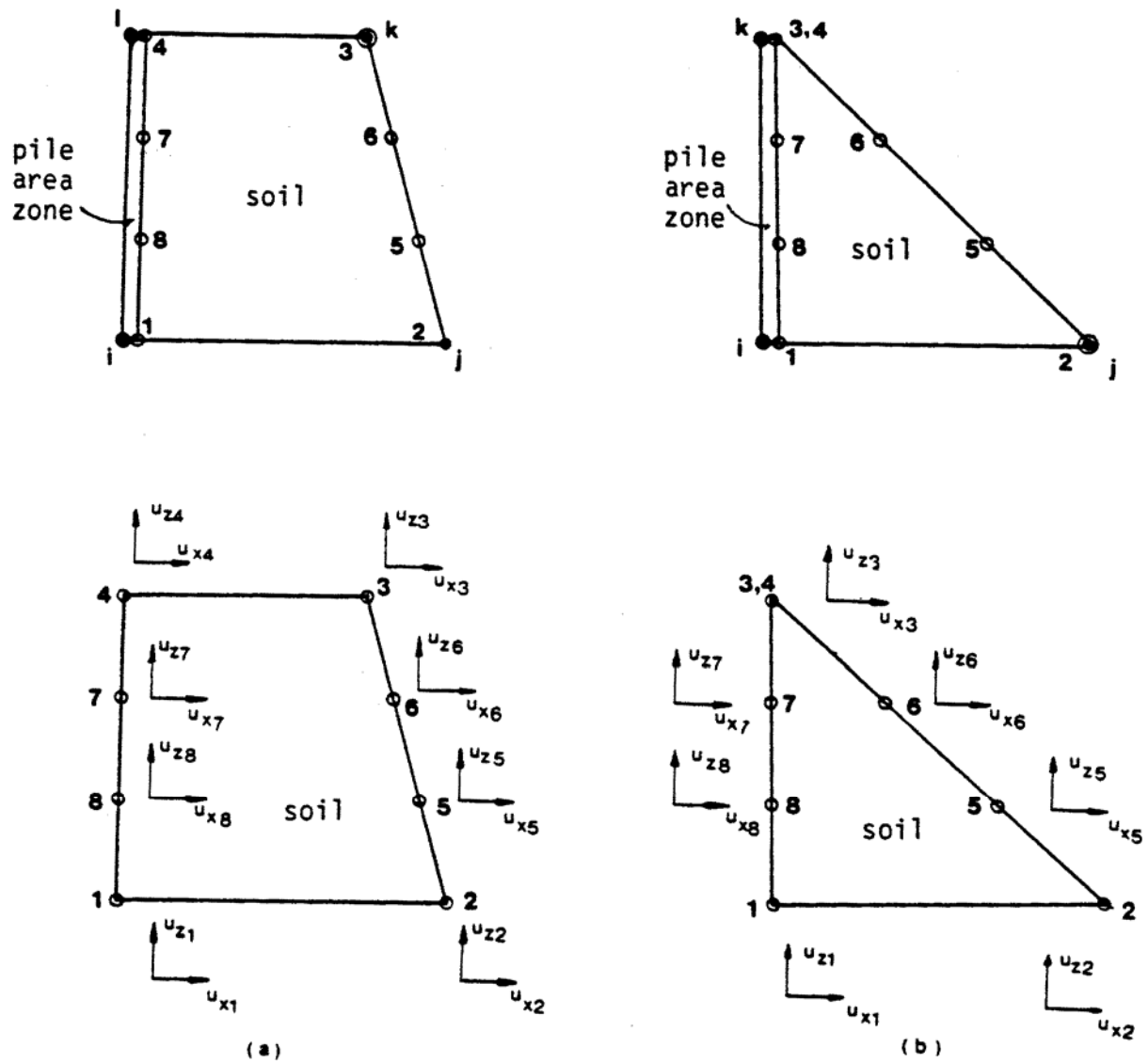


Figure 5.3-4. Soil Element for Special Cases with Internal Nodes (Two-dimensional Case)

In Section 5.3.5 the relationships between the global displacements, U , and the internal displacements, u , will be established and the total element mass and stiffness matrices will be expressed in terms of global degrees of freedom.

a. Global and Natural Coordinate Systems

The basic equations from which the stiffness of an element can be determined is Eq. (5.1). It is simpler to perform the numerical operations in this equation in a natural coordinate system in which each element is scaled to fixed dimensions. Figure 5.3-5 shows an element in both global (x, z) and natural (s, t) coordinates. The relationship between the two sets of coordinates is defined by

$$x = \sum_{i=1}^4 Q_i(s, t) x_i \quad (5.57a)$$

$$z = \sum_{i=1}^4 Q_i(s, t) z_i \quad (5.57b)$$

In these equations x_i and z_i are the coordinates of Node i in the

xz system and

$$Q(1) = 1/4(1 - s) (1 - t) \quad (5.58a)$$

$$Q(2) = 1/4 (1 + s) (1 - t) \quad (5.58b)$$

$$Q(3) = 1/4 (1 + s) (1 + t) \quad (5.58c)$$

$$Q(4) = 1/4 (1 - s) (1 + t) \quad (5.58d)$$

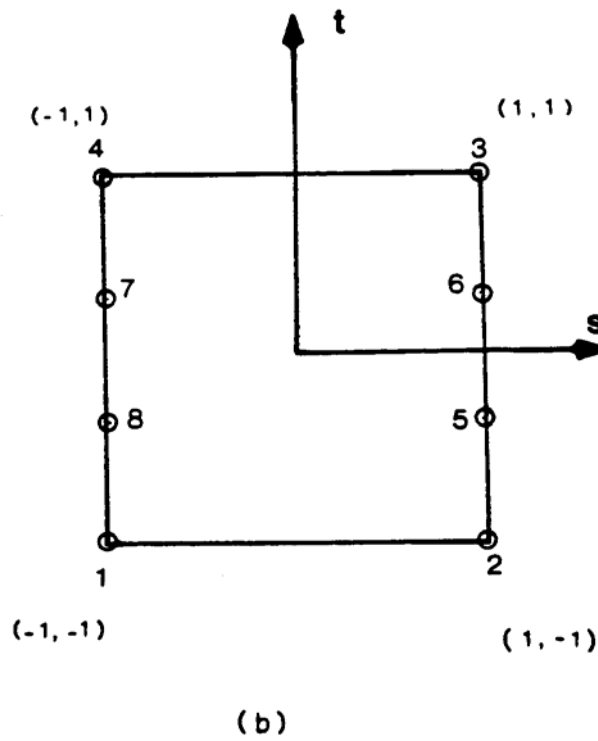
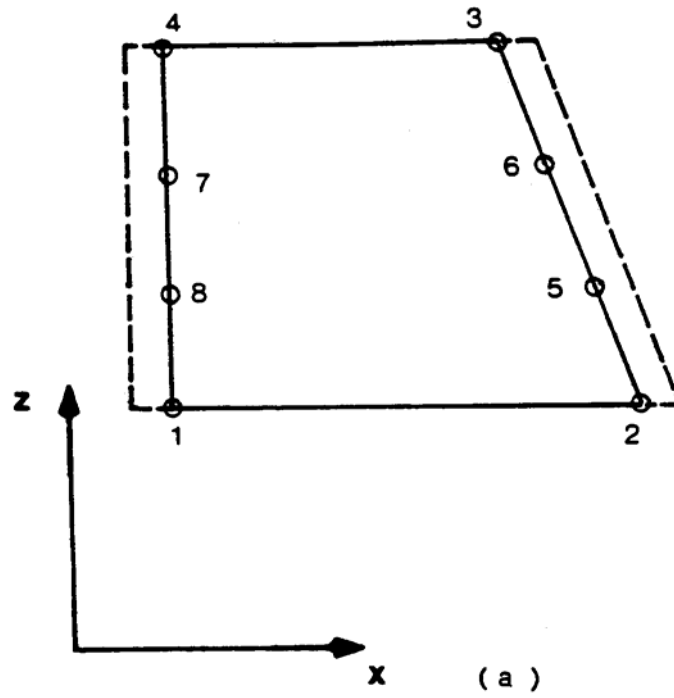


Figure 5.3-5. Soil Element in (a) Global, and (b) Natural Coordinate System

b. Displacement Field

The basic assumption in finite element analysis is that the displacements $u_x(x, z)$ and $u_z(x, z)$ of any point inside an element can be expressed in terms of the nodal point displacements u_{xi} and u_{zi} of the element. For the soil element discussed above this relationship can be written

$$u_x(x, z) = \sum_{i=1}^8 H_i(s, t) u_{xi} \quad (5.59a)$$

$$u_z(x, z) = \sum_{i=1}^8 H_i(s, t) u_{zi} \quad (5.59b)$$

where H_i are the interpolation functions

$$H(1) = Q(1) - 2/3H(8) - 1/3H(7) \quad (5.60a)$$

$$H(2) = Q(2) - 2/3H(5) - 1/3H(6) \quad (5.60b)$$

$$H(3) = Q(3) - 2/3H(6) - 1/3H(5) \quad (5.60c)$$

$$H(4) = Q(4) - 2/3H(7) - 1/3H(8) \quad (5.60d)$$

$$H(5) = 27/32 (1-t) (1+t) (1/3 - t) (1 + s) \quad (5.60e)$$

$$H(6) = 27/32 (1-t) (1+t) (1/3 + t) (1 + s) \quad (5.60f)$$

$$H(7) = 27/32 (1-t) (1+t) (1/3 + t) (1 - s) \quad (5.60g)$$

$$H(8) = 27/32 (1-t) (1+t) (1/3 - t) (1 - s) \quad (5.60h)$$

These functions have been designed in such a way that compatibility is retained on the pile-soil interface.

For an isotropic element the interpolation functions H_i in Eq. (5.60) should be the same as the functions Q_i in Eq. (5.58). However, for the soil element in question this is not the case because the special locations of the nodes 5 to 8 on the straight sides of the element make it possible to use lower order functions, Q_i , for the transformation from (s, t) to (x, z) coordinates. The element is in fact subparametric and, therefore, satisfy the conditions of compatibility and completeness [Bathe and Wilson, 1976].

c. Strain-Displacement Relationship

The strain-displacement relationship is

$$\{\varepsilon\}_{xz} = \begin{Bmatrix} \varepsilon_{xx} \\ \varepsilon_{zz} \\ \varepsilon_{xz} \end{Bmatrix} = \begin{bmatrix} \frac{\partial}{\partial x} & 0 \\ 0 & \frac{\partial}{\partial z} \\ \frac{\partial}{\partial z} & \frac{\partial}{\partial x} \end{bmatrix} \begin{Bmatrix} u_x \\ u_z \end{Bmatrix} \quad (5.61)$$

In order to determine the displacement derivatives in this equation one needs to evaluate the Jacobian

$$[J] = \begin{bmatrix} \frac{\partial x}{\partial s} & \frac{\partial z}{\partial s} \\ \frac{\partial x}{\partial t} & \frac{\partial z}{\partial t} \end{bmatrix} \quad (5.62)$$

from Eqs. (5.57) and (5.58). The Jacobian satisfies the relation

$$\begin{Bmatrix} \frac{\partial}{\partial s} \\ \frac{\partial}{\partial t} \end{Bmatrix} = [J] \begin{Bmatrix} \frac{\partial}{\partial x} \\ \frac{\partial}{\partial z} \end{Bmatrix} \quad (5.63)$$

Hence

$$\begin{Bmatrix} \frac{\partial u_x}{\partial x} \\ \frac{\partial u_x}{\partial z} \end{Bmatrix} = [J]^{-1} \begin{Bmatrix} \frac{\partial u_x}{\partial s} \\ \frac{\partial u_x}{\partial t} \end{Bmatrix} \quad \text{and} \quad \begin{Bmatrix} \frac{\partial u_z}{\partial x} \\ \frac{\partial u_z}{\partial z} \end{Bmatrix} = [J]^{-1} \begin{Bmatrix} \frac{\partial u_z}{\partial s} \\ \frac{\partial u_z}{\partial t} \end{Bmatrix} \quad (5.64)$$

which with Eq. (5.59) implies

$$\begin{Bmatrix} \frac{\partial u_x}{\partial x} \\ \frac{\partial u_x}{\partial z} \end{Bmatrix} = [J]^{-1} \begin{bmatrix} \frac{\partial H_1}{\partial s} & 0 & \frac{\partial H_2}{\partial s} & 0 & \dots & \frac{\partial H_8}{\partial s} & 0 \\ \frac{\partial H_1}{\partial t} & 0 & \frac{\partial H_2}{\partial t} & 0 & \dots & \frac{\partial H_8}{\partial t} & 0 \end{bmatrix} \{u\} \quad (5.65a)$$

Similarly

$$\begin{Bmatrix} \frac{u_z}{\partial x} \\ \frac{u_z}{\partial z} \end{Bmatrix} = [J]^{-1} \begin{bmatrix} 0 & \frac{\partial H_1}{\partial s} & 0 & \frac{\partial H_2}{\partial s} & \dots & 0 & \frac{\partial H_8}{\partial s} \\ 0 & \frac{\partial H_1}{\partial t} & 0 & \frac{\partial H_2}{\partial t} & \dots & 0 & \frac{\partial H_8}{\partial t} \end{bmatrix} \{u\} \quad (5.65b)$$

where $\{u\}$ is the displacement vector defined at internal nodes, i.e.

$$\{u\}^T = \langle u_{x1}, u_{z1}, u_{x2}, \dots, u_{z7}, u_{x8}, u_{z8} \rangle \quad (5.66)$$

By substitution of Eqs. (5.65) into Eq. (5.61) the strains in the element can be expressed in the form

$$\{\varepsilon\} = [B]_{st} \{u\} \quad (5.67)$$

where the coefficients of B_{st} are functions of s and t . The volume element (actually an area element for the two-dimensional case) in Eq. (5.1) is $dV = \det \mathbf{J} \cdot ds \, dt$. Hence the stiffness matrix in Eq. (5.1) can be evaluated from

$$[K]^{(m)} = \int_{-1}^1 ds \int_{-1}^1 [B]_{st}^{(m)T} [C]^{(m)} [B]_{st}^{(m)} \cdot \det \mathbf{J} \cdot dt \quad (5.68)$$

d. Stress-Strain Relationship

The basic stress-strain relations are those of linear elasticity. For two-dimensional isotropic materials deforming in plane strain these relations can be expressed as follows:

$$\{\alpha\} = [C]\{\varepsilon\} \quad (5.69)$$

where

$$\{\alpha\} = (\alpha_{xx} \alpha_{zz} \alpha_{xz}) \quad (5.70a)$$

$$\{\varepsilon\} = (\varepsilon_{xx} \varepsilon_{zz} \varepsilon_{xz}) \quad (5.70b)$$

and

$$[C] = \begin{bmatrix} M & M-2G & 0 \\ M-2G & M & 0 \\ 0 & 0 & G \end{bmatrix} \quad (5.71)$$

For viscoelastic materials and harmonic motion M and G are the complex constrained and shear moduli, respectively.

e. Numerical Integration

By using Gauss-quadrature Eq. (5.68) can be reformulated as follows

$$[K]^{(m)} = \sum_{i=1}^{n_2} \sum_{j=1}^{n_1} [B]_{ij}^{(m)T} [C]^{(m)} [B]_{ij}^{(m)} \det J_{ij} \alpha_{ij} \quad (5.72)$$

where (i, j) is the Gauss point and α_{ij} is the corresponding weighting factor. The indices i and j correspond to discretization in the s- and t-directions, respectively. As was discussed for the case of a three-dimensional element, the number of Gauss points required depend on the order of the integrand. The integrand in Eq. (5.72) is of higher order in t than in s. Hence the number of points, n_1 , in the s direction can be chosen smaller than the number, n_2 , in the t-direction. Experience with Eq. (5.72) for the evaluation of the stiffness matrix has shown that the choice $n_2 = 4$ and $n_1 = 2$ leads to

good results provided the element shape does not degenerate too far away from the rectangular shape. The resulting 16 X 16 stiffness matrix for the soil part of the element will have complex terms if soil damping is specified.

5.3.4 MASS MATRIX FORMULATION

As for the three-dimensional case, the mixed mass matrix defined by Eq. (5.16) is used. The consistent mass matrix is evaluated by Gauss-quadrature in a manner very similar to, but simpler than, the one presented for the stiffness matrix in the previous section. The lumped mass matrix is a simple diagonal matrix whose terms are obtained by distributing the total mass in proportion to the diagonal terms of the consistent mass matrix.

The procedures developed above for the evaluation of the stiffness and mass matrices of the soil element are also applicable to the soil parts of the special inter-pile elements shown in Figure 5.3-2. In the case of the triangular element(Figure 5.3-2(b)), Nodes 3 and 4 coincide (see Figure 5.3-4). However, the procedures developed for the quadrilateral soil part of the element are still valid provided both nodes are considered.

5.3.5 GLOBAL SOIL ELEMENT MASS AND STIFFNESS MATRICES

The stiffness matrix developed in the previous section relates the forces $\{P\}$ and the displacements $\{u\}$ of the internal nodes, 1 to 8, of the soil part of the inter-pile element shown in Figure 5.3-6. The relationship is:

$$\{P\}_{(16 \times 1)} = [K]_{(16 \times 16)} \{u\}_{(16 \times 1)} \quad (5.73)$$

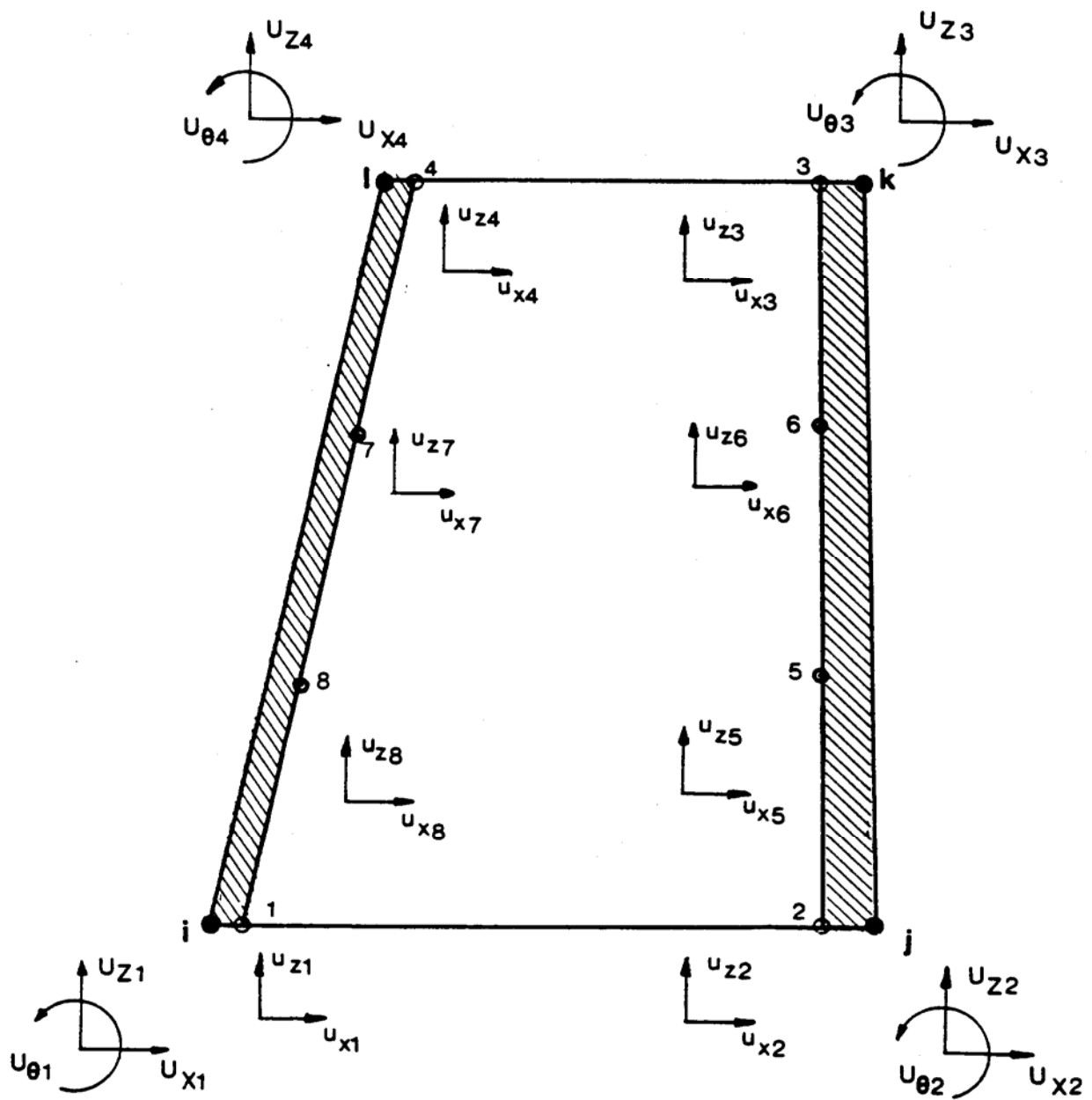


Figure 5.3-6. Degrees of Freedom at the Global and Internal Nodes (Two-dimensional Case)

In order to develop a similar relationship between the corresponding forces $\{R\}$ and displacements $\{U\}$ at the global nodes i, j, k and ℓ at the pile centers, a transformation matrix $[A]$ is introduced as follows

$$\{u\}_{(16 \times 1)} = [A]_{(16 \times 12)} \{U\}_{(12 \times 1)} \quad (5.74)$$

This matrix is designed in such a manner that compatibility is retained between the displacements of the soil part and pile surface zones of the inter-pile element. The elements of $[A]$ can be computed by a procedure similar to the one presented in Section 5.2.6 for the more complicated three-dimensional case.

The force system $\{P\}$ and $\{R\}$ must be statically equivalent. This equivalence, as was discussed in Section 5.2.5, implies that

$$\{R\} = [A]^T \{P\} \quad (5.75)$$

Substituting for $\{P\}$ using Eqs. (5.73) and (5.74), the above equation can be written in the following form

$$\{R\} = [K^g] \{U\} \quad (5.76)$$

where

$$[K^g]_{(12 \times 12)} = [A]_{(12 \times 16)}^T [K]_{(16 \times 16)} [A]_{(16 \times 12)} \quad (5.77)$$

The same procedure can be used for the set of accelerations and inertia forces at internal and global nodes to obtain the global mass matrix. The resulting mass matrix is

$$[M^g]_{(12 \times 12)} = [A]_{(12 \times 16)}^T [M]_{(16 \times 16)} [A]_{(16 \times 12)} \quad (5.78)$$

In the case of special configurations of the inter-pile element, shown in Figure 5.3-2, the matrix A used in Eqs. (5.77) and (5.78) must be modified. The procedure for modifying the matrix is similar to the one presented in Section 5.2.7 for the three-dimensional case.

5.4 IMPLEMENTATION AND FURTHER CAPABILITIES OF THE SPECIAL ELEMENTS

The elements developed for the two- and three-dimensional cases are coded in two separate subprograms which can be executed with program HOUSE in SASSI. For every element, the coordinates of the global nodes and the cross-sectional areas of the piles are used as input. The output of the subprograms are the global mass and stiffness matrices of the element. Due to the size of the subprograms they should only be loaded with program HOUSE if they are actually used.

Further capabilities of the elements are as follows.

- 1) The equivalent linear method described in Chapter 3 can be used to iterate on soil properties adjacent to the piles. Every inter-pile element can be further subdivided to obtain more accurate strain values in the soil. As was discussed previously, it is possible to consider the secondary nonlinearity such that the expensive evaluation of the impedance matrix does not have to be repeated.
- 2) By modeling the pile cap, the effects of pile-soil-pile interaction and soil-cap interaction can be considered simultaneously.
- 3) Tapered piles can be modeled using different cross-sectional areas in the t- and b-planes.
- 4) Hollow piles such as pipe piles can be treated such that the effect of their diameter along with the appropriate mass and stiffness of the piles are considered.

5.5 PILE IMPEDANCE METHOD

5.5.1 INTRODUCTION

In this section a simple method for analyzing single vertical piles in a horizontally layered medium is presented first. Later the method is extended such that it can be applied to more general soil-structure systems involving piloted foundations with vertical piles. The method is applicable only to the case of directly loaded pile foundations to develop frequency dependent impedance functions for pile group.

5.5.2 ANALYTICAL MODEL FOR SINGLE PILES

Figure 5.5-1 shows the general configuration of the proposed model. The model consists of a column of axisymmetric elements which model the pile and the soil above and below the pile. The pile head may be located below the ground surface. This latter feature will be used in a sub-structuring scheme which, as will be discussed later, is applicable to soil-pile-structure systems with embedded pile caps. The name "cylindrical core" used throughout the chapter refers to the pile and to the soil columns at its ends. The soil medium is horizontally layered and is either resting on bedrock or is underlain by a homogeneous half space.

The model is used to determine the response of a pile subjected to direct harmonic loads and the resulting displacement field in the soil medium.

As shown in Figure 5.5-1, the nodes and the degrees of freedom are defined at the axis and perimeter of the cylindrical core. Using the complex response method and omitting the common factor $\exp(i\omega t)$ the equation of harmonic motion for the entire model can be written

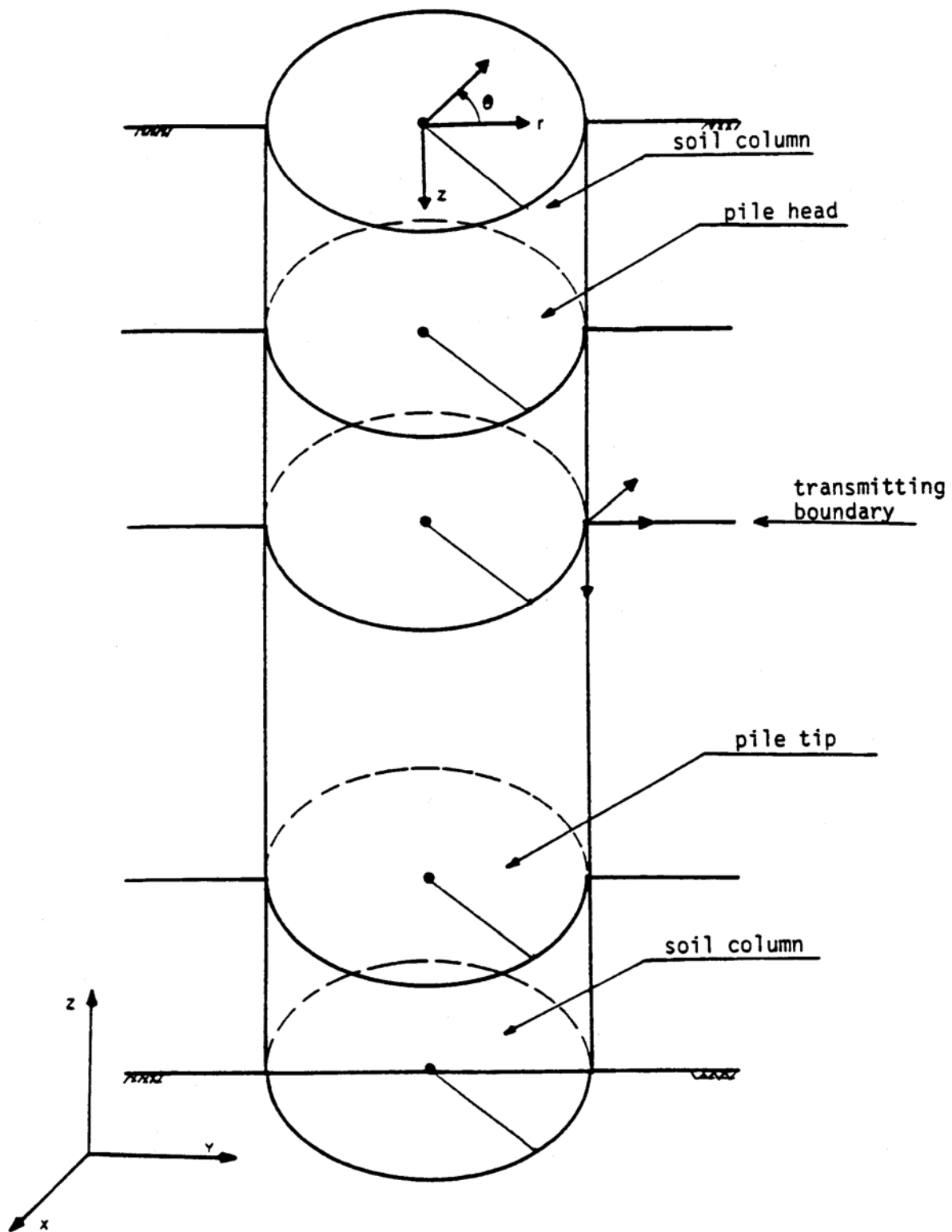


Figure 5.5-1. Single Pile in Horizontally Layered System

$$([K] - \omega^2[M]) \begin{Bmatrix} U_a \\ U_b \end{Bmatrix} = \begin{Bmatrix} P \\ -RU_b \end{Bmatrix} \quad (5.81a)$$

where $\{U_a\}$ and $\{U_b\}$ are the displacement amplitudes at the axis and perimeter of the cylindrical core, respectively. The load vector contains the external load amplitudes applied at the cylindrical core axis, $\{P\}$, and the reactions, $-[R]\{U_b\}$ from the surrounding layered half space. The matrix $[R]$ which expresses the transmitting boundary conditions will be developed in Section 5.6.8. The matrices $[K]$ and $[M]$ are the stiffness and mass matrices, respectively, and ω is the circular frequency. As will be described, the degrees of freedom may be specified such that advantage is taken from symmetry and antisymmetry.

Equation (5.81a) may be rearranged and partitioned as follows:

$$\left(\begin{bmatrix} K_{aa} & K_{ab} \\ K_{ba} & K_{bb} \end{bmatrix} - \omega^2 \begin{bmatrix} M_{aa} & M_{ab} \\ M_{ba} & M_{bb} \end{bmatrix} + \begin{bmatrix} 0 & 0 \\ 0 & R \end{bmatrix} \right) \begin{Bmatrix} U_a \\ U_b \end{Bmatrix} = \begin{Bmatrix} P \\ 0 \end{Bmatrix} \quad (5.81b)$$

In formulating the element stiffness $[K]$ and the mass matrix $[M]$ and also in developing the boundary matrix $[R]$ it will be assumed that displacements vary linearly with depth within each layer. This assumption is acceptable since a finer discretization of the model will effectively yield more accurate results. It is possible to use a higher order variation of the displacement field with depth. However, this possibility will not be pursued herein.

5.5.3 FORMULATION OF THE AXISYMMETRIC ELEMENT

In this section the displacement field for the cylindrical elements and the loads are expressed in terms of the cylindrical coordinates shown in Figure 5.5-1.

The displacement components U_r , U_z , and U_θ in the r -, z - and θ -directions, respectively, may be expanded in the θ -direction as follows:

$$U_r(r, z, \theta) = \sum_{m=0}^M U_r^m(r, z) \cos m\theta + \hat{U}_r^m(r, z) \sin m\theta \quad (5.82a)$$

$$U_z(r, z, \theta) = \sum_{m=0}^M U_z^m(r, z) \cos m\theta + \hat{U}_z^m(r, z) \sin m\theta \quad (5.82b)$$

$$U_\theta(r, z, \theta) = \sum_{m=0}^M -U_\theta^m(r, z) \sin m\theta + \hat{U}_\theta^m(r, z) \cos m\theta \quad (5.82c)$$

where m is the Fourier harmonic number and M is the total number of harmonics required to represent the displacement field. $U^m(r, z)$ and $\hat{U}^m(r, z)$ represent the m^{th} harmonic of the symmetric and antisymmetric displacement amplitudes, respectively.

The loading may similarly be expanded into Fourier harmonics. The load components P_r , P_z and P_θ in the r -, z - and θ -directions are expanded in the θ -direction using

$$P_r(r, z, \theta) = \sum_{m=0}^M P_r^m(r, z) \cos m\theta + \hat{P}_r^m(r, z) \sin m\theta \quad (5.83a)$$

$$P_z(r, z, \theta) = \sum_{m=0}^M P_z^m(r, z) \cos m\theta + \hat{P}_z^m(r, z) \sin m\theta \quad (5.83b)$$

$$P_\theta(r, z, \theta) = \sum_{m=0}^M -P_\theta^m(r, z) \sin m\theta + \hat{P}_\theta^m(r, z) \cos m\theta \quad (5.83c)$$

where P^m and \hat{P}^m correspond to the symmetric and antisymmetric amplitudes of the loads, respectively.

In the development of the mass and stiffness matrices of the element only the first two terms of Eq. (5.82) are considered, i.e. $M = 1$. In the case of symmetric loading (vertical force) only the terms corresponding to the zero-harmonic ($m = 0$) need to be considered. In the case of antisymmetric loadings (lateral forces and rocking moments) the terms corresponding to the first harmonic ($m = 1$) are used.

Since the piles are considerably stiffer than the soil, their cross sections will not significantly deform, but will behave approximately as rigid planes. Under this assumption it is a simple matter to show that the two Fourier harmonic terms corresponding to $M = 1$ are sufficient to represent the displacements of the pile and the surrounding soil.

Actually, the formulation of the cylindrical elements to be discussed in the next section will allow small deformations of the cross sections of the element. Thus, the use of only the first two harmonics is an approximation which, however, is justified in view of the accuracy of the results proven in later sections. The same Fourier harmonics are used for all the elements of the cylindrical core. Furthermore, it is assumed that the pile does not rotate about its own axis.

5.5.4 STIFFNESS MATRIX FORMULATION

The stiffness matrix of the axisymmetric element, e , may be obtained from the following equation

$$[K]^{(e)} = \int_{V^e} [B]^{(e)T} [C]^{(e)} [B]^{(e)} dV \quad (5.84)$$

The matrix $[B]^{(e)}$ represents the strain-displacement relationship in Element e . $[C]^{(e)}$ is the matrix which relates the stresses to strains. It is simpler to perform the operations in Eq. (5.84) in a natural coordinate system in which each element is scaled to fixed dimensions. The natural coordinate system and the matrices $[B]^{(e)}$ and $[C]^{(e)}$ are described in the following sections.

The following conventions are used with respect to the development of the mass and stiffness matrices of the element.

- 1) $u_r(r, z, \theta)$, $u_z(r, z, \theta)$ and $u_\theta(r, z, \theta)$ are the displacement amplitudes of the general point (r, z, θ) in the r -, z - and θ -directions for the zero harmonic case.

For the case of the first harmonic the amplitudes are $\hat{u}_r(r, z, \theta)$, $\hat{u}_z(r, z, \theta)$ and $\hat{u}_\theta(r, z, \theta)$, respectively.

- 2) The nodal displacement amplitudes are denoted U_r , U_z and U for the zero harmonic case and \hat{U}_r , \hat{U}_z and \hat{U}_θ for the first harmonic case. In later sections additional subscripts will be introduced to specify particular degrees of freedom.

5.5.4.1 Global and Natural Coordinate Systems

Figure 5.5-2 shows an element in both global (r,z) and natural (s,t) coordinates. The relationship between the two sets of coordinates is defined by

$$r = \sum_{i=1}^4 Q_i(s, t) r_i \quad (5.85a)$$

$$z = \sum_{i=1}^4 Q_i(s, t) z_i \quad (5.85b)$$

In these equations r_i and z_i are the coordinates of Node i in the rz system and

$$Q_1 = \frac{1}{4}(1-s)(1+t) \quad (5.86a)$$

$$Q_2 = \frac{1}{4}(1-s)(1-t) \quad (5.86b)$$

$$Q_3 = \frac{1}{4}(1+s)(1-t) \quad (5.86c)$$

$$Q_4 = \frac{1}{4}(1+s)(1+t) \quad (5.86d)$$

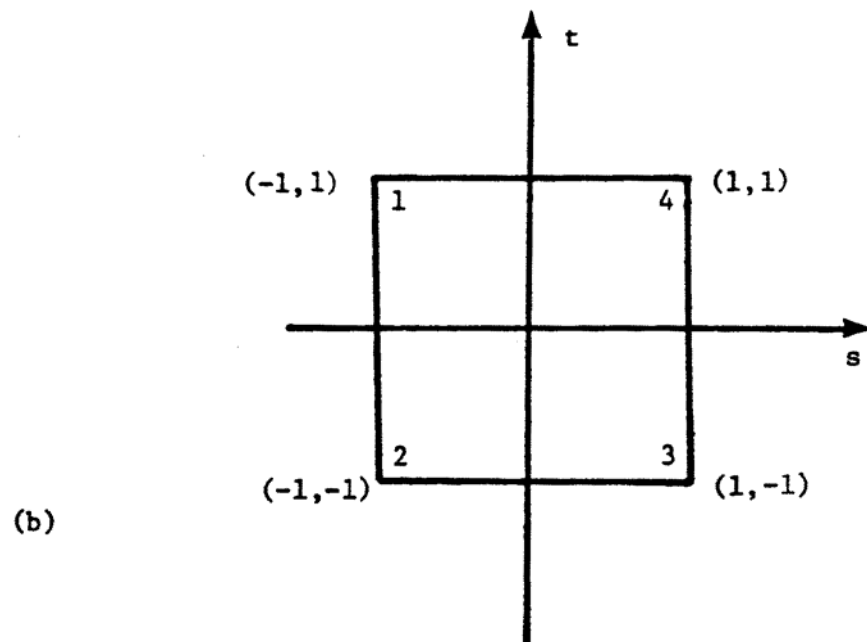
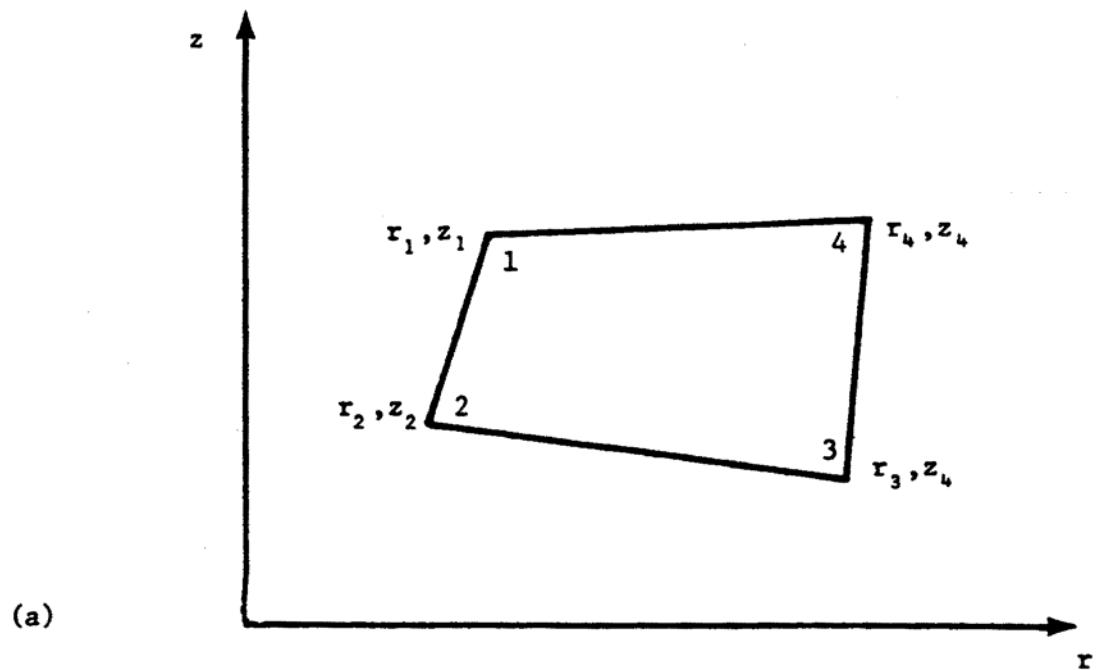


Figure 5.5-2. (a) Element in Global Coordinate System, (b) Element in Natural Coordinate System

5.5.4.2 Displacement Field

The local degrees of freedom for each element for the zero and first harmonic case are shown in Figures 5.5-3(a) and 5.5-3(b), respectively (see Tajirian [Ref. 31]).

The displacements of any point in the element can be expressed in terms of nodal displacements.

For the case of the zero harmonic the relations are:

$$U_r(r, z, \theta) = \sum_{i=1}^4 Q_i U_{ri} \quad (5.87a)$$

$$U_z(r, z, \theta) = \sum_{i=1}^4 Q_i U_{zi} \quad (5.87b)$$

$$U_\theta(r, z, \theta) = 0 \quad (5.87c)$$

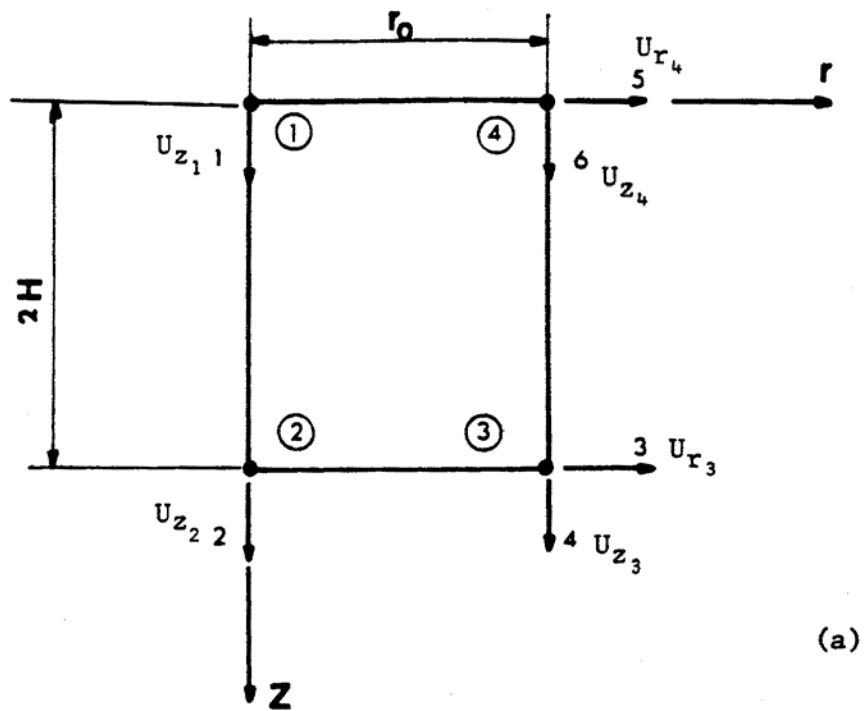
The interpolations Q_1 to Q_4 are defined by Eqs. (5.86).

The nodal displacement vector $\{U_i\}$ of the element for the zero harmonic case is

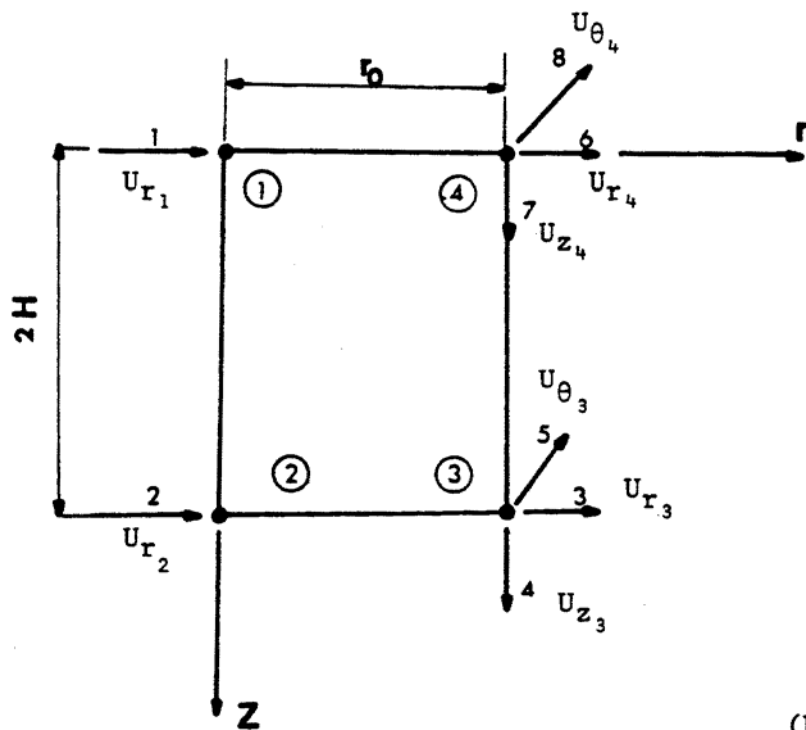
$$\{U_i\}^T = \langle U_{r_1} U_{z_1} U_{r_2} U_{z_2} U_{r_3} U_{z_3} U_{r_4} U_{z_4} \rangle \quad (5.88)$$

as it is described in the next section and shown in Figure 5.5-3(a), the components U_{r_1} and U_{r_2} are set to zero.

In the case of the first harmonic, the displacements of a point in the element may be written as



(a)



(b)

Figure 5.5-3. Local Degrees of Freedom for (a) Zero Harmonic, and (b) First Harmonic Case

$$\hat{U}_r(r, z, \theta) = \sum_{i=1}^4 Q_i \hat{U}_{ri} \cos \theta + (\alpha_1 Q_5 + \alpha_2 Q_6) \cos \theta \quad (5.89a)$$

$$\hat{U}_z(r, z, \theta) = \sum_{i=1}^4 Q_i \hat{U}_{zi} \cos \theta + (\alpha_3 Q_5 + \alpha_4 Q_6) \cos \theta \quad (5.89b)$$

$$\hat{U}_\theta(r, z, \theta) = \sum_{i=1}^4 Q_i \hat{U}_{\theta i} \sin \theta + (\alpha_5 Q_5 + \alpha_6 Q_6) \sin \theta \quad (5.89c)$$

The interpolations Q_5 and Q_6 may be used to define incompatible modes in the element and they are

$$Q_5 = 1 - s^2 \quad (5.90a)$$

$$Q_6 = 1 - t^2 \quad (5.90b)$$

The coefficients α_1 to α_6 are additional degrees of freedom which are not associated with any element nodal point and, when used, they will be eliminated by static condensation. As described in Section 5.6.6 the incompatible modes may be used in a special method for reducing parasitic shear in the pile elements.

The displacement vector of the element for this case is

$$\{\hat{U}_i\}^T = \langle \hat{U}_{r_1} \hat{U}_{z_1} \hat{U}_{\theta_1} \hat{U}_{r_2} \dots \hat{U}_{r_4} \hat{U}_{z_4} \hat{U}_{\theta_4} \rangle \quad (5.91)$$

As shown in Figure 5.5-3(b), the nodal displacements \hat{U}_{z_1} , \hat{U}_{θ_1} , \hat{U}_{z_2} and \hat{U}_{θ_2} are set to zero.

5.5.4.3 Strain-displacement Relationship

The strain-displacement relationship for the zero harmonic case can be expressed as

$$\{\varepsilon\} = \begin{Bmatrix} \varepsilon_{rr} \\ \varepsilon_{zz} \\ \varepsilon_{\theta\theta} \\ \gamma_{rz} \end{Bmatrix} = \begin{bmatrix} \frac{\partial}{\partial r} & 0 \\ 0 & \frac{\partial}{\partial z} \\ \frac{1}{r} & 0 \\ \frac{\partial}{\partial z} & \frac{\partial}{\partial r} \end{bmatrix} \begin{Bmatrix} U_r \\ U_z \end{Bmatrix} \quad (5.92)$$

where ε_{rr} , ε_{zz} and $\varepsilon_{\theta\theta}$ represent the normal strains in the r-, z- and θ -directions, respectively, and γ_{rz} is the shear strain. Since U_{r_1} and U_{r_2} have been set to zero, strain continuity is retained at $r = 0$.

Using the Eqs. (5.85) and (5.87), the strain displacement transformation matrix $B(r,z)$ or $B(s,t)$ can be constructed such that

$$\{\varepsilon\} = [B]\{U_i\} \quad (5.93)$$

where $\{U_i\}$ is defined in Eq. (5.88).

In the case of first harmonic the strain-displacement relationship can be written as

$$\{\hat{\varepsilon}\} = \begin{Bmatrix} \hat{\varepsilon}_{rr} \\ \hat{\varepsilon}_{zz} \\ \hat{\varepsilon}_{\theta\theta} \\ \hat{\gamma}_{rz} \\ \hat{\gamma}_{r\theta} \\ \hat{\gamma}_{z\theta} \end{Bmatrix} = \begin{bmatrix} \frac{\partial}{\partial r} \cos \theta & 0 & 0 \\ 0 & \frac{\partial}{\partial z} \cos \theta & 0 \\ \frac{\cos \theta}{r} & 0 & -\frac{\cos \theta}{r} \\ \frac{\partial}{\partial z} \cos \theta & \frac{\partial}{\partial r} \cos \theta & 0 \\ -\frac{\sin \theta}{r} & 0 & \left(\frac{1}{r} - \frac{\partial}{\partial r}\right) \sin \theta \\ 0 & -\frac{\sin \theta}{r} & \frac{\partial}{\partial r} \sin \theta \end{bmatrix} \begin{Bmatrix} \hat{U}_r \\ \hat{U}_z \\ \hat{U}_\theta \end{Bmatrix} \quad (5.94)$$

Since r goes to zero along the central axis, it is clear from the above equation that $\hat{\varepsilon}_{\theta\theta}$, $\hat{\gamma}_{r\theta}$ and $\hat{\gamma}_{z\theta}$ will be infinite on this axis. The singularity is removed by the following boundary conditions

$$\hat{U}_r(0, z) = \hat{U}_\theta(0, z) \quad (5.95a)$$

and

$$\hat{U}_z(0, z) = 0. \quad (5.95b)$$

Using Eqs. (5.85) and (5.89) the strain-displacement transformation matrix $[\hat{B}(r, z, \theta)]$ or $[\hat{B}(s, t, \theta)]$ can be constructed such that

$$\{\hat{\varepsilon}\} = [\hat{B}]\{\hat{U}_i\}. \quad (5.96)$$

The displacement vector $\{\hat{U}_i\}$ is defined by Eq. (5.91).

5.5.4.4 Stress-strain Relationship

The stress-strain relations are those of linear elasticity. For a three-dimensional isotropic material these relations are as follows:

a. Zero harmonic case

$$\{\sigma\} = [C]\{\varepsilon\} \quad (5.97)$$

where

$$\{\sigma\} = \langle \sigma_{rr} \quad \sigma_{zz} \quad \sigma_{\theta\theta} \quad \tau_{rz} \rangle \quad (5.98)$$

which corresponds to the strain components defined by Eq. (5.92) and

$$[C] = \begin{bmatrix} M & M-2G & M-2G & 0 \\ M-2G & M & M-2G & 0 \\ M-2G & M-2G & M & 0 \\ 0 & 0 & 0 & G \end{bmatrix} \quad (5.99)$$

For viscoelastic materials and harmonic motion M and G are the complex constrained and shear moduli, respectively.

b. First harmonic case

The relations for the first harmonic case are similarly

$$\{\hat{\sigma}\} = [\hat{C}] \{\hat{\varepsilon}\} \quad (5.100)$$

where

$$\{\hat{\sigma}\}^T = \langle \hat{\sigma}_{rr} \quad \hat{\sigma}_{zz} \quad \hat{\sigma}_{\theta\theta} \quad \hat{\tau}_{rz} \quad \hat{\tau}_{r\theta} \quad \hat{\tau}_{z\theta} \rangle.$$

which corresponds to the strain components defined by Eq. (5.94) and

$$[\hat{C}] = \begin{bmatrix} M & M-2G & M-2G & 0 & 0 & 0 \\ M-2G & M & M-2G & 0 & 0 & 0 \\ M-2G & M-2G & M & 0 & 0 & 0 \\ 0 & 0 & 0 & G & 0 & 0 \\ 0 & 0 & 0 & 0 & G & 0 \\ 0 & 0 & 0 & 0 & 0 & G \end{bmatrix} \quad (5.101)$$

5.5.4.5 Numerical Integration

Following the computation of the matrices [B] and [C] for the zero harmonic case and $[\hat{B}]$ and $[\hat{C}]$ for the first harmonic case, the corresponding stiffness matrices can be computed from Eq. (5.84) by Gauss integration in natural coordinates. The resulting stiffness matrices are (6 x 6) and (8 x 8) for the zero and the first harmonic case, respectively.

5.5.5 MASS MATRIX FORMULATION

The mass matrix is the combination of the lumped and consistent mass matrix determined by

$$[M]^{(e)} = \alpha [M^C]^{(e)} + (1 - \alpha) [M^L]^{(e)} \quad (5.102)$$

where $[M^C]^{(e)}$ and $[M^L]^{(e)}$ are the consistent and lumped mass matrices respectively and α is a constant coefficient chosen to be .50.

The consistent and lumped mass matrices for the zero harmonic case are

$$[M^C]^{(e)} = \pi r_0^2 H^{(e)} \rho^{(e)} \begin{bmatrix} 1/9 & 1/18 & 0 & 1/18 & 0 & 1/9 \\ 1/18 & 1/9 & 0 & 1/9 & 0 & 1/18 \\ 0 & 0 & 1/3 & 0 & 1/6 & 0 \\ 1/18 & 1/9 & 0 & 1/3 & 0 & 1/6 \\ 0 & 0 & 1/6 & 0 & 1/3 & 0 \\ 1/9 & 1/18 & 0 & 1/6 & 0 & 1/3 \end{bmatrix} \quad (5.103a)$$

$$[\hat{\mathbf{M}}^L]^{(e)} = \pi r_0^2 H^{(e)} \rho^{(e)} \begin{bmatrix} 1/4 & & & & & & & \\ & 1/4 & & & & & & \\ & & 3/4 & & & & & \\ & & & 3/4 & & & & \\ & & & & 3/4 & & & \\ & & & & & 3/4 & & \\ & & & & & & 3/4 & \\ & & & & & & & 3/4 \end{bmatrix} \quad (5.103b)$$

where $\rho^{(e)}$ is the mass density of the element and r_0 and H are the dimensions shown in Figure 5.5-3.

The corresponding mass matrices for the first Fourier harmonic case are

$$[\hat{\mathbf{M}}^C]^{(e)} = \pi r_0^2 H^{(e)} \rho^{(e)} \begin{bmatrix} 1/9 & 1/18 & 1/36 & 0 & 1/36 & 1/18 & 0 & 1/18 \\ 1/18 & 1/9 & 1/18 & 0 & 1/18 & 1/36 & 0 & 1/36 \\ 1/36 & 1/18 & 1/6 & 0 & 0 & 1/12 & 0 & 0 \\ 0 & 0 & 0 & 1/6 & 0 & 0 & 1/12 & 0 \\ 1/36 & 1/18 & 0 & 0 & 1/6 & 0 & 0 & 1/12 \\ 1/18 & 1/36 & 1/12 & 0 & 0 & 1/6 & 0 & 0 \\ 0 & 0 & 0 & 1/12 & 0 & 0 & 1/6 & 0 \\ 1/18 & 1/36 & 0 & 0 & 1/12 & 0 & 0 & 1/6 \end{bmatrix} \quad (5.104a)$$

$$[\hat{M}^L] = \pi r_0^2 H^{(e)} \rho^{(e)} \begin{bmatrix} 2/5 & & & & & \\ & 2/5 & & & & \\ & & 3/5 & & & \\ & & & 3/4 & & \\ & & & & 3/4 & \\ & & & & & 3/5 \\ & & & & & & 3/4 \\ & & & & & & & 3/4 \end{bmatrix} \quad (5.104b)$$

Using the methods described above, the mass and stiffness matrices of all elements in the cylindrical core can be evaluated.

From the above element matrices the mass and stiffness matrices for the entire cylindrical core can be assembled. For a system with n soil layers the assembled matrices associated with the zero and first harmonics have the dimensions $3n \times 3n$ and $4n \times 4n$ respectively.

5.5.6 IMPROVING THE BENDING BEHAVIOR OF THE ELEMENTS

The standard method for computing the stiffness matrix of the axisymmetric elements will result in poor behavior of the piles in bending. This is because, in numerical integration of the stiffness in Eq. (5.84) using Gauss quadrature, the Gauss points are distributed such that the shear energy part of the integrand is computed too large and is sufficient to lock the element in shear deformation. To remedy this problem, one of the following techniques may be used.

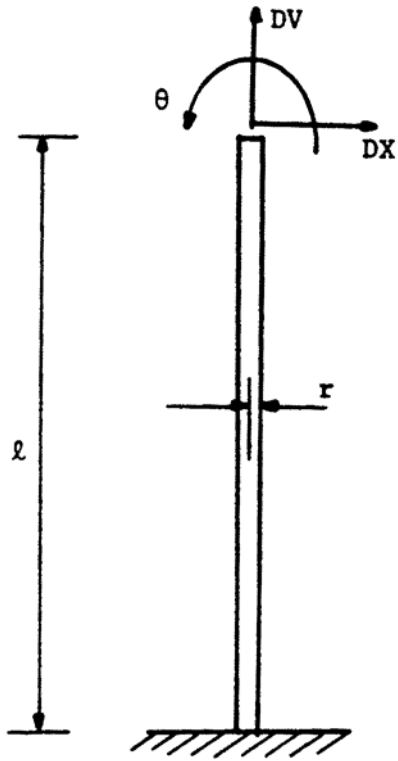
One technique is to remove the so called "parasitic shear" by selecting special Gauss points. This technique has successfully been used by Zienkiewicz et al [Ref. 35] and later was applied by Kuhlemeyer [Ref. 47]. The strain energy in the element, represented by Eq. (5.84), is the sum of the normal and the shear strain energy. Since there is no coupling between the normal strains and shear strains in the stress-strain relationships (see Eqs. (5.99) and (5.101)), the normal and shear strain energy can be computed separately (see Zienkiewicz [Ref. 35]). In the numerical integration, different numbers of Gauss points may be used for each part. As will be seen, the use of 2 x 2 Gauss points for the normal strain energy and 1 x 1 Gauss points for the shear strain energy yields accurate results for the piles. It should be noted, also, that this technique not only improves the bending behavior of the piles but also reduces the numerical operations needed to compute the stiffness of each element.

An alternative technique is to use incompatible modes. These higher modes can model the strains in the element in bending behavior more accurately. The use of incompatible modes results in a more flexible element.

In order to investigate the improvement obtainable by the above techniques the static displacements of the cylindrical cantilever beam shown in Figure 5.5-4 were determined using several methods and discretizations of the beam.

The results of this investigation are shown in Figures 5.5-5 to 5.5-7 Each figure corresponds to a given slenderness ratio, ℓ/r , of the beam and contains four subfigures which represent (a) vertical displacements due to vertical load, (b) rotation due to horizontal load, (c) horizontal displacements due to horizontal load (free rotation at top), and (d) horizontal displacement due to horizontal load (fixed rotation at top). All displacements refer to the top of the beam and have been normalized with respect to "exact" values from beam theory (B.T.). The abscissa in all subfigures indicates the number of elements used to represent the beam.

The curve marked "element" in Figure 5.5-5(c) shows results obtained when the coefficients α_1 to α_6 in Eq. (5.89) are set to zero (standard case) and 2x 2 Gauss points are used for both the normal and shear strain energy parts of Eq. (5.84). The curve deviates significantly from unity and this method is therefore not acceptable for piles.



$$r = 1.0 \text{ ft}$$

$$E = 8.82 \times 10^8 \text{ psf}$$

$$\nu = .25$$

$$l = 10, 30, 60 \text{ ft}$$

Figure 5.5-4. Cantilever Beam

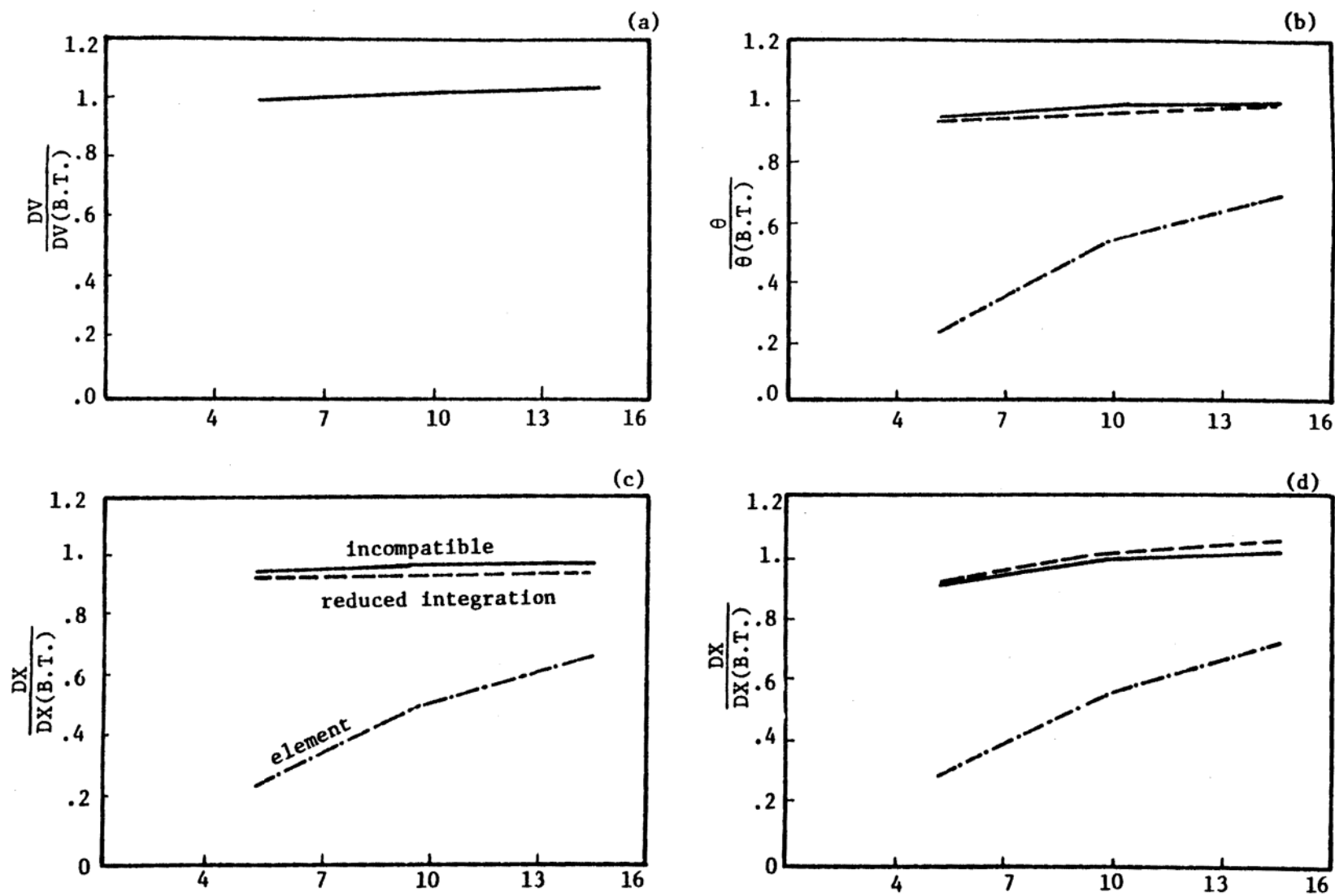


Figure 5.5-5. Comparison of the Pile ($l/r = 10$) with beam theory. (a) Axial Displacement; (b) Head Rotation; (c) Lateral Displacement (Free Rotation); (d) Lateral Displacement (Fixed Rotation)

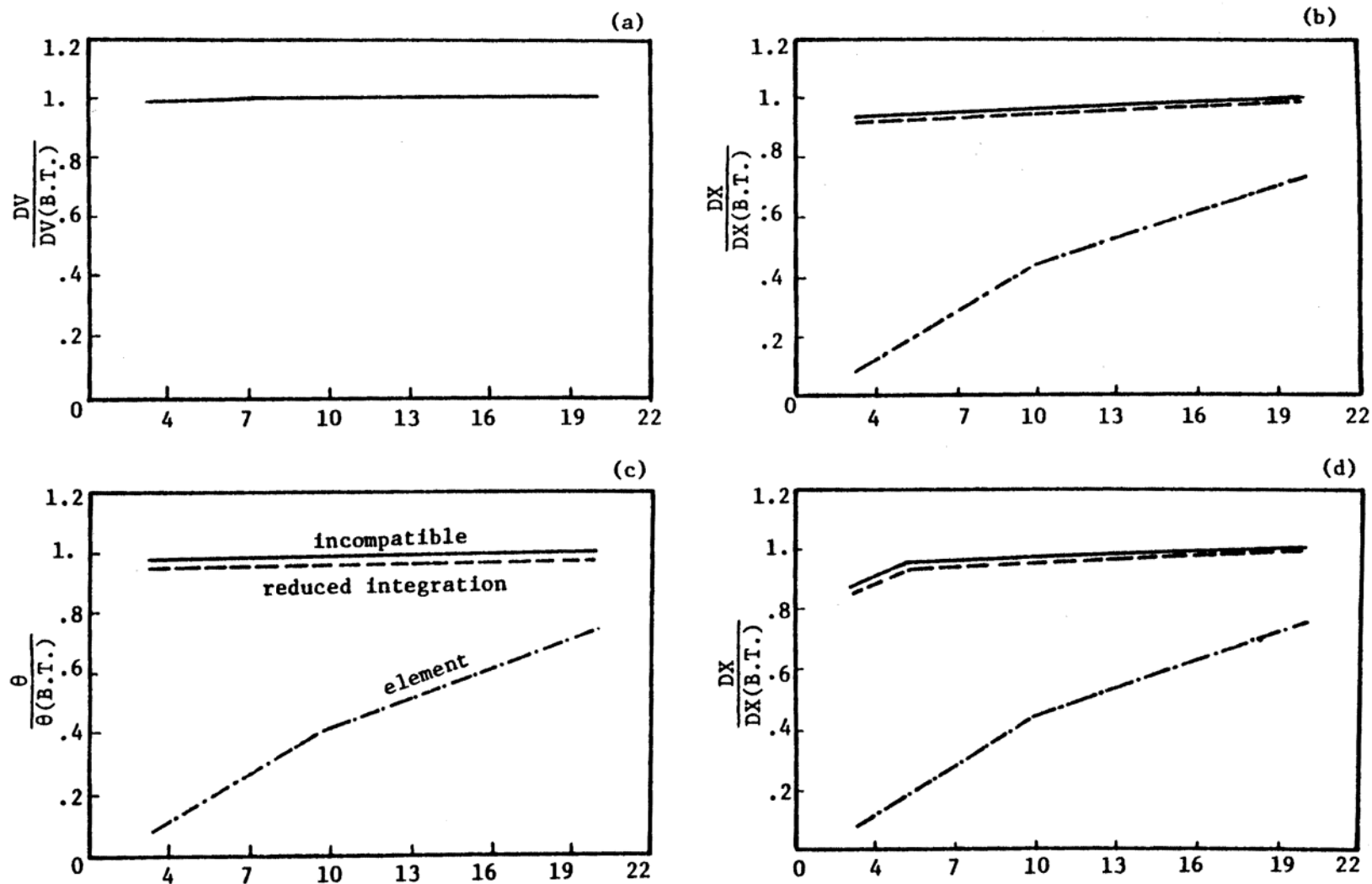


Figure 5.5-6. Comparison of the Pile ($l/r = 30$) with beam theory. (a) Axial Displacement; (b) Lateral Displacement (Free Rotation); (c) Head Rotation; (d) Lateral Displacement (Fixed Rotation)

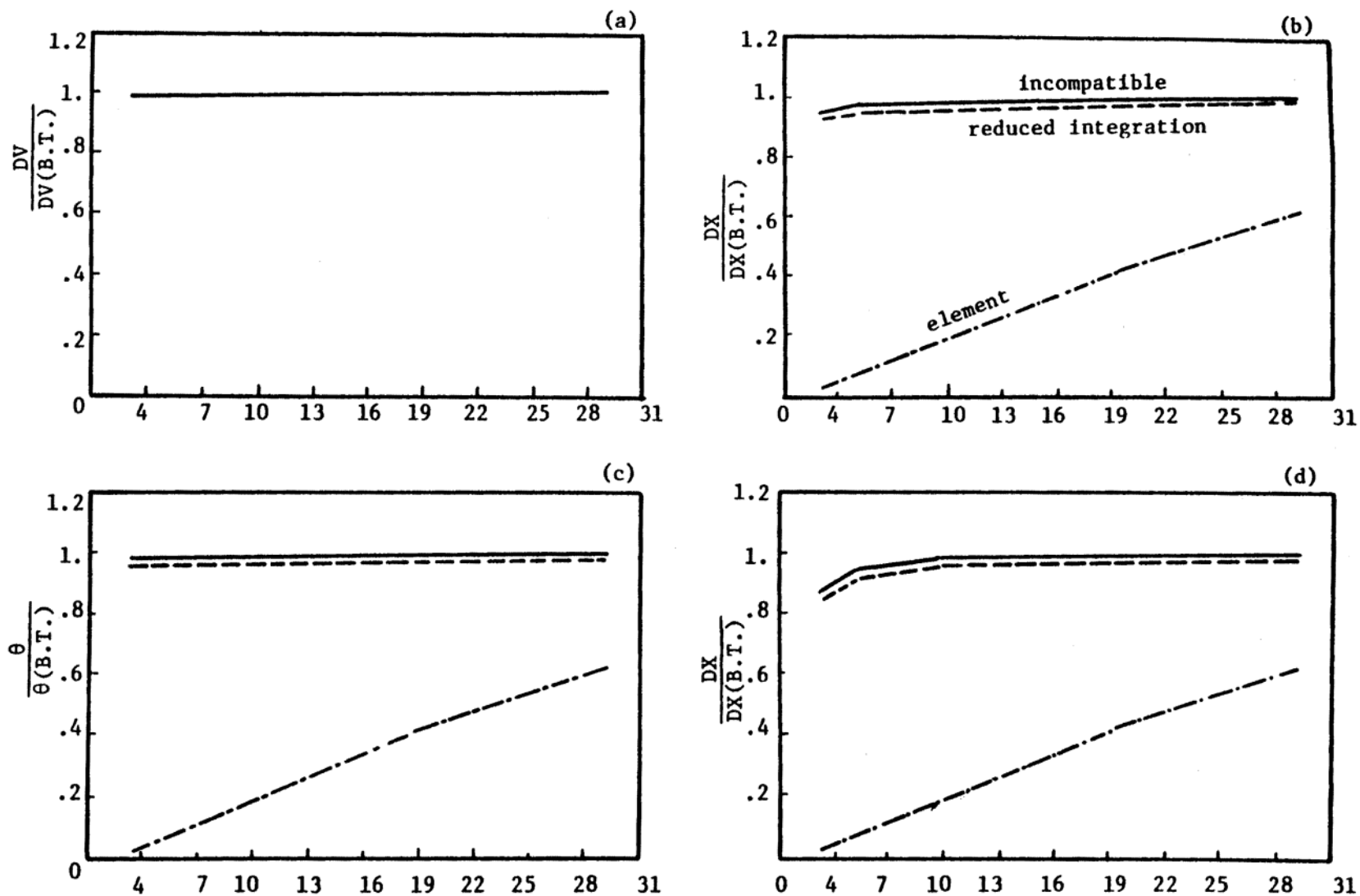


Figure 5.5-7. Comparison of the Pile ($\ell/r = 60$) with beam theory. (a) Axial Displacement; (b) Lateral Displacement (Free Rotation); (c) Head Rotation; (d) Lateral Displacement (Fixed Rotation)

The curve marked "reduced integration" was obtained by using 2 x 2 Gauss points for the normal strain energy and 1 x 1 Gauss points for the shear strain energy part of Eq. (5.84). Finally the curve marked "incompatible" was obtained by using incompatible modes. Both of the latter curves are close to unity for all load cases. Any of these methods are therefore acceptable and both options are provided in the computer program PILE which implements the method.

It should be noted, however, that the normalized axial deformations shown in Figures 5.5-5(a), 5.5-6 (a) and 5.5-7(a) are not horizontal. This is due to the fact that the degrees of freedom U_{z_1} and U_{z_4} shown in Figure 5.5-3(a) are not forced to be equal as they would be in standard beam theory. It would be possible to enforce this condition. However, this option was not chosen in the current work.

5.5.7 CONSIDERATIONS FOR PIPE PILES

The governing factors in the stiffness of the pile itself are EA and EI, where E is the Young's modulus, A is the axial area, and I is the moment of inertia. For the case of a pipe pile, A and I are computed from the actual solid sectional area and the thickness of the pipe wall. The axisymmetric elements, described in the previous sections, model the pipe piles as a solid cylinder. Since the displacement field caused by the vibration of a single pile will be used later to construct the flexibility matrix for pile groups it is important to use the actual radius, r, of the pipe pile in the model. In order to retain the actual EA and EI stiffness components in the model, without changing the radius, the following adjustments are made to the data:

Once the radius is fixed, the cross-sectional area A' and moment of inertia I' for a solid cylinder with radius r can be determined and adjusted. Young's moduli E'_1 and E'_2 to be used in the stiffness computation for the zero and first harmonics, respectively, can be determined from

$$E'_1 A' = EA ,$$

$$E'_2 I' = EI .$$

Similarly an adjusted mass density ρ' can be determined from the actual mass density ρ such that

$$\rho' A' = \rho A$$

or

$$\rho' = \rho \frac{A}{A'}.$$

5.5.8 THE SEMI-INFINITE REGION

Both the general flexible volume method and the special method discussed in this chapter requires the use of special boundary conditions to simulate the semi-infinite extent of the layered medium outside the region modeled by finite elements. A perfect transmitting boundary for plane strain analysis was developed by Waas [Ref. 32] and his method was later extended by Kausel [Ref. 66] to the axisymmetric case. Only the latter case will be discussed herein.

The discussion is divided into three parts. First, in Section 5.5.8.1, a general solution is presented for the motion outside the boundary. Second, in Section 5.5.8.2, the boundary condition is developed and, third, in Section 5.5.8.2, a method is presented for computing the actual motions outside the transmitting boundary.

5.5.8.1 The General Solution

As in the impedance analysis described in Section 4.2, it is assumed that the site consists of n horizontal layers over a rigid base and that within each layer all displacements vary linearly with depth. Thus, working in cylindrical coordinates, a harmonic displacement field is completely determined by a vector $\{U(r, \theta)\}$ which contains the $3n$ displacement amplitudes at the layer interfaces. Using Fourier expansion in the θ -direction the above vector can be written

$$\{U(r, \theta)\} = \sum_{m=0}^M \{U(r)\}_m \exp(im\theta). \quad (5.105)$$

In analogy with Section 5.5.3 only the first two terms of this series need to be considered, i.e. $M = 1$.

Using a technique first developed by Lysmer [Ref. 8] and Waas [Ref. 33] for the plane strain case, Kausel [Ref. 66] set up the equations of motion for the axisymmetric system defined above and showed that in the region outside the cylindrical core, i.e. $r \geq r_0$, the solution for the m^{th} Fourier harmonic is of the form

$$\{U(r)\}_m = [W(r)]_m \{\Gamma\}_m \quad (5.106)$$

where

$$\{\Gamma\}_m^T = \langle \alpha_1, \dots, \alpha_{3n} \rangle \quad (5.107)$$

is a constant vector. The elements α_s , $s = 1, \dots, 3n$, are called mode participation factors and depend on the boundary conditions of $r = r_0$.

The $3n \times 3n$ matrix $[W(r)]_m$ has the general elements

$$w_{is}(r) = \begin{cases} H'_m(k_s r) \cdot x_{i,s} + \frac{m}{r} H_m(k_s r) \cdot x_{i+2,s}, & \text{for } i = 1, 4, \dots, 3n-2 \\ H_m(k_s r) \cdot k_s \cdot x_{i,s}, & \text{for } i = 2, 5, \dots, 3n-1 \\ \frac{m}{r} H_m(k_s r) x_{i-2,s} + H'_m(k_s r) \cdot x_{i,s}, & \text{for } i = 3, 6, \dots, 3n \end{cases} \quad (5.108)$$

where H_m is the Hankel function of order m of the second kind (usually denoted $H_m^{(2)}$) and H'_m is the derivative of this function.

The coefficients k_s are called wave numbers and the coefficients $x_{i,s}$ are the elements of certain mode shape vectors $\{x\}_s$. These elements will be defined later, see Eqs. (5.119) and (5.120). Each wave number and its associated mode shape define a cylindrical Rayleigh or Love wave motion propagating in the positive r -direction

Equation (5.106) defines a complete system of such waves with amplitudes defined by the mode participation factors.

The wave numbers and the associated mode shapes are independent of the order, m , of the Fourier term and can be determined from the eigenvalues and associated eigenvectors of two uncoupled algebraic eigenvalue problems. One for Rayleigh wave motion

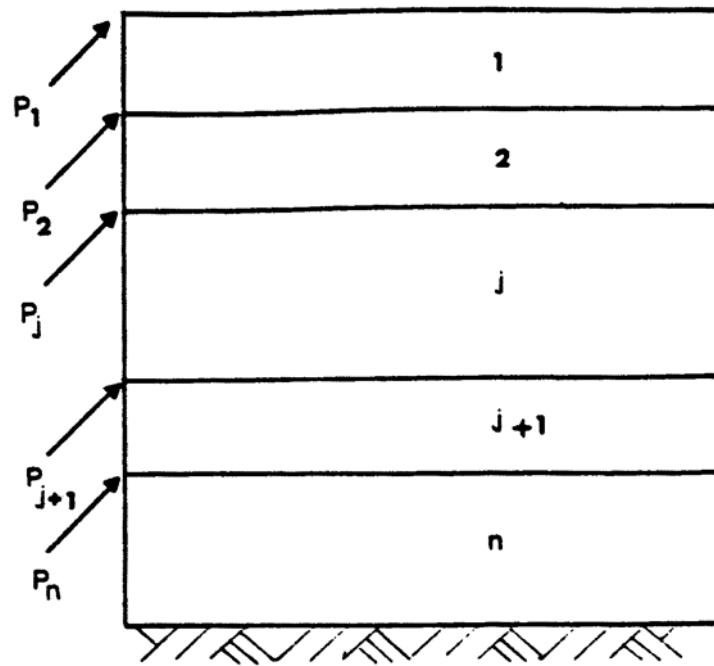
$$([A]_{2n}k^2 + i[B]_{2n}k + [G]_{2n} - \omega^2[M]_{2n})\{Y\}_{2n} = 0 \quad (5.109)$$

and another for Love wave motion

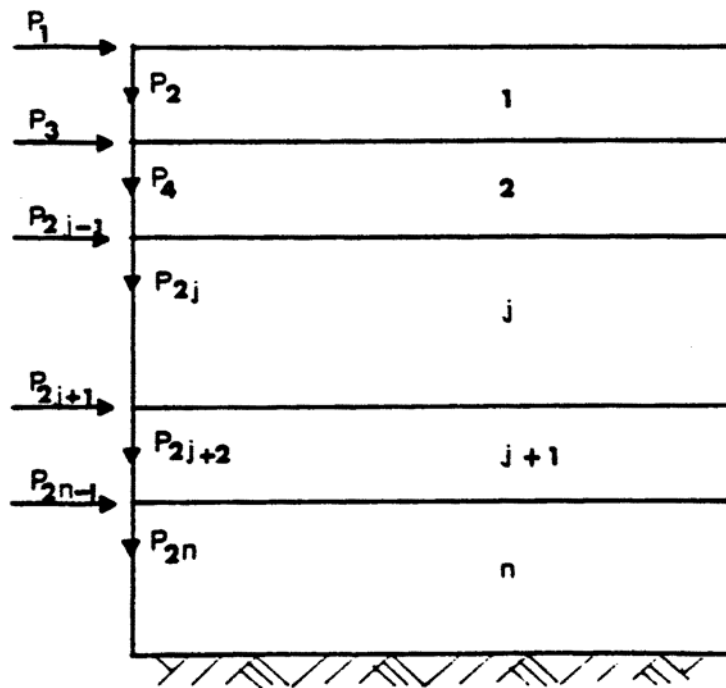
$$([A]_n k^2 + [G]_n - \omega^2[M]_n)\{Y\}_n = 0. \quad (5.110)$$

These equations, which are actually a reduced form of the equations of motion, are identical to the set of equations previously developed by Waas [1972) for the plane strain case.

In the above equations the subscripts $2n$ and n indicate the dimensions for the square matrices and vectors involved for an n -layer system. ω^2 is the known frequency of excitation, k is an unknown wave number (eigenvalue) and $\{Y\}_{2n}$ and $\{Y\}_n$ are the associated eigenvectors which correspond to the degrees of freedom shown in Figure 5.5-8.



(a)



(b)

Figure 5.5-8. Degrees of Freedom: (a) Love Wave, and (b) Rayleigh Wave

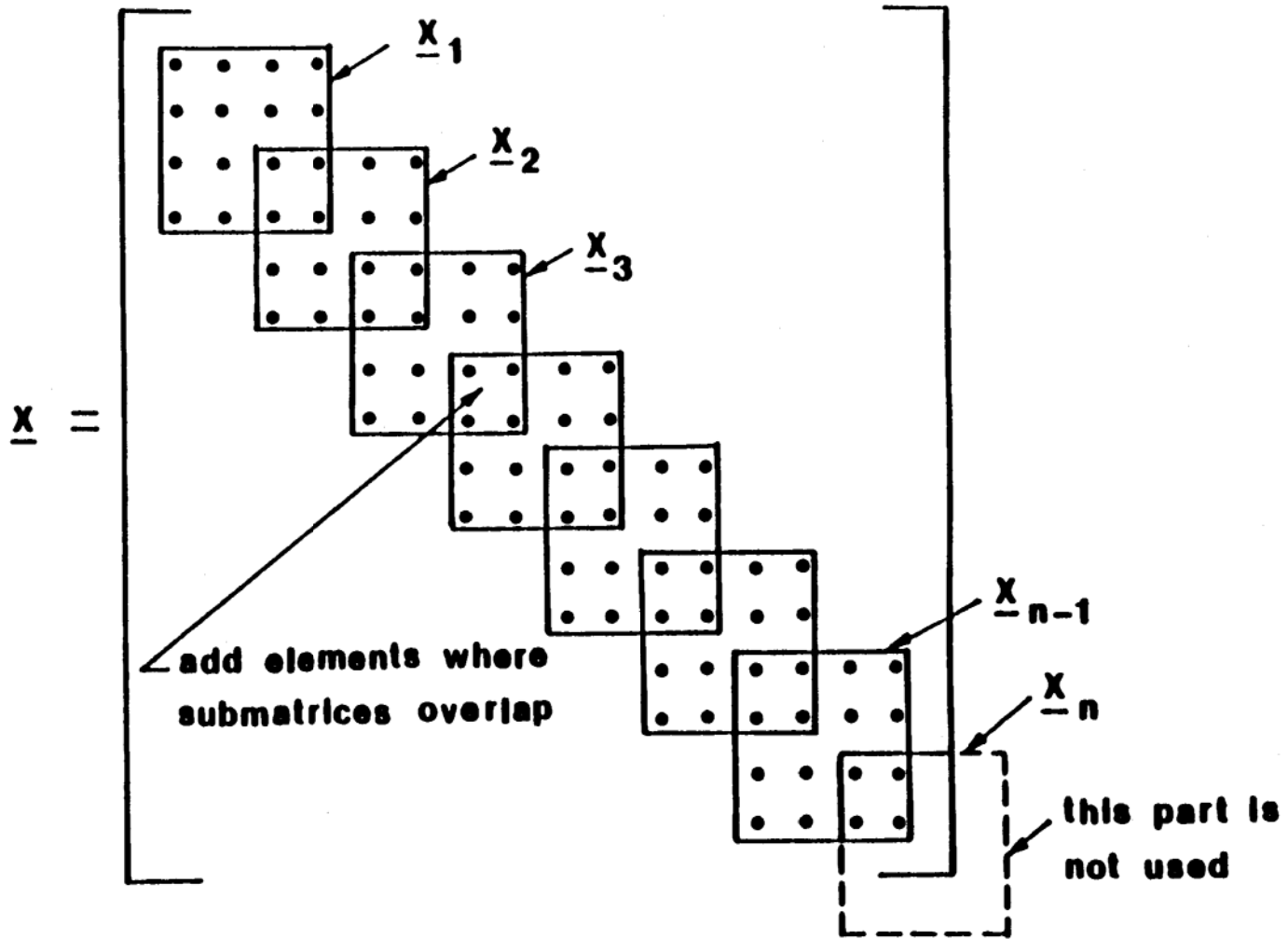


Figure 5.5-9. Structure of Matrices [A], [B], [G], [M]

a. Rayleigh wave case

The matrices $[A]_{2n}$, $[B]_{2n}$, $[G]_{2n}$ and $[M]_{2n}$ in Eq. (5.109) are assembled from submatrices according to the scheme shown in Figure 5.5-9. Each submatrix corresponds to a soil layer. Denoting the thickness of the j^{th} layer from the top by h_j , the mass density by ρ_j , the shear modulus by G_j , and Lamé's constant by λ_j , these layer submatrices are:

$$[A_j]_{2n} = \frac{h_j}{6} \begin{bmatrix} 2(\lambda_j + 2G_j) & 0 & (\lambda_j + 2G_j) & 0 \\ 0 & 2G_j & 0 & G_j \\ (\lambda_j + 2G_j) & 0 & 2(\lambda_j + 2G_j) & 0 \\ 0 & G_j & 0 & 2G_j \end{bmatrix} \quad (5.111)$$

$$[B_j]_{2n} = \frac{1}{2} \begin{bmatrix} 0 & -(\lambda_j - G_j) & 0 & (\lambda_j + G_j) \\ (\lambda_j - G_j) & 0 & (\lambda_j + G_j) & 0 \\ 0 & -(\lambda_j + G_j) & 0 & (\lambda_j - G_j) \\ -(\lambda_j + G_j) & 0 & -(\lambda_j - G_j) & 0 \end{bmatrix} \quad (5.112)$$

$$[G_j]_{2n} = \frac{1}{h_j} \begin{bmatrix} G_j & 0 & -G_j & 0 \\ 0 & (\lambda_j + 2G_j) & 0 & -(\lambda_j + 2G_j) \\ -G_j & 0 & G_j & 0 \\ 0 & -(\lambda_j + 2G_j) & 0 & (\lambda_j + 2G_j) \end{bmatrix} \quad (5.113)$$

$$[M_j]_{2n}^{(c)} = \frac{\rho_j h_j}{6} \begin{bmatrix} 2 & 0 & 1 & 0 \\ 0 & 2 & 0 & 1 \\ 1 & 0 & 2 & 0 \\ 0 & 1 & 0 & 2 \end{bmatrix} \quad (5.114a)$$

$$[M_j]_{2n}^{(\ell)} = \frac{\rho_j h_j}{2} \begin{bmatrix} 1 & 0 & 0 & 0 \\ 0 & 1 & 0 & 0 \\ 0 & 0 & 1 & 0 \\ 0 & 0 & 0 & 1 \end{bmatrix} \quad (5.114b)$$

b. Love wave case

The matrices $[A]_n$, $[B]_n$, $[G]_n$ and $[M]_n$ in Eq. (5.110) are assembled in a similar manner from the 2 x 2 layer submatrices defined below

$$[A_j]_n = h_j G_j \begin{bmatrix} 1/3 & 1/6 \\ 1/6 & 1/3 \end{bmatrix} \quad (5.115)$$

$$[G_j]_n = \frac{G_j}{h_j} \begin{bmatrix} 1 & -1 \\ -1 & 1 \end{bmatrix} \quad (5.116)$$

$$[M_j]_n^{(c)} = \frac{\rho_j h_j}{6} \begin{bmatrix} 2 & 1 \\ 1 & 2 \end{bmatrix} \quad (5.117a)$$

$$[M_j]_n^{(\ell)} = \frac{\rho_j h_j}{2} \begin{bmatrix} 1 & 0 \\ 0 & 1 \end{bmatrix} \quad (5.117b)$$

In each case a combination of consistent and lumped mass matrices is used. The combined mass matrix is

$$[M_j] = \alpha [M_j]^{(c)} + (1 - \alpha) [M_j]^{(l)} \quad (5.118)$$

where α is a constant coefficient chosen to be .50.

The solutions to the eigen equations (5.108) and (5.109) consist of two sets of $4n$ and $2n$ wave numbers and associated mode shapes, respectively. Each wave number and its associated mode shape represent a possible cylindrical surface wave. For the damped system considered herein all wave numbers are complex and occur in pairs of opposite signs. Only modes which propagate energy in the positive r -direction are of interest. These can be isolated by taking only the $2n$ Rayleigh modes and the n Love modes for which the wave number, k , has a negative imaginary part. The relationship between the mode shape coefficients in Eq. (5.108) and the eigenvectors obtained from Eqs. (5.109) and (5.110) can be expressed as follows:

For each eigen solution k_s , $\{Y\}_{2n,s}$, $s = 1, \dots, 2n$, of Eq. (5.109)

$$x_{i,s} = \begin{cases} y_{(i+2)/3}, & \text{for } i = 1, 4, \dots, 3n - 2 \\ y_{(i+1)/3}, & \text{for } i = 2, 5, \dots, 3n - 1 \end{cases} \quad (5.119)$$

For each eigen solution k_s , $\{Y\}_{n,s}$, $s = 2n+1, 3n$ of Eq. (5.110)

$$x_{i,s} = y_{i/3}, \quad \text{for } i = 3, 6, \dots, 3n. \quad (5.120)$$

The above Eqs. (5.108) to (5.120) completely define the matrix $[W(r)]_m$ in Eq. (4.26) and thus the entire displacement field for $r > r_0$ in terms of the unknown mode participation factors α_s , $s = 1, \dots, 3n$, in Eq. (5.107).

5.5.8.2 The Boundary Condition

Since the form of the displacement field is now known, the strain field can be obtained by differentiation of Eq. (5.106). From the strains the stresses in each layer can be computed and these can again be integrated to find the equivalent nodal forces, $\{P_b\}_m$, at $r = r_0$ shown in Figure 5. 5-10. The expression for these forces will depend linearly on the unknown mode participation factors defined by Eq. (5.107). Hence, $\{\Gamma\}_m$ can be eliminated by Eq. (5.106) and the relationship between the nodal displacement amplitudes and force amplitudes at $r = r_0$ can be expressed in the linear form

$$\{P\}_m = [R]_m \{U_b\}_m \quad (5.121)$$

which is the boundary condition which appears in Eq. (5.90). The matrix $[R]_m$ is frequency dependent and can be thought of as a dynamic stiffness matrix for the entire region $r \geq r_0$.

The algebraic manipulations required to develop the $3n \times 3n$ symmetric matrix $[R]_m$ have been completed by Kausel [Ref. 66]. They are rather extensive and will not be repeated herein. The final result is

$$[R]_m = r_0 \left\{ [A][\psi]_m [K^2] + ([D] - [E] + m[N])(\phi)_m [K] - m \left(\frac{m+1}{2} [L] + [Q] \right) [\psi]_m \right\} [W(r_0)]^{-1} \quad (5.122)$$

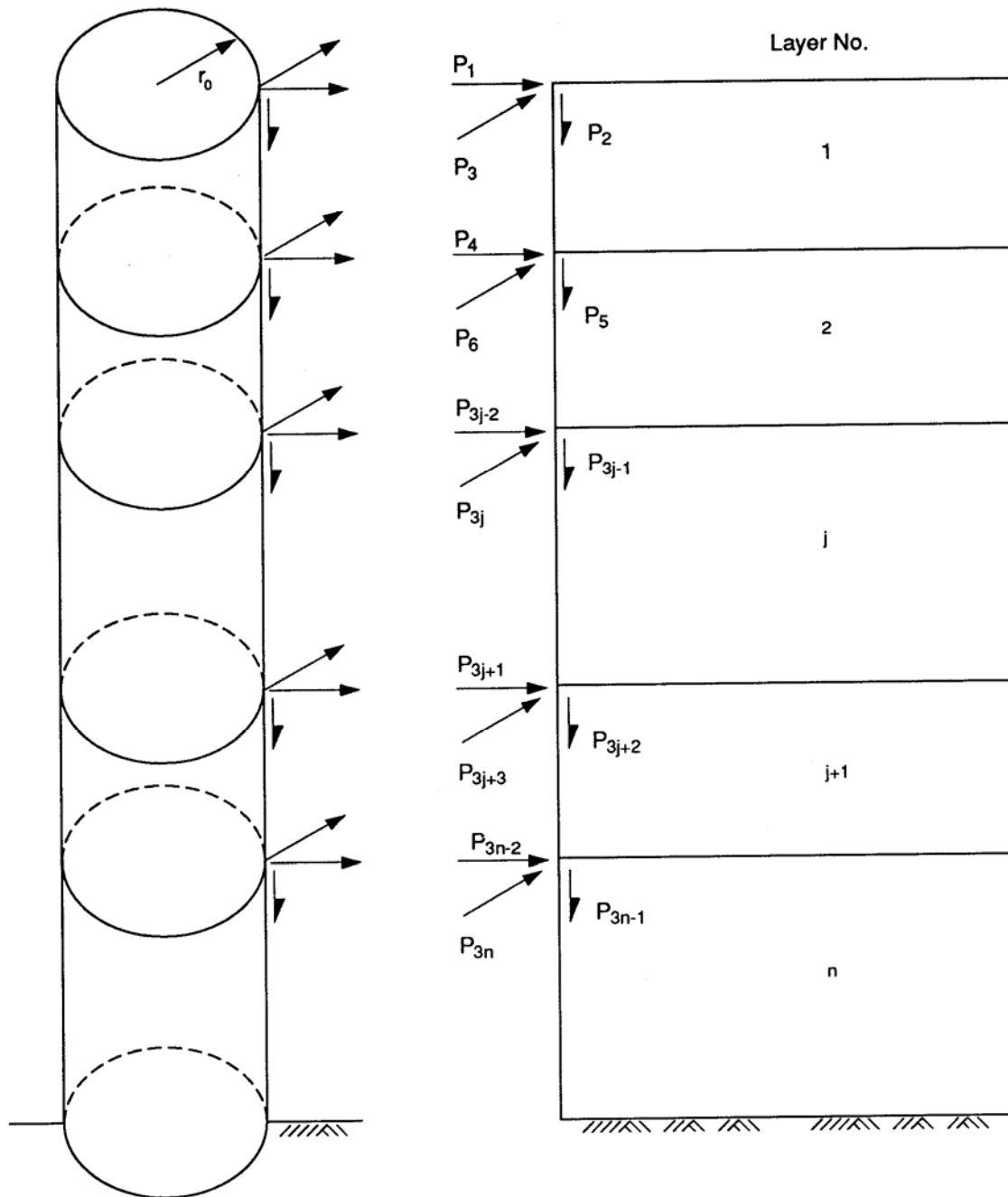


Figure 5.5-10. Degrees of Freedom on Transmitting Boundary

where m is the number of the harmonic considered, r_0 is the radial distance from the central axis to the transmitting boundary. The matrices $[K]$ and $[K^2]$ are simple diagonal matrices which contain the wave numbers k_s and k_s^2 , respectively, on their diagonals in the same order as the columns of $[W(r_0)]$.

The matrices $[A]$, $[D]$, $[E]$, $[N]$, $[L]$ and $[Q]$ are assembled from submatrices according to the scheme shown in Figure 5.5-9. The submatrices are:

$$[A]_j = \frac{h_j}{6} \begin{bmatrix} 2(\lambda_j + 2G_j) & 0 & 0 & (\lambda_j + 2G_j) & 0 & 0 \\ 0 & 2G_j & 0 & 0 & G_j & 0 \\ 0 & 0 & 2G_j & 0 & 0 & G_j \\ 2(\lambda_j + 2G_j) & 0 & 0 & 2(\lambda_j + 2G_j) & 0 & 0 \\ 0 & G_j & 0 & 0 & 2G_j & 0 \\ 0 & 0 & G_j & 0 & 0 & 2G_j \end{bmatrix} \quad (5.123)$$

which is related to the matrices defined by Eqs. (4.31) and (4.35).

$$[D]_j = \frac{1}{2} \begin{bmatrix} 0 & \lambda_j & 0 & 0 & -\lambda_j & 0 \\ -G_j & 0 & 0 & G_j & 0 & 0 \\ 0 & 0 & 0 & 0 & 0 & 0 \\ 0 & \lambda_j & 0 & 0 & -\lambda_j & 0 \\ -G_j & 0 & 0 & G_j & 0 & 0 \\ 0 & 0 & 0 & 0 & 0 & 0 \end{bmatrix} \quad (5.124)$$

$$[E_j] = \frac{G_j h_j}{3r_0} \begin{bmatrix} 2 & 0 & 0 & 1 & 0 & 0 \\ 0 & 0 & 0 & 0 & 0 & 0 \\ 0 & 0 & 2 & 0 & 0 & 1 \\ 1 & 0 & 0 & 2 & 0 & 0 \\ 0 & 0 & 0 & 0 & 0 & 0 \\ 0 & 0 & 1 & 0 & 0 & 2 \end{bmatrix} \quad (5.125)$$

$$[N_j] = \frac{G_j h_j}{6r_0} \begin{bmatrix} 0 & 0 & 4 & 0 & 0 & 2 \\ 0 & 2 & 0 & 0 & 1 & 0 \\ 4 & 0 & 0 & 2 & 0 & 0 \\ 0 & 0 & 2 & 0 & 0 & 4 \\ 0 & 1 & 0 & 0 & 2 & 0 \\ 2 & 0 & 0 & 4 & 0 & 2 \end{bmatrix} \quad (5.126)$$

$$[L_j] = \frac{2}{3} \frac{G_j h_j}{r_0^2} \begin{bmatrix} 2 & 0 & -2 & 1 & 0 & -1 \\ 0 & 0 & 0 & 0 & 0 & 0 \\ -2 & 0 & 2 & -1 & 0 & 1 \\ 1 & 0 & -1 & 2 & 0 & -2 \\ 0 & 0 & 0 & 0 & 0 & 0 \\ -1 & 0 & 1 & -2 & 0 & 2 \end{bmatrix} \quad (5.127)$$

$$[Q_j] = \frac{G_j}{2r_0} \begin{bmatrix} 0 & 0 & 0 & 0 & 0 & 0 \\ 1 & 0 & -1 & -1 & 0 & 1 \\ 0 & 0 & 0 & 0 & 0 & 0 \\ 0 & 0 & 0 & 0 & 0 & 0 \\ 1 & 0 & -1 & -1 & 0 & 1 \\ 0 & 0 & 0 & 0 & 0 & 0 \end{bmatrix} \quad (5.128)$$

The $3n \times 3n$ matrices $[\psi]_m$ and $[\phi]_m$ are related to the mode shape vectors $\{x\}_s$. They have the elements

$$\psi_{i,s} = \begin{cases} H_m(k_s r_0) \cdot x_{i,s} & , \quad \text{for } i = 1, 4, \dots, 3n-2 \\ -H_{m-1}(k_s r_0) \cdot x_{i,s} & , \quad \text{for } i = 2, 5, \dots, 3n-1 \\ H_m(k_s r_0) \cdot x_{i,s} & , \quad \text{for } i = 3, 6, \dots, 3n \end{cases} \quad (5.129)$$

$$\phi_{i,s} = \begin{cases} -H_{m-1}(k_s r_0) \cdot x_{i,s} & , \quad \text{for } i = 1, 4, \dots, 3n-2 \\ H_m(k_s r_0) \cdot x_{i,s} & , \quad \text{for } i = 2, 5, \dots, 3n-1 \\ -H_{m-1}(k_s r_0) \cdot x_{i,s} & , \quad \text{for } i = 3, 6, \dots, 3n \end{cases} \quad (5.130)$$

In using the above formulas for $m = 0$ and 1 , observe that $H_{-1} = -H_1$.

The above formulas, Eqs. (5.122) to (5.130), completely define the boundary condition expressed by Eq. (5.121).

5.5.8.3 Motions Outside the Boundary

Assuming that the loading on the piles are given and having determined the boundary condition, Eq. (5.81b) can now be solved for each harmonic, $m = 0, 1$. The solution yields both the displacement amplitudes on the axis, $\{U_a\}_m$, and those on the boundary of the cylindrical core, $\{U_b\}_m$.

The former defines the motions of the pile and the latter may be used to compute the mode participation factors from Eq. (5.106), i.e.

$$\{\Gamma\}_m = [W(r_0)]_m^{-1} \{U_b\}_m, \quad m=0,1 \quad (5.131)$$

which is a simple calculation since $[W(r_0)]^{-1}$ has already been determined in connection with the computation of the matrix $[R]_m$, see Eq. (5.122).

Knowing $\{\Gamma\}_m$ the entire displacement field for $r > r_0$ can be computed from Eq. (5.106). This ability will be used in the following sections to evaluate pile-to-pile interaction.

5.5.9 SOIL-PILE-STRUCTURE SYSTEMS

Using the substructuring scheme shown in Figure 5.5-11, the above method for a single pile can be developed into a simplified method for a complete piloted system involving vertical piles and direct loads on the structure.

The substructuring is very similar to that used in the flexible volume method, see Figure 2.2-1. The basic difference is that in the new method the piles are considered to be parts of the foundation, see Figure 5.5-11(b), while in the standard flexible volume method they are considered to be parts of the structure.

With the new substructuring scheme the equations of motion for the superstructure, Eq. (2.42), remains unchanged except that the impedance matrix, $[x_f]$, must now include the effects of the embedded piles. This matrix can still be determined as the inverse of the flexibility matrix $[F]$ for the piloted foundation shown in Figure 5.5-11(b). Thus, the main difference between the new and the original method relates to the formation of the flexibility matrix. This topic will be discussed in the next section.

The seismic motions, U_f , in Eq. (2.2-6) can in principle be determined by performing a separate soil-structure interaction analysis of the soil-pile systems shown in Figure 5.5-11(b). However, this would greatly complicate the total analysis since it would require the introduction of many additional interaction nodes. For this reason seismic excitation will not be considered for the pile impedance method.

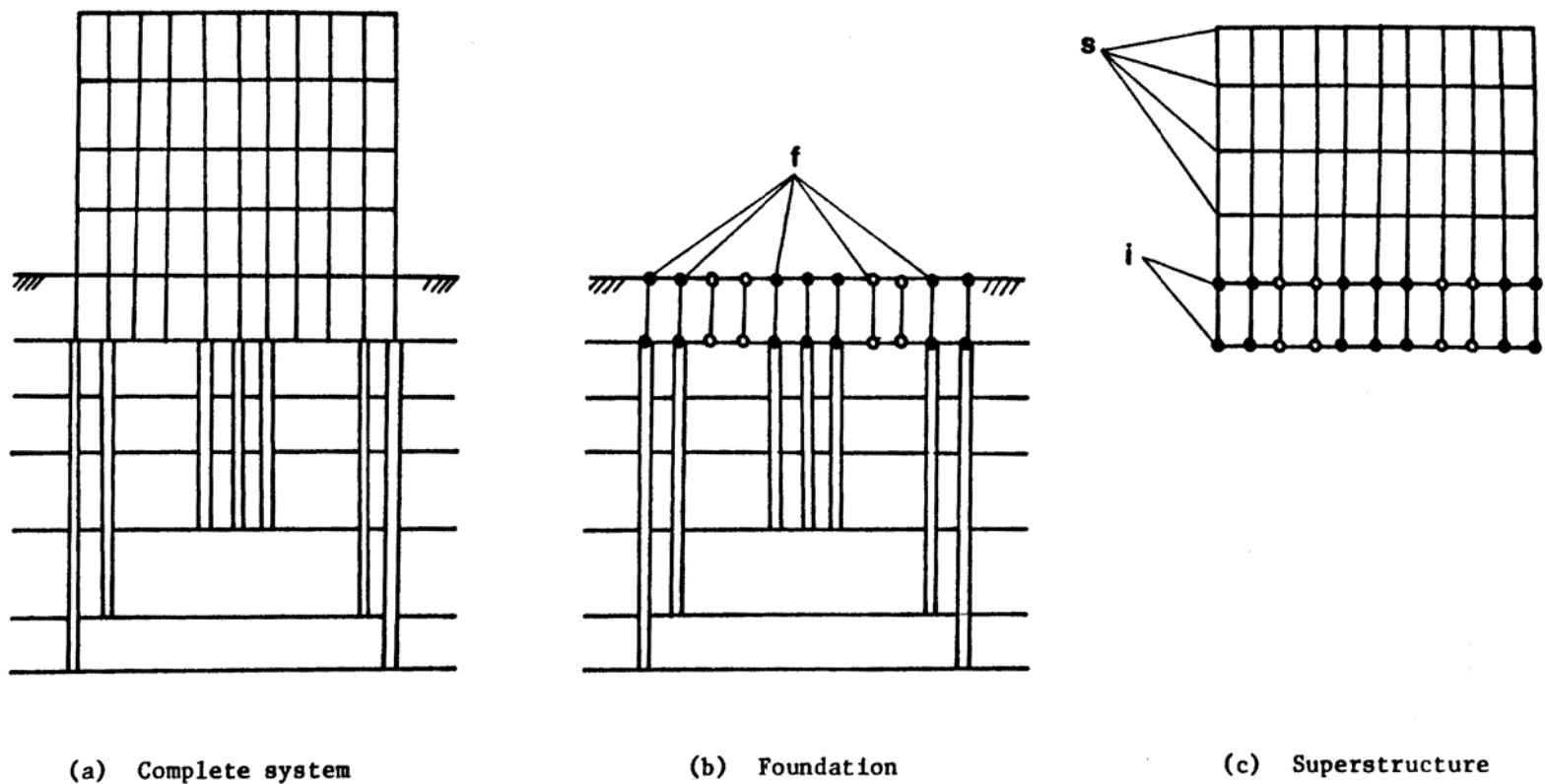


Figure 5.5-11. Substructuring for the Simplified Method

5.5.9.1 Global Flexibility Matrix

As in the flexible volume method, the columns of the flexibility matrix for the interaction nodes in Figure 5.5-11(b) are determined by successively applying harmonic loads of unit amplitude at each degree of freedom of the interaction nodes and evaluating the displacements of all interaction nodes. In order to facilitate this process these nodes are divided into two groups:

- Group 1 nodes, shown by open circles in Figure 5. 5-11(b), are those not located at a pile head or an extension of a pile axis.
- Group 2 nodes, shown by solid circles in Figure 5. 5-11(b), are those located at a pile head or on an extension of a pile axis.

Furthermore, it is assumed that the interaction nodes have only translational degrees of freedom and that displacements can be computed as if neighboring piles did not exist. These assumptions and their effects will be further discussed below.

With the above assumptions the displacements due to a unit load at a node of Group 1 can be determined exactly as for the flexible volume method, see Section 2.2. Only one cylindrical core model of the type shown in Figure 4.2-1 needs to be analyzed to handle all of the nodes of Group 1.

The nodes of Group 2 may be located above piles of different stiffness, diameter and length. The displacements caused by loads at nodes of this group can be determined using the simplified method for a single pile developed in the beginning of this chapter. Only one cylindrical core needs to be analyzed for each pile type (combination of stiffness, diameter and length).

Except for the different properties and dimensions of the cylindrical cores used, the computations for nodes of the two groups proceed in a similar manner and the following applies to both groups.

For each Fourier harmonic, m , the matrices in Eq. (5.81b) are formed and the total coefficient matrix on the left side is triangularized. Next the elements of P in Eq. (5.81b)

are successively set to unity and the solution $\langle U_a, U_b \rangle$ is obtained by back substitution. Since for any given cylindrical core the interaction nodes are limited to the upper, say j , layers, the above operation needs to be repeated for only the first $3j$ elements of P . The process is further simplified by the fact that for loads of any given interface, say at the top of layer ℓ , the solution for the vertical unit load $P_{3\ell-2}$ involves only the zero mode ($m = 0$) and the solution for the two horizontal loads, $P_{3\ell-1}$ and $P_{3\ell}$, involves only a single first mode ($m = 1$) solution.

For each of the load cases the displacements of the interaction nodes on the axis of the cylindrical core follow from $\{U_a\}$. The displacement amplitudes of the interaction nodes outside the cylinder can be computed from $\{U_b\}$ through Eqs. (5.131) and (5.132). The latter amplitudes will be obtained in cylindrical coordinates and are then transformed to Cartesian coordinates to determine the relevant column of the flexibility matrix. The transformation is as follows:

Displacements due to unit force in z direction

$$\bar{u}_x^z = u_r^z \cos \theta$$

$$\bar{u}_y^z = u_r^z \sin \theta$$

$$\bar{u}_z^z = u_z^z$$

where \bar{u}_x , \bar{u}_y , and \bar{u}_z is the displacement in x, y and z directions respectively, and u_r^z , u_r , and u_z^z are the amplitudes in cylindrical coordinates obtained from an $m = 0$ analysis.

Displacements due to unit force in the x direction

$$\bar{u}_x^x = u_r^x \cos^2 \theta + u_\theta^x \sin^2 \theta$$

$$\bar{u}_y^x = (u_r^r - u_\theta^r) \sin \theta \cos \theta$$

$$\bar{u}_z^x = -u_z^r \cos \theta$$

Displacements due to unit force in the y direction

$$u^y = (u_r^r - u_\theta^r) \sin \theta \cos \theta$$

$$\bar{u}_y^y = u_r^r \sin^2 \theta + u_\theta^r \cos^2 \theta$$

$$\bar{u}_z^y = -u_z^r \sin \theta$$

The displacements u_r^r , u_θ^r , and u_z^r are the displacement amplitudes in the $\theta = 0$ plane obtained from an $m = 1$ analysis for a unit load in the radial direction.

The procedure described in this section completely defines how to determine the individual columns of the flexibility matrix; and thus the entire matrix.

As discussed in Section 4.3, this matrix is then inverted to form the impedance matrix for the foundation substructure in Figure 5.5-11(b) and the remaining part of the analysis proceeds as in the standard flexible volume method.

5.5.10 CAPABILITIES AND LIMITATIONS OF THE PILE IMPEDANCE METHOD

The major advantage of the pile impedance method over the full method described earlier is a dramatic saving in computational effort and thus cost. The saving is achieved through the substructuring scheme which for the pile impedance method contains much fewer interaction nodes. In fact, with the pile impedance method, the number of interaction nodes for a problem with piles is about the same as for the corresponding problem without piles. Since the number of interaction nodes is the major factor in determining the cost of a total analysis, the pile impedance method reduces the cost of

an analysis of piloted structures to nearly that of an analysis for a directly founded structure.

The capability of the pile impedance method to include the effects of embedment and flexible pile caps (which are treated as part of the structure, see Figure 5. 5-11(c)) is a new feature which has not been part of previously published methods for analysis of piloted structures. It should be mentioned here that while Figure 5. 5-11 (c) shows a system for which all the pile caps are at the same level, this is not a limitation of the method.

Pile to pile interaction is treated by an approximate method. However, several verification studies, one of which is presented in the next section, have shown that the approximation is justified. Thus, the approximate method used imposes no limitations on the practical applications of the method.

The major limitations of the simplified method are: (1) that the piles must be vertical, and (2) that the seismic case cannot be considered. The latter limitation may not be too important since numerous studies have shown that in many practical situations the presence of piles have only minor effects on the seismic response of structures. The limitation in this respect is that the pile impedance method provides no means for estimating seismic forces in piles and pile caps.

Further limitations of the simplified method are that, as opposed to the complete method described in Chapter 3, the simplified method has no potential for handling the effects of nonlinearities of the soil between the piles by the equivalent linear method.

5.5.11 IMPLEMENTATION

The simplified method has been implemented in the form of a number of subroutines to and modifications of the computer program SASSI.

The method for analyzing single piles is coded in subprogram SPILE. The free field is solved by subprogram SITE and the necessary information such as soil properties, mode shapes and wave numbers are transferred to subprogram SPILE by Tape 2. In

SPILE one may request stiffness and damping coefficients of the head of one or more single piles. The boundary condition at the pile head and pile tip and different loadings may be specified by the user. It is also possible to assign different material properties for the elements along the pile. Information required to compute the flexibility matrix is saved on Tape 31 for use in program ANALYS.

CHAPTER 6

STRUCTURAL ANALYSIS

In this chapter, computation of the structural and excavated soil properties used in the coefficient matrix of the equations of motion, namely, the components C_{ss} , C_{si} , and C_{ii} , in Eqs. (2.2-6) or (2.3-3) or (2.3-3) or (2.3-4) are described.

6.1 MODELLING OF STRUCTURE

The structure, which consists of the superstructure and the basement, is modeled by finite elements. Several types of elements are included in the finite element library of SASSI. These elements include 3- to 4-node plane-strain elements (Ref. 1), 4- to 8-node three-dimensional solid elements (Ref. 1), thick shell element (Refs. 61, 62 and 64, to be completed) straight beam elements (Ref. 1), spring elements (Ref. 1), thin shell elements (LSST9, Ref. 1), inter-pile elements, and special matrix elements to assign stiffness or inertia relating any two nodes in the model. Formulation of mass and stiffness matrices for the above element types is not described but may be obtained from the reference cited. Basic theory for formulation of finite elements may be obtained from general finite element text books (e.g., Refs. 35 and 64).

The material damping is incorporated in the stiffness matrix using the complex modulus representation as described in Section 3.6. With this representation, the material damping ratio defined at the element level will be used to compute the complex stiffness of the element, thus allowing for variation of damping from element to element in the model. The mass matrices are either computed by the program by specifying the density for each element or assembled from the nodal lump mass input at the nodal points. When the mass matrix is computed by the program, the matrix consists of the summation of half lump mass and half consistent mass except for the plate and beam elements for which only lump mass and consistent mass matrices are computed, respectively.

Once the mass and stiffness elements are formed, they are assembled into global matrices. These matrices are frequency independent and need to be formed only once. Furthermore, they are symmetric and sparse and therefore can be stored in blocks using the active column method (Ref. 34) to minimize computer storage.

6.2 MODELLING OF EXCAVATED SOIL

The excavated soil is modeled using either plane-strain or three-dimensional solid elements for two- and three-dimensional problems, respectively. These elements are assigned two or three translational degrees of freedom per node. Thus, the moments from beam or plate elements are transferred to the soil through several common connecting nodes.

6.3 EXTENDED NEAR FIELD ZONE

In some cases it may become necessary to include an additional volume of the soil in the immediate vicinity of the basement in the SSI model. This may be the case where the soil properties around the basement are different from those of the otherwise horizontal layered site (e.g., due to backfilling) or when the magnitude of the stress and strain in the soil around the basement is needed to measure the secondary nonlinear effects. For these cases, an additional soil volume is modeled with plane strain or brick elements and these elements are treated as structural elements. Subsequently, the excavated soil elements must cover the additional soil volume already modeled as structural elements.

6.4 FINITE ELEMENT SIZE

The accuracy of a finite element analysis depends on the type of interpolation function used to represent the displacement field in the element and element sizes. The interpolation functions which are used for solid and plane strain elements in SASSI vary linearly within the element.

It has been shown (Ref. 8) that for such elements the accuracy of the solution is a function of the method used to compute the mass matrix and an accuracy better than 10 percent for wave amplitude is obtained if the element size h follows the relations shown below:

$$\left\{ \begin{array}{l} 1/8 \lambda_s \text{ for lumped mass matrix} \\ 1/8 \lambda_s \text{ for consistent mass matrix} \\ 1/5 \lambda_s \text{ for mixed mass matrix} \end{array} \right. \quad (6.4-1)$$

In the above relation λ_s is the shortest wavelength which occurs in the volume represented by the elements. The shortest wavelength is obtained from

$$\lambda_s = \frac{V_s}{f_{\max}} \quad (6.4-2)$$

where V_s is the shear wave velocity and f_{\max} is the maximum frequency of analysis which must be transmitted through the finite elements. Thus, larger element size can be used in the zones with higher shear wave velocity.

In calculating the mass matrices for brick and plane-strain elements, combination of half consistent mass matrix with half lump mass matrix is used. Thus, the criteria of $h < 1/5\lambda$ need to be followed in selecting the finite element sizes.

These criteria along with the appropriate choice of f_{\max} for the problem control the size of the model in terms of the degrees of freedom and subsequently the cost of analysis.

CHAPTER 7

SOLUTION OF THE EQUATION OF MOTION

Following the computations of free-field motion, $\left\{U_f'\right\}$, as described in Chapter 3, impedance matrix $[X_{ff}]$ as presented in Chapter 4, and the coefficient matrix of the structures and excavated soil volume as described in Chapter 6, the equations of motion can be formed and solved. Depending on the types of excitations, the following solution techniques are used.

7.1 STEADY STATE RESPONSE ANALYSIS

For steady state response analysis such as force vibration or seismic excitation of the SSI system at discrete harmonic frequencies, Eqs. (2.2-6) and (2.2-7) or (2.3-3) and (2.3-4) are formed for each selected frequency of analysis and solved. The results of analysis (U_s and U_f) are the harmonic complex displacement transfer functions for the case of external loading with units consistent with the selected system of units for the analysis. For the case of harmonic seismic excitation, the results (U_s and U_f) are the harmonic complex acceleration transfer functions representing the total response with respect to the harmonic input motion at control point.

7.2 TRANSIENT RESPONSE ANALYSIS

The complex response method described in Section 3.6 is formulated for steady state vibrations. However, transient motions such as earthquake motions or impulse loads can be analyzed using discrete Fourier transform techniques. These techniques are described for the case of transient external loading. However, they are equally applicable to transient earthquake motions.

Using these techniques the basic input is specified at N discrete points uniformly distributed over the period T . The given function values are

$$P_j(t) = P(j \cdot \Delta t) ; j = 0, 1, \dots, N-1 \quad (7.2-1)$$

where Δt is the time interval (T/N). The input can then be extended using trigonometric functions

$$P_j(t) = R_e \sum_{j=0}^{N/2} P_j \exp(i\omega_j t) \quad (7.2-2)$$

where ω_j are the frequencies,

$$\omega_j = \frac{2\pi j}{N\Delta t} \quad (7.3-3)$$

and P_j are complex amplitudes

$$P_j = \frac{2}{N} \sum_{j=0}^{N-1} P_j \exp(-i\omega_j \Delta t) \quad (7.2-4)$$

which can be computed by the very efficient Fast Fourier Transform (FFT) algorithm, developed by Cooley and Tukey (Ref. 6), which requires that N be a power of two. A further requirement is that since Eq. (7.2-2) is a truncated Fourier series, the function $P_j(t)$ has to be periodic over the period T . Actual earthquakes or impact loads are not periodic. However, by the addition of a "quiet zone" consisting of a limited number of trailing zeroes to the input, both the above requirements can be met. The quiet zone should be chosen sufficiently long such that the response occurring at the beginning of the next cycle is very small due to the system damping. In this case, the response within each cycle is not influenced by the previous cycle.

The solution for a single harmonic can be obtained by solving the equations of motion in Eq. (2.2-7) or Eq. (2.3-4). Since superposition of solutions is valid for linear systems, the solution of Eq. (2.2-7) or Eq. (2.3-4) is obtained independently at each frequency, and

the results are superimposed to obtain the complete response, using the following equation:

$$\begin{Bmatrix} U_s(t) \\ U_f(t) \end{Bmatrix} = R_e \sum_{j=0}^{N/2} \begin{Bmatrix} U_{sj} \\ U_{fj} \end{Bmatrix} \exp(i\omega_j t) \quad (7.2-5)$$

Discrete values of $\{u(t)\}$ at time intervals Δt can be computed by using the inverse Fourier transform on $\{U_j\}$ which is the solution for a single harmonic input.

To obtain a complete solution, the system of linear equations in Eq. (2.2-7) or Eq. (2.3-4). must, in principle, be formed and solved for all of the following FFT frequencies.

$$f_j = \frac{\omega_j}{2\pi} = \frac{j}{T}, \quad j = 1, \dots, N/2 \quad (7.2-6)$$

This is a formidable computational task. To minimize the cost, a cutoff frequency is introduced whereby the response for frequencies above a given f_{\max} are set to zero. The choice of f_{\max} depends on the SSI problem and type of the loading. This feature will considerably cut the number of frequencies to be solved. To further reduce the number of frequencies to be solved, the SASSI program uses an efficient interpolation scheme, whereby the complex response amplitudes U_s and U_f are computed for a certain number of selected frequencies, and the values for the rest of the FFT frequencies are obtained by interpolation. One interpolation technique that has been used previously is the interpolation based on the single-degree-of-freedom complex response function (Lysmer et al., Ref. 9).

For the program SASSI, a new technique based on the two-degrees-of-freedom complex response function is developed and used. This technique is more general and it is possible to choose the computed frequencies at wider intervals to further reduce the cost of analysis. This interpolation technique is described below.

7.3 SASSI INTERPOLATION TECHNIQUE

The interpolation technique used in SASSI to interpolate the response for frequencies in between the calculated frequencies and to obtain the response for all FFT frequencies is based on the frequency response function of a two-degree-of-freedom system. The total response of a two-degree-of-freedom system subjected to harmonic base excitation for each degree-of-freedom has the following general form:

$$r(\omega) = \frac{a_1\omega^4 + a_2\omega^2 + a_3}{\omega^4 + a_4\omega^2 + a_5} \quad (7.3-1)$$

where $r(\omega)$ is the response at frequency ω and a_1 , a_2 , a_3 , a_4 , and a_5 are the constants. Thus, if the response of the system is known at 5 frequencies i.e., r_1 , r_2 , r_3 , r_4 , and r_5 are known at frequencies ω_1 , ω_2 , ω_3 , ω_4 , and ω_5 , the constants in Eq. (7.3-1) can be obtained from

$$\begin{bmatrix} \omega_1^4 & \omega_1^2 & 1 & -\omega_1^2 & -r_1 \\ \omega_2^4 & \omega_2^2 & 1 & -\omega_2^2 & -r_2 \\ \omega_3^4 & \omega_3^2 & 1 & -\omega_3^2 & -r_3 \\ \omega_4^4 & \omega_4^2 & 1 & -\omega_4^2 & -r_4 \\ \omega_5^4 & \omega_5^2 & 1 & -\omega_5^2 & -r_5 \end{bmatrix} \begin{Bmatrix} a_1 \\ a_2 \\ a_3 \\ a_4 \\ a_5 \end{Bmatrix} = \begin{Bmatrix} \omega_1^4 r_1 \\ \omega_2^4 r_2 \\ \omega_3^4 r_3 \\ \omega_4^4 r_4 \\ \omega_5^4 r_5 \end{Bmatrix} \quad (7.3-2)$$

Following the computation of the 5 constants from the above equation, Eq. (7.3-1) can be used to compute the response (the interpolated response) for all the frequencies in the range ω_1 to ω_5 .

The interpolation technique described above can be used for interpolating transfer functions for multi-degree-of-freedom when the transfer functions behave like those of the two-degree-of-freedom system within small frequency regions. Following this technique, the frequency range for which Eqs. (2.2-6) and (2.2-7) or (2.3-3) and (2.3-4) are solved is subdivided into smaller regions each of which contains the transfer function solution for 5 frequencies of the analysis. For the last region, the solution from the previous region can be augmented, if necessary, to form the solution of 5 frequencies

needed for the interpolation. Using the above technique, the transfer function in each region is interpolated so that by covering all the regions, the transfer function values are computed for all FFT frequencies shown in Eq. (7.2-6).

7.4 CRITERIA FOR CHOOSING FREQUENCIES OF ANALYSIS

The frequencies to be selected for the analysis depend on the number of peaks in the transfer function at the specific response location and how close these peaks are located relative to each other. This information can be obtained from the fixed-base modal analysis of the structure. The modal properties show the significance of different frequencies in the response of the structure depending on the modal participation factors. The frequencies of analysis can be selected by recognizing that the SSI effects usually shift the frequencies to the lower frequency range and tend to flatten the sharp peaks or sometimes even eliminate the fixed-base response peaks. For most of the practical problems it is sufficient to solve the system for 10 to 20 frequencies. In the event that the fixed-base modal properties are not available, it is necessary to select adequate number of frequencies with uniform increment throughout the frequency range of interest.

In SASSI, it is possible to first calculate the transfer functions based on an initial set of selected frequencies and by examining this initial transfer function, if additional frequencies need be added, the program SASSI has the capability to obtain and combine the solutions from several sets of frequencies and subsequently interpolates the transfer function of the response based on the combined solution set.

CHAPTER 8

COMPUTER PROGRAM ORGANIZATION

The program SASSI (Ref. 12) is originally written in the Fortran IV language. The new additions also use Fortran 77 and Fortran 90. The program is organized in modules and the analysis steps as described in Section 2.4 are handled by separate modules. The program layout, operational features, its capabilities and limitations, and a summary description of its validation and application are presented in this section.

8.1 PROGRAM LAYOUT

Fig. 8.1-1 shows the layout of the SASSI program. A brief description of the function of each module and its interaction with other modules are presented in the following:

a. HOUSE

In this program the mass and stiffness matrices of all the elements used in the model are computed and stored on Tape 4. These properties are frequency independent and the computation is performed only once.

b. MOTOR

This program forms the load vector in Eq. (2.2-7) or (2.3-4). The loads may correspond to impact forces, rotating machinery, or simple unit forces to be used to determine the impedance of a foundation. It is possible to allow for loads acting out of phase. The results are stored on Tape 9.

c. SITE

This program solves the site response problem. The control point and wave composition of the control motion are defined. The information needed to compute vector $\{U_f'\}$ used in Eq. (2.2-6) or (2.3-3) is computed at this stage and is saved on

Tape 1. The program also stores information required for the transmitting boundary calculation on Tape 2. The actual time history of the control motion is not required in this program.

d. POINT

This program consists of two subprograms, namely, POINT2 and POINT3 for two- and three-dimensional problems, respectively. The modules described in Sections 4.1 and 4.2 are solved and the results, which provide the information required to form the flexibility matrix, are saved on Tape 3. Tape 2 created by program SITE is used as input.

e. INCOH

This program is used to develop the free field reactor following the formulation of incoherence models described in Chapter 2. This program uses Tape 1 from SITE and Tape 7 from HOUSE and generates Tape 11 for input to ANALYS. **This program is not completed at this time and is not available.**

f. SPILE

This program is used to solve for single pile and pile groups using pile impedance method described in Chapter 5. This program uses Tape 2 from SITE and generates tape 31 for use in ANALYSIS.

g. MATRIX

In this program, Tapes 3 and 4 are used as input to form the impedance matrix $[X_{ff}]$, for each frequency. The impedance matrix is saved on Tape 5. The coefficient matrix in Eqs. (2.2-6), (2.2-7), (2.3-3) and (2.3-4) is also formed, triangularized, and stored on Tape 6.

h. LOADS

Using the data of Tapes 1 and 9, this program computes the load vectors in Eqs. (2.2-6), (2.2-7), (2.3-3) or (2.3-4) for each frequency and stores them on an internal tape.

i. SOLVE

In this program the reduced stiffness matrices are read from Tape 6. The program then performs the back-substitution using the load vectors on the internal tape. If Eq. (2.2-6) or (2.3-3) is being solved, the solution is the transfer functions from the control motion to the final motions. If Eq. (2.2-7) or (2.3-4) is being solved, the solution is a set of transfer functions from external loads to total displacements. In either case, the results are stored on Tape 8.

The subprograms MATRIX, LOAD, and SOLVE are combined into a controlling program called ANALYS.

Interpolation of the transfer functions in the frequency domain and further output requirements are handled by the following subprograms.

j. MOTION

This program is a post-processor. It reads the transfer functions from Tape 8, performs the interpolations described in Section 6.3, and computes the final response at a specified node selected by the user. The information relating slave master nodes are read from Tape 4 generated by HOUSE as input to MOTION. Acceleration, velocity, or displacement of the response in terms of time history, peak value, or the response spectrum may be requested.

k. STRESS

This program reads Tapes 8 and 4 and computes requested stress, strain, and forces time histories and peak values in structural members.

l. COMBINE

If after interpolation it is found that some additional frequencies need to be included, this program combines the corresponding Tapes 8s and produces a new Tape 8.

m. PLOT

This program reads the nodal data and all finite element group data from Tape 7 made by HOUSE and generates the plots of the model. The plots can be made on various element groups or nodal groups for all or parts of the model. The plots can be viewed on the screen, plotted by the printer or imported to WORD or EXCEL for further processing.

8.2 OPERATIONAL FEATURES

If some changes occur in the design parameters, only part of SASSI system would need to be re-executed. This feature makes it possible to perform parametric studies in a very effective manner. The following examples illustrate the possible uses of the restart capabilities:

a. Change in seismic environment

The seismic environment is defined in terms of (1) the time history of the control motion, (2) the location of the control point, and (3) the composition as to type and direction of the waves assumed to cause the control motion. A re-analysis with a different time history requires only a simple re-execution of the program MOTION. If the control point and/or the wave composition are changed, only the programs SITE, ANALYS (LOAD, SOLVE), and MOTION need to be re-executed. This takes only a

small fraction of a complete re-analysis time since the expensive impedance matrix calculation does not have to be repeated.

b. Change in structure

If part of the structure is changed by changing material properties or by adding or subtracting elements, only HOUSE, part of MATRIX, SOLVE, and MOTION would have to be re-executed, as long as no new interaction nodes are added.

8.3 CAPABILITIES AND LIMITATIONS

The current version of computer program SASSI has the following capabilities and limitations:

- The site consists of semi-infinite horizontal layers resting on a rigid base or a semi-infinite halfspace.
- The seismic environment consists of an arbitrary three-dimensional superposition of inclined body waves and surface waves. It is also possible to introduce external forces such as impact loads, wave forces, or loads from rotating machinery acting directly on the structure.
- The structure(s) are represented by standard two- or three-dimensional finite element models.
- The method is restricted to linear analysis. However, approximate nonlinear analysis can be performed by the equivalent linear method.
- Primary nonlinear effects in the free-field and secondary nonlinear effects in a limited region near the structure can be considered.

Within the above limitations and that of available computer capacity the system can handle:

- Two- and three-dimensional SSI problems involving single or multiple structures
- Structure with rigid or flexible embedded foundation of arbitrary shape
- Machine foundation vibration problems
- Pile foundations
- Impact problems or problems involving wave and ice loadings
- Seismic loadings involving body waves and surface waves
- Effects of torsional ground motions
- Incoherent ground motion (to be completed)

8.4 PROGRAM VALIDATION AND APPLICATION

During the development of the theory and the corresponding analytical models, many example problems were analyzed to test the modules. These example problems and comparisons of the results with reference solutions are reported in Refs. 13, 30, 31, and 32. A comprehensive validation of the program has been carried out to benchmark the SASSI solutions against the published solutions (Ref. 2). The benchmark solutions consist of simple hand solutions, analytical or closed form solutions reported in the literature, and solutions obtained from other validated computer programs. The validation covers many capabilities of the program ranging from calculation of finite element mass and stiffness properties, impedance analysis of surface and embedded single and multiple foundations with rigid and flexible properties, scattering analysis of surface and embedded foundation subjected to vertical and inclined P-, SV-, and SH-waves, and surface Rayleigh and Love waves; and SSI analysis of surface and embedded structures. The favorable agreements between the SASSI results and the benchmark solutions obtained for all problem cases validate many capabilities of

computer program SASSI. In addition to the above validation report, SASSI capabilities have also been tested through the course of application of the program to an SSI experiment conducted by the U.S. NRC and EPRI. The objective of this project was to evaluate the validities of the current industry SSI methodologies by using the forced-vibration test data and the recorded actual earthquake response data obtained from a 1/4-scale containment structure constructed and instrumented in Lotung, Taiwan. The results of the SASSI analyses and correlation with the test results and the results of other SSI methods used are reported in Refs. 3 and 21. Results of this study provide the validation of the SASSI analysis capability for embedded structures against test results.

SASSI has been applied to many engineering projects. The first application of the program for analyses of an embedded power plant structure, an offshore structure, and an underground structure is reported in Ref. 12. The recent applications of the program are reported in Refs. 19 through 26.

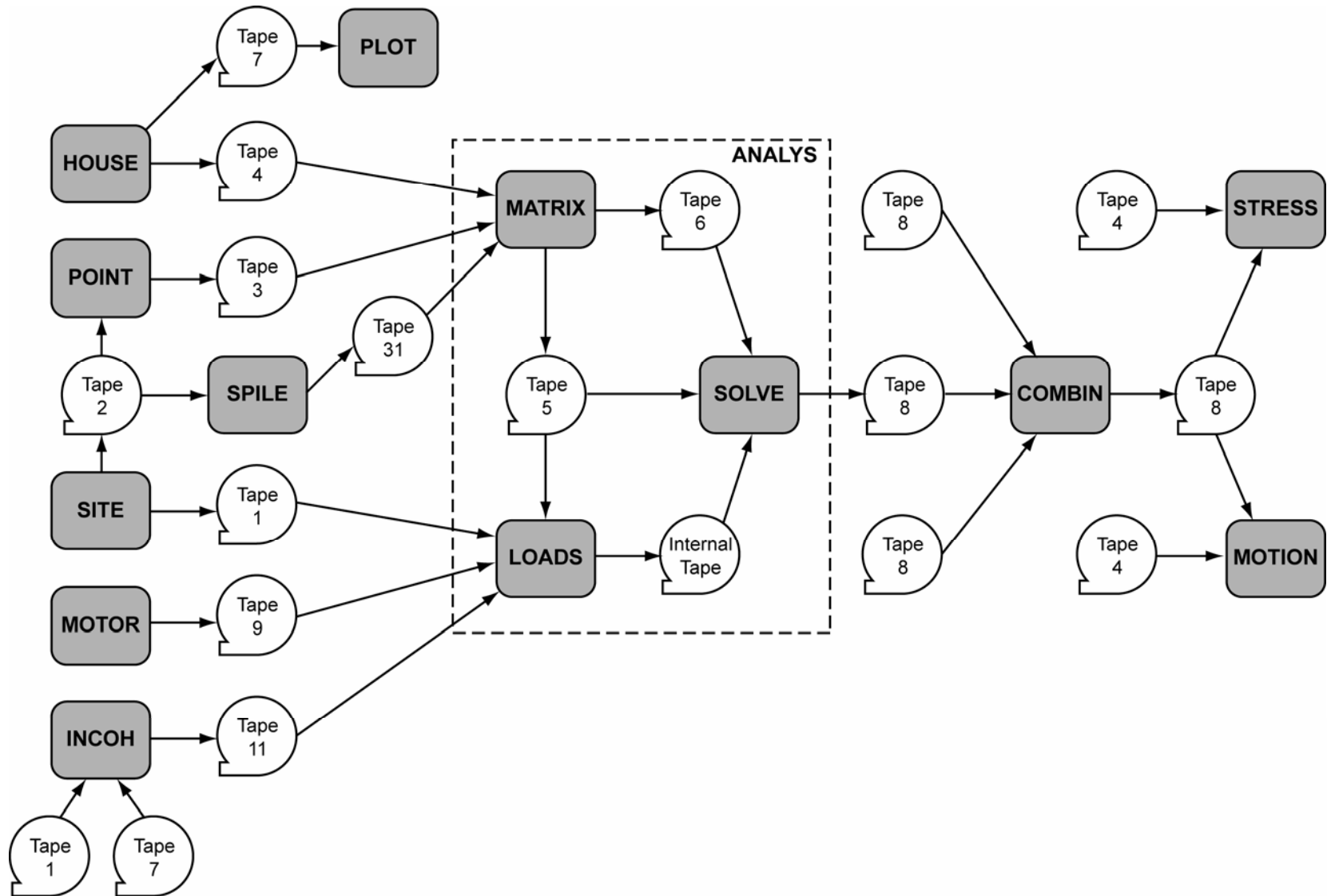


Figure 8.1 Layout of Computer Program SASSI

CHAPTER 9

REFERENCES

1. Bathe, K. L., Wilson, E. L., Peterson, F. E. (1974) "SAP IV - A Structural Analysis Program for Static and Dynamic Response of Linear Systems," Report No. EERC 73-11, Earthquake Engineering Center, UCB, April.
2. Ostadan, F. (2000): "SASSI 2000 Validation Report,".
3. Ostadan, F., et al. (1987): "Soil-Structure Interaction Analyses of Quarter-Scale Containment Model Experiment in Lotung, Taiwan," Bechtel Corporation, San Francisco, CA, prepared for Electric Power Research Institute, Palo Alto, CA, December.
4. Chen, J-C. (1980): "Analysis of Local Variation in Free-Field Seismic Ground Motions," Ph.D. Dissertation, University of California, Berkeley, November.
5. Chin, Chih-Cheng (1998): "Substructure Subtraction Method and Dynamic Analysis of Pile Foundations," Ph.D. Dissertation, University of California, Berkeley.
6. Cooley, J. W. and Tukey, J. W. (1965): "An algorithm for the machine calculation of complex Fourier series," Mathematics of Computation, Vol. 19, No. 19, 297-301.
7. Hardin, B. O. and Drnevich, V. P. (1972): "Shear modulus and damping in soils: design equations and curves," Journal of the Soil Mechanics and Foundations Division, ASCE, Vol. 98, No., SM7, 667-692.
8. Lysmer, J. and Kuhlemeyer, R. L. (1969): "Finite dynamic model for infinite media," Journal of Engineering Mechanics Division, ASCE, Vol. 95, No. EM4, 859-877.
9. Lysmer, J., Udaka, T., Seed, H. B., and Hwang, R. (1974): "LUSH - A computer program for complex response analysis of soil-structure systems," Report No. EERC 74-4, Earthquake Engineering Research Center, UCB, April.
10. Lysmer, J., Udaka, T., Tsai, C-F., and Seed, H. B. (1975): "FLUSH - A computer program for approximate 3-D analysis of soil structure interaction problems," Report No. EERC 75-30, Earthquake Engineering Research Center, UCB, November.
11. Lysmer, J. (1978): "Analytical procedures in soil dynamics," Report No. EERC 78/29, Earthquake Engineering Research Center, University of California, Berkeley, December.
12. Lysmer, J., Tabatabaie-Raissi, M., Tajirian, F., Vahdani, S., and Ostadan, F. (1981): "SASSI - A system for analysis of soil-structure interaction," Report No. UCB/GT/81-02, Geotechnical Engineering, University of California, Berkeley, April.
13. Ostadan, F. (1983): "Dynamic Analysis of Soil-Pile-Structure Systems," Ph.D. Dissertation, University of California, Berkeley.

14. Ostadan, F., Lysmer, J. (1985): "Dynamic Analysis of Directly Loaded Structures on Pile Foundations," 8th SMiRT Conference, Brussels, Belgium.
15. Ostadan, F., Lysmer, J. (1986): "Simplified Dynamic Analysis of Soil-Pile-Structure Systems," 5th International Symposium & Exhibition on Offshore Mechanics and Arctic Engineering, Tokyo, Japan.
16. Ostadan, F., et al. (1987): "Application of Flexible Volume Method to Soil-Structure Interaction Analysis of Flexible and Embedded Foundation," 9th SMiRT Conference, Lausanne, Switzerland.
17. Ostadan, F., et al. (1988): "Effect of Foundation Flexibility and Embedment on the Soil-Structure Interaction Response," 9th World Conference on Earthquake Engineering, Tokyo, Japan, August.
18. Ostadan, F., et al. (1989): "Effect of Site Soil Properties on Seismic SSI Response of Embedded Structures," ASCE Foundation Engineering Congress, Evanston, Illinois.
19. Ostadan, F., et al. (1989): "The Effect of Embedment Depth on Seismic Response of a Nuclear Reactor Building," 10th SMiRT Conference, Los Angeles, California, U.S.A.
20. Ostadan, F., et al. (1991): "Radially Loaded Circular Tunnel Structure," IX Panamerican Conference on Soil Mechanics and Foundation Engineering, Vina Del Mar, Chile.
21. Ostadan, F., et al. (1991): "Effect of Intermediate SSI Solutions on Final Responses," 11th SMiRT Conference, Tokyo, Japan, 1991.
22. Ostadan, F., et al. (1993): "Seismic Design of ABWR and SBWR Standard Plants," ICONE2, San Francisco, California, March.
23. Ostadan, F., et al. (1993): "Seismic Considerations for the Standardized Advanced Light Water Reactor (ALWR) Plant Design," American Power Conference, Chicago, Illinois, April.
24. Ostadan, F., et al. (1996): "Design Soil Profiles for Seismic Analyses of AP600 Plant Standard Design," ASME PVP & ICVT Pressure Vessel and Piping Conference, Montreal, Quebec, Canada, July 21-26.
25. Ostadan, F., et al. (1997): "Seismic Qualification of New Underground Diesel Fuel Tanks at the Diablo Canyon Nuclear Power Plant Site," ASME PVP & ICVT Pressure Vessel and Piping Conference, Orlando, Florida, July 27-31.
26. Ostadan, F., et al. (1998): "Lateral Seismic Soil Pressure-An Updated Approach," US-Japan Workshop on Soil-Structure Interaction, USGS, Menlo Park, CA, September 22-23 also published in Earthquake Engineering and Soil Dynamics Journal, April 2005.
- 26b. Ostadan, F., Penzien, J. (2001): "Seismic Design of Cut-and-Cover Sections of the Bay Area Rapid Transit Extension to San Francisco Airport," 2nd US-Japan Workshop on Soil-Structure Interaction, Tsubuka, Japan, March 6-8, 2001.

- 26c. Ostadan, F., Deng, N., Costantino, C. (2003): "River Protection Project Seismic Analysis of Vitrification Buildings," Structural Mechanics in Reactor Technology, Czech Republic, August.
27. Schnabel, P. B., Lysmer, J. and Seed, H. B. (1972): "SHAKE - A computer program for earthquake response analysis of horizontally layered sites," Report No. EERC 72-12, Earthquake Engineering Research Center, UCB, December.
28. Seed, H. B. and Idriss, I. M. (1969): "The influence of soil conditions on ground motion during earthquake," Journal of Soil Mechanics and Foundations Division, ASCE, Vol. 94, No., SM1, 99-137, December.
29. Seed, H. B. and Idriss, I. M. (1970): "Soil moduli and damping factors for dynamic response analysis," Report EERC 70-10, Earthquake Engineering Research Center, UCB, December.
30. Tabatabaie-Raissi, M. (1982): "The Flexible Volume Method for Dynamic Soil-Structure Interaction Analysis," Ph.D. Dissertation, University of California, Berkeley.
31. Tajirian, F. (1981): "Impedance Matrices and Interpolation Techniques for 3-D Interaction Analysis by the Flexible Volume Method," Ph.D. Dissertation, University of California, Berkeley.
32. Vahdani, S. (1984): "Impedance Matrices for Soil-Structure Interaction Analysis by the Flexible Volume Method," Ph.D. Dissertation, University of California, Berkeley.
33. Waas, G. (1972): "Earth vibration effects and abatement for military facilities - analysis method for footing vibrations through layered media," Technical Report 5-71-14, U.S. Army Engineer Waterways Experimental Station, Vicksburg, Mississippi, September. (Also a Ph.D. Dissertation entitled, "Linear Two-Dimensional Analysis of Soil Dynamics Problems in Semi-Infinite Layered Media," University of California, Berkeley).
34. Wilson, E. L. and Dovey, H. H. (1978): "Solution or reduction of equilibrium equations for large complex structural systems," Advances in Engineering Software, Vol. 1, No. 1, 19-25.
35. Zienkiewicz, O. C., (1977): The Finite Element Method, 3rd edition, (McGraw-Hill).
36. Kausel, E. and Manolis G. (2000): "Wave Motion in Earthquake Engineering," WIT Press, Southampton, Boston.
37. Mita, A. and Luco J.E. (1986): "Response of Structures to Spatially Random Ground Motion," 3rd U.S. Conference on Earthquake Engineering, Charleston, South Carolina.
38. Abrahamson, N.A. (2005): "Recommended Coherency Model," A report Prepared for EPRI.
39. Angelides, D.C. and Roesset, J.M. (1981): "Nonlinear lateral dynamic stiffness of piles," Journal of the Geotechnical Engineering, ASCE, Vol. 107, No. GT11, November, 1443-

1460.

40. Apsel, R.J. and Luco, J.E. (1976): "Torsional response of rigid embedded foundations," *Journal of the Engineering Mechanics*, Division, ASCE Vol. 102, 957-970.
41. Blaney, G.W., Kausel, E. and Roesset, J.M. (1976): "Dynamic stiffness of piles," *Second International Conference on Numerical Methods in Geomechanics*, Vol. II, Virginia Polytechnic Institute and State University, Blacksburg, VA, June 1976, pp. 1001-1012
42. Butterfield, R. and Banerjee, P.K. (1971): "The elastic analysis of compressible piles and pile groups," *Geotechnique* 21, No. 1, 43-60.
43. Dobry, R., Vicente, E., O'Rourke, M.J. and Roesset, J.M. (1982): "Horizontal stiffness and damping of single piles," *Journal of the Geotechnical Division, ASCE*, Vol. 108, No. GT3, 439-459, March.
44. Flores-Berrones, R. and Whitman, R. (1982): "Seismic response of end bearing piles," *Journal of the Geotechnical Engineering Division, ASCE*, Vol. 108, No. GT4, 554-569, April.
45. Kagawa, T. and Kraft, L.M., Jr. (1980): "Seismic P-y response of flexible piles," *Journal of the Geotechnical Division, ASCE*, Vol. 106, No. GT8, August, 899-918.
46. Kaynia, A.M. (1982): "Dynamic stiffness and seismic response of pile groups," Research report R82-03, School of Civil Engineering, Constructed Facilities Division, MIT, Cambridge, Massachusetts.
47. Kuhlemeyer, R.L. (1979): "Dynamic response curves for vertically loaded floating pile foundations," Research report No. CE79-5, Department of Civil Engineering, University of Calgary, Calgary, Alberta, Canada.
48. Matlock, H. (1970): "Correlations for design of laterally loaded piles in soft clay," *Proceedings of the 2nd Offshore Technology Conference*, Houston, Texas, Vol. 1, pp. 577-594.
49. Mindlin, R.D. (1936): "Forced at a point in the interior of a semi-infinite solid," *Physics* 7, 195-202.
50. Nogami, T. (1979): "Dynamic group effect of multiple piles under vertical vibration," *Proceedings of 3rd Engineering Mechanics Division Specialty Conference*, University of Texas at Austin, September 17-19.
51. Nogami, T. and Novak, M. (1977): "Resistance of soil to a horizontally vibrating pile," *Earthquake Engineering and Structural Dynamics*, Vol. 5, 249-261.
52. Novak, M. (1974): "Dynamic stiffness and damping of piles," *Canadian Geotechnical Journal*, vol. II, No. 4, 574-598.
53. Novak, M. (1977): "Vertical vibrations of floating piles," *Journal of the Engineering*

Mechanics Division, ASCE, Vol. 103, No. EMI, 153-168, February.

54. Novak, M. and Howell, J.F. (1977): "Torsional vibration of pile foundations," Journal of the Geotechnical Engineering Divisions, ASCE, Vol. 103, No. GT4, 271-285, April.
55. Novak, M. and Aboul-Ella, F. (1978): "Impedance functions of piles in layered media," Journal of the Engineering Mechanics Division, ASCE, Vol. 104, No. EM6, 643-661, June.
56. Penzien, J. (1970): "Soil-pile foundation interaction," Chapter 14 of Earthquake Engineering, (Prentice-Hall, Inc.).
57. Poulos, H.G., Aust. A.M.I.E. (1968): "Analysis of the settlement of pile groups," Geotechnique 18, 449-471.
58. Poulos, H.G. (1971): "Behavior of laterally loaded piles. II: Pile groups," Journal of the Soil Mechanics and Foundations Division, ASCE, Vol. 97, No. SM5, 733-751, May.
59. Poulos, H.G. (1972): "Behavior of laterally loaded piles. III: Socketed piles," Journal of the Soil Mechanics and Foundations Division, ASCE, Vol. 98, No. SM4, 341-360, April.
60. Wolf, J.P. and Von Arx, G.A. (1978): "Impedance functions of a group of vertical piles," Proceedings of the Specialty Conference on Soil Dynamics and Earthquake Engineering, ASCE, Pasadena, California, Vol. 2, pp. 1024-1041.
61. Weismann, Shmuel L. and Taylor, Robert L. (1989): "Resultants fields for mixed plate bending elements/Report/Structural Engineering, Mechanics and Materials; no. UCB/SEMM-89/13 Berkeley, California.: Dept. of Civil Engineering, University of California at Berkeley.
62. Weismann, Shmuel L. and Taylor, Robert L. (1990): "Mixed formulations for plate bending elements/Report; NO. ucb/sem-90/13 Berkeley, Calif.: Dept. of Civil Engineering, University of California.
63. Reese, L.C., Cox W.R. and Koop, F.D. (1974): "Analysis of laterally loaded piles in and," Proceedings of the 6th Offshore Technology Conference, Houston, Texas, paper OTC-2080.
64. Zienkiewicz, O. C., Taylor, R. L. (2002), "The Finite Element method," Butterworth Heinemann, 3 Volumes.
65. Tajimi, H. (1969), "Dynamic analysis of a structure embedded in an elastic stratum," Proceedings of the 4th World Conference on earthquake Engineering, Santiago, Chile, Vol. III.
66. Kausel, E. (1974), "Forced vibrations of circular foundations on layered media," Soils Publication No. 336, Department of Civil Engineering, MIT, Cambridge.

APPENDIX A

**COMMENT FORMS
AND
ERROR REPORTS**

S A S S I

READER'S COMMENT FORM

Manual Title: _____ Revision No.: _____

Please complete this form and return to:

sassi@sassi2000.net

Your comments and suggestions about this manual are requested to improve the manual and the program itself. Your comments may include clarity, accuracy, completeness, organization, index, etc.

COMMENTS: (Please give specific page and line reference where appropriate.)

FROM Name or Title (incl. email): _____

Company Name: _____

Company Address: _____

City: _____ State: _____ Zip Code: _____

Country: _____

S A S S I

SUSPECTED ERROR REPORT

Please complete this form and return to:

sassi@sassi2000.net

This form is for reporting a suspected error in the computer program.

Program Module Name: _____ Revision No.: _____

Computer Systems: _____ System: _____

REPORTED BY: Name or Title (incl. email): _____

Company Name: _____

Company Address: _____

City: _____ State: _____ Zip Code: _____

Country: _____

DESCRIPTION (Please be complete. Append relevant files, listings, core dumps, etc.)